

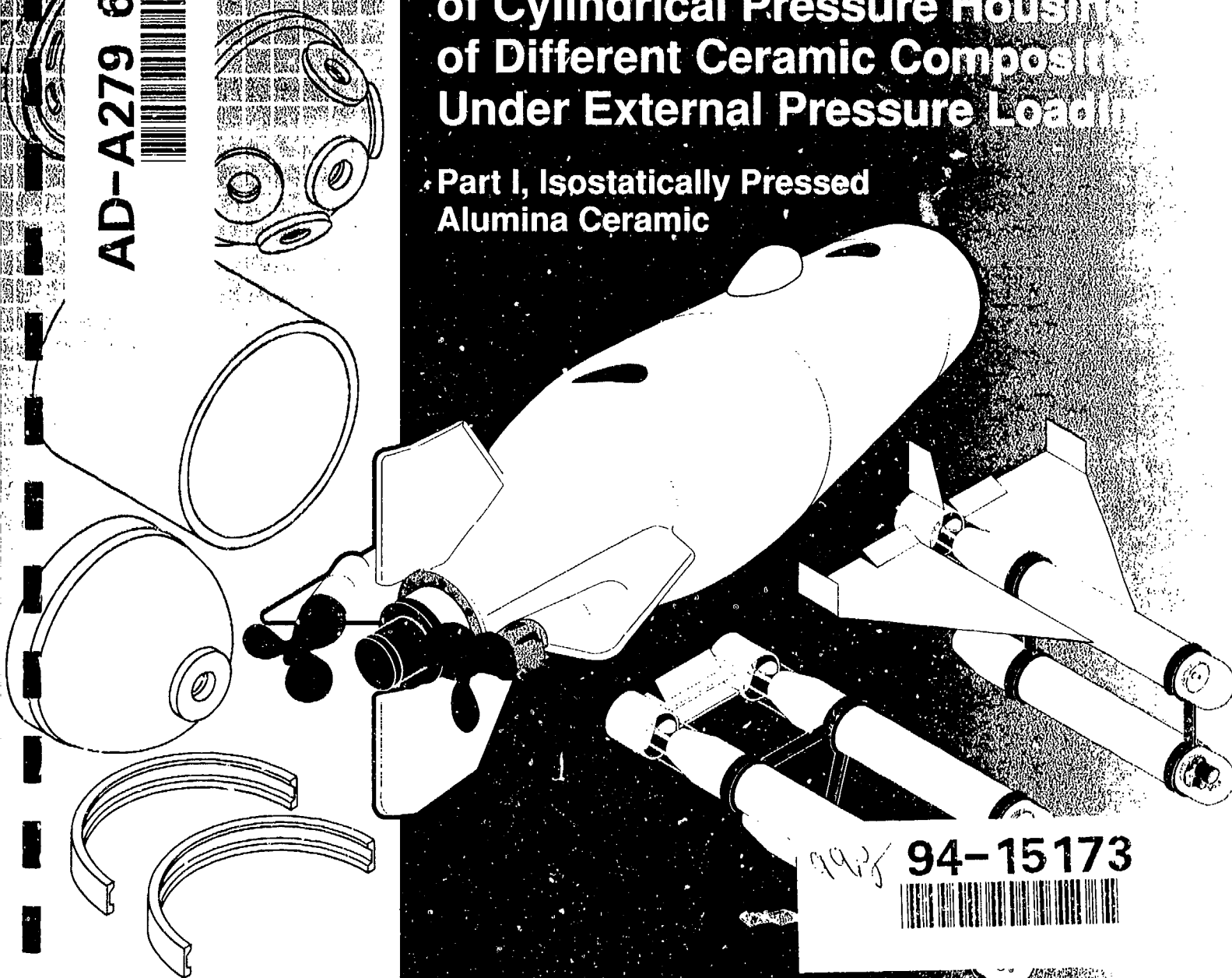
MAY 20 1994

AD-A279 669



# Structural Performance of Cylindrical Pressure Housing of Different Ceramic Compositions Under External Pressure Loading

Part I, Isostatically Pressed  
Alumina Ceramic



992 94-15173



R. P. Johnson  
R. R. Kurkchubasche  
J. D. Stachiw

Technical Report 1590  
August 1993

Approved for public release; distribution is unlimited.



**Technical Report 1590**  
August 1993

**Structural Performance of  
Cylindrical Pressure Housings  
of Different Ceramic Compositions  
Under External Pressure Loading**

**Part I, Isostatically Pressed Alumina Ceramic**

R. P. Johnson  
R. R. Kurkchubasche  
J. D. Stachiw

**NAVAL COMMAND, CONTROL AND  
OCEAN SURVEILLANCE CENTER  
RDT&E DIVISION  
San Diego, California 92152-5001**

**K. E. EVANS, CAPT, USN**  
Commanding Officer

**R. T. SHEARER**  
Executive Director

**ADMINISTRATIVE INFORMATION**

This work was performed by the Marine Materials Technical Staff, RDT&E Division of the Naval Command, Control and Ocean Surveillance Center, for the Naval Sea Systems Command, Washington, DC 20362.

Released by  
J. D. Stachiw  
Marine Materials  
Technical Staff

Under authority of  
N. B. Estabrook, Head  
Ocean Engineering  
Division

Accession For		<input checked="checked" type="checkbox"/>
NTIS GRA&I		<input type="checkbox"/>
DTIC TAB		<input type="checkbox"/>
Unannounced		
Justification		
By _____		
Distribution _____		
Availability _____		
Special _____		
Dist	A-1	

## SUMMARY

Ten 12-inch-OD by 18-inch-long by 0.412-inch-thick monocoque cylinders fabricated by WESGO, Inc. from 96-percent alumina ceramic were assembled into external pressure housings and experimentally evaluated under short-term, static, and cyclic pressure loadings. Each external pressure housing that was tested consisted of an alumina cylinder with adhesively bonded titanium end-cap joint rings for sealing and mating with end closures. This study was undertaken as part of a program to promote the application of ceramic to large external pressure housings for underwater vehicles (reference 14). Pressure testing was performed in order to generate structural performance data that could be used to establish design criteria for external pressure housings constructed using 96-percent alumina ceramic as the primary hull material. The 96-percent alumina composition (density 3.74 g/cc) used in the test cylinders was found to have the following minimum mechanical and physical properties:

- compressive strength: 350 kpsi
- flexural strength: 47 kpsi
- Weibull modulus: 20
- fracture toughness ( $K_{IC}$ ): 2.50 kpsi ( $\text{in}^{1/2}$ )
- elastic modulus: 43E6 psi

Two of the alumina cylinders were subjected to short-term pressure tests to determine the elastic stability of the monocoque alumina-ceramic pressure housing assembly. When capped with flat-steel end closures, one of the 96-percent alumina cylinders failed by buckling at an external pressure of 23,730 psi. Seven of the alumina cylinders were external pressure cycled to peak pressures varying from 9,000 to 15,000 psi to determine cyclic life as a function of the applied load level during each cycle. At an external pressure of 11,000 psi generating nominal maximum membrane stresses of -160,000 psi in the hoop direction and -80,000 psi

in the axial direction in the ceramic shell wall, the 96-percent alumina cylinders were found to have a cyclic fatigue life in excess of 1,000 dive cycles. Finally, one cylinder was subjected to long-term external pressurization at 11,000 psi generating nominal maximum membrane stresses of -160,000 psi in the hoop direction and -80,000 psi in the axial direction in the ceramic shell wall. From this test, the alumina cylinder demonstrated a static fatigue life in excess of 1,000 hours.

The monocoque 96-percent alumina-ceramic cylinders with  $t/OD = 0.034$  tested for this report have a weight-to-displacement (W/D) ratio of 0.49 in seawater (0.55 including two titanium end-cap joint rings). The submerged lift generated by alumina-ceramic pressure housings exceeds that which can be obtained using an equivalent metallic housing for the same design depth. This enables alumina-ceramic housings to carry more than three times the payload capacity of an equivalent titanium housing while remaining neutrally buoyant. Consequently, the incorporation of ceramic materials like 96-percent alumina into external pressure housings allows hull designs with improved performance when minimum dry weight and maximum in-service buoyancy are required.

The cyclic fatigue life of cylindrical external pressure housings assembled with a 96-percent alumina monocoque cylinder and capped at both ends with adhesive-bonded type Mod 1 titanium joint rings was found to be a function of the peak stresses generated in the ceramic during each dive cycle. Failure by cyclic fatigue occurred through the initiation and propagation of cracks from the plane-bearing surfaces of the cylinder ends at the interface with the titanium joint rings. Based on experimental testing performed for this report, design curves for 96-percent alumina external pressure housings are presented that relate the maximum number of operational dive cycles to the maximum allowable stresses in the ceramic housing during each dive cycle.

## CONTENTS

INTRODUCTION	1
TESTING CONFIGURATIONS	2
FABRICATION	4
BACKGROUND	4
MANUFACTURING	4
INSPECTION	6
MATERIAL PROPERTIES	7
TESTING	8
PLAN	8
STRUCTURAL ANALYSIS	9
TEST RESULTS	12
FINDINGS	14
CONCLUSIONS	17
RECOMMENDATIONS	17
REFERENCES	20
GLOSSARY	22
APPENDIX	
A: QUALITY CONTROL DATA	A-1

## FIGURES

1. 25-inch-OD 96-percent alumina-ceramic cylindrical assembly for ocean depth service of 20,000 feet	23
2. 25-inch-OD 96-percent alumina-ceramic hemispherical end-closure assembly for ocean depth service of 20,000 feet	23
3. Sub-critical crack growth in a ceramic cylinder	24
4. 96-percent alumina-ceramic AL-600 stress rupture curve	24
5. 12-inch cylinder test assembly I configuration, Sheet 1	25
5. 12-inch cylinder test assembly I configuration, Sheet 2	26

## FEATURED RESEARCH

---

5. 12-inch cylinder test assembly I configuration, Sheet 3	27
6. 12-inch cylinder Mod 1, Type 2 end-cap joint ring	28
7. 12-inch cylinder spacer	29
8. 12-inch hemisphere	30
9. 12-inch cylinder Mod 1 end-cap joint ring O-ring	31
10. 12-inch hemisphere clamp band	32
11. 12-inch hemisphere plug	33
12. 12-inch hemisphere washer	34
13. 12-inch hemisphere wood plug	35
14. 12-inch cylinder test assembly II configuration, Sheet 1	36
14. 12-inch cylinder test assembly II configuration, Sheet 2	37
15. 12-inch flat end plate	38
16. 12-inch cylinder test assembly III configuration, Sheet 1	39
16. 12-inch cylinder test assembly III configuration, Sheet 2	40
17. 12-inch cylinder Mod 1, Type 1 end-cap joint ring	41
18. 12-inch flat end-plate tie rod	42
19. 12-inch flat end-plate feed through	43
20. 12-inch flat end-plate wood plug	44
21. Alumina-ceramic 12-inch cylinder	45
22. Alumina-ceramic manufacturing steps	46
23. Alumina-ceramic NDE calibration standards	47
24. NDE calibration standards mounting fixture	48
25. Alumina ceramic calibration standards assembly	49
26. Bonding of Mod 1 end-cap joint rings	50
27. 12-inch alumina cylinder with Mod 1, Type 2 end-cap joint rings	50
28. 12-inch alumina cylinder with Mod 1, Type 2 end-cap joint rings	51
29. Test assembly I configuration	51
30. Preparation of test assembly I configuration for pressure testing	52
31. Preparation of test assembly II configuration for pressure testing	52
32. FEA solid model of test assembly I configuration	53
33. Test assembly I radial stress plot at 9,000 psi	55
34. Detail of test assembly I radial stress plot at 9,000 psi	57

35. Test assembly I axial stress plot at 9,000 psi	59
36. Test assembly I hoop stress plot at 9,000 psi	61
37. FEA solid model of test assembly II configuration	63
38. Detail of FEA solid model of test assembly II configuration	65
39. Test assembly II radial stress plot at 15,000 psi	67
40. Plot of strains recorded during pressurization of test 1 cylinder	69
41. Circumferential cracks on the bearing surface of test 1 cylinder	69
42. Ultrasonic C-scan of sub critical crack growth in test 1 cylinder	70
43. Plot of strains recorded during pressurization of test 2 cylinder	71
44. Plot of strains recorded during pressurization of test 3 cylinder	71
45. Plot of strains recorded during pressurization of test 4 cylinder	72
46. Plot of strains recorded during pressurization of test 5 cylinder	72
47. Plot of strains recorded during pressurization of test 6 cylinder	73
48. Plot of strains recorded during pressurization of test 7 cylinder	73
49. Remains of cylinder assembly after failure from test 3	74
50. Remains of cylinder assembly after failure from test 7	74
51. Plot of strains recorded during pressurization of test 8 cylinder	75
52. Plot of strains recorded during pressurization of test 9 cylinder	75
53. Cyclic external pressure loading test data for test 1 through 7 cylinders	76
54. AL-600 alumina cyclic life versus maximum calculated tensile bearing surface stress	76
55. AL-600 alumina cyclic life versus maximum calculated compressive hoop stress	77
56. Design curve for external pressure cyclic loading of AL-600 alumina cylinders	77
57. t/OD ratios of monocoque AL-600 alumina cylinders for 1,000 cycles to design depth	78
58. W/D ratios of monocoque AL-600 alumina cylinders for 1,000 cycles to design depth	78
59. t/OD ratios of monocoque AL-600 alumina cylinders for 100 cycles to design depth	79
60. W/D ratios of monocoque AL-600 alumina cylinders for 100 cycles to design depth	79
61. t/OD ratios of monocoque AL-600 alumina cylinders for 10 cycles to design depth	80
62. W/D ratios of monocoque AL-600 alumina cylinders for 10 cycles to design depth	80

## TABLES

1. Material properties for WESGO, Inc. alumina-ceramic composites	81
2. Internal defects detected in alumina cylinders using ultrasonic NDE techniques	82

## FEATURED RESEARCH

---

3. External pressure test plan for alumina cylinders _____	83
4. Calculated stresses (psi) in alumina cylinders for test assembly I configuration _____	84
5. Calculated stresses (psi) in alumina cylinders for test assembly II and III configurations _____	85
6. External pressure test results for alumina cylinders _____	86



## INTRODUCTION

Alumina ceramic is an excellent material choice for designing pressure-resistant housings because of its outstanding high specific compressive strength and elastic modulus, resistance to corrosion, and good thermal conductivity. In underwater applications where maximum housing buoyancy is required, the use of ceramics-like alumina for constructing the major hull components offers a clear advantage over traditional metallic alloys.

Prior ceramic pressure housing development focused on demonstrating the feasibility of alumina for the primary structural material used in progressively larger external pressure housings (references 8 and 20 through 24). Design concepts for alumina housings were proven by pressure testing 6-inch, 12-inch, 20-inch, and 25-inch outside diameter (OD) cylindrical and hemispherical alumina hull components. Figure 1<sup>1</sup> shows a 25-inch-OD by 64.84-inch-long cylindrical pressure assembly (reference 8) designed for ocean depth service down to 20,000 feet (9,030 psi). This housing is built up using two 96-percent alumina-ceramic cylinders and a central titanium joint ring. Figure 2 shows a 25-inch-OD 96-percent alumina-ceramic hemispherical end closure also designed for ocean depth service down to 20,000 feet (reference 8).

The hemispherical end closure shown in figure 2 was proof tested to 10,000 psi external pressure and cycled to 9,000 psi external pressure 500 times. These 25-inch-OD alumina housing components could be joined together to construct an external pressure housing with a weight-to-displacement (W/D) ratio of 0.585 in sea water providing a net lift of 620 pounds. This report supplements this current design philosophy with additional data on the structural performance of isostatically pressed alumina-ceramic cylindrical hulls used in pressure-resistant housings for deep submergence applications.

Alumina housings must be designed to withstand a variety of environments associated with the

specific service for which they are intended. Consideration must be given to the housings' ability to withstand handling, thermal and depth loads, as well as the reactive environment of the sea. In most cases, the design of alumina hull components will be driven by their ability to perform reliably at the service depths at which the housing assembly is intended to operate. There are two primary failure modes that have been observed for alumina housings subjected to external pressure loading which must be addressed. The first failure mode that must be considered is cyclic fatigue of the alumina hull components subjected to external pressure cycles. The second failure mode which must be addressed is buckling of the ceramic housing under depth loading. Low-cycle fatigue failure is specifically of concern for pressure housings constructed from brittle materials like alumina, whereas buckling is a potential failure mode for all external pressure housings and for any compressively loaded structure in general.

Alumina housings can fail by low-cycle fatigue because of localized tension that occurs at bearing surfaces at the ends of alumina hull components when subjected to pressure loading on the external surfaces of the housing.

Bearing-surface tensile stresses occur during depth loading due to material and geometric discontinuities that exist at joint interfaces at alumina component ends. Circumferential cracks have been observed to initiate from pre-existing flaws on the bearing surfaces of alumina-housing sections where pressure-induced tensile stresses are calculated to exist. These flaws can be in the form of intrinsic-surface or sub-surface pores or micro-cracks (references 2 and 15).

Crack propagation from the bearing surfaces of externally pressure-cycled alumina hull components appears to be characterized by distinct growth stages as indicated by acoustic emissions data recorded during testing (reference 23) and subsequent fractographic examinations of exposed fracture surfaces (reference 7). These observations indicate that stable crack growth occurs in a sequence of bursts and arrests and originates from point sources on the bearing surfaces of the alumina hull ends. Over repeated pressure cycles, the

<sup>1</sup>Figures and tables are placed at the end of the text.

sub-critical cracks can propagate meridionally into the alumina shell wall as shown in figure 3. The structural integrity of the alumina hull only becomes compromised when these cracks have propagated to the point that flakes of the wall spall off from the cylinder OD or inner diameter (ID) and failure occurs due to leakage and/or a reduction in the amount of material in the shell wall that can bear compressive load.

Tensile stresses at levels well below the flexural strength of alumina are known to be sufficient to induce crack growth when present over a number of external pressure cycles. A substantial amount of research has been invested in developing joint designs and assembly techniques to reduce the potential for crack growth from the bearing surfaces of ceramic-housing component ends when subjected to external pressure loading. Much of this effort has focused on the use of interface gasket materials between the bearing surfaces of the ceramic hull and the metallic joint rings (references 3, 11, and 23). The key to designing alumina housings to ensure against low-cycle fatigue failure is to determine safe-operating stress levels at which spalling, resulting in leakage and/or collapse of the ceramic housing, will not occur. As with most fatigue analysis, safe-operating stress levels depend on the number of pressure cycles for which the ceramic housing is intended to perform.

Structural instability can occur in underwater pressure housings under external hydrostatic load if there is a means by which the strain energy associated with *compression* of the shell membrane can be converted to strain energy associated with *bending* of the shell membrane. Large deflections associated with bending of the pressure housing shell wall is known as buckling and is one of the primary failure mechanisms for ceramic pressure housings. Buckling analysis of an alumina housing must be performed to ensure the housing will adequately resist failure from general instability.

Stress rupture due to long-term static loading is a third failure mode that has not been directly observed in previous external pressure testing of

alumina housings, but was investigated for this report. Prior research (references 7 and 17) has indicated that the flexural strength of alumina modulus-of-rupture (MOR) test specimens is dependent on the duration of the applied load. Flexural strength data presented for alumina is typically based on failure by fast fracture of MOR test specimens. A sample group of alumina test specimens were statically loaded at different load levels and the time required for failure was recorded. Figure 4 shows the time/load curve that was generated for a particular alumina composition that had a fast fracture flexural strength of 43.9 kpsi. It was found that extended submersion in salt water has relatively little effect on the stress-rupture characteristics of alumina. It was also found that the strength of alumina ceramic subjected to long-term loading has an endurance limit of approximately 50 to 60 percent of the fast fracture strength for load durations exceeding 2,000 hours.

This report serves to provide documentation of the structural performance of 12-inch-OD 96-percent alumina-ceramic cylinders that were subjected to cyclic external pressure loading, short-term external pressure loading, and long-term external pressure loading. This information will provide a data base to ensure that future alumina hull components are adequately designed against structural failure during service in external pressure-resistant housings.

## TESTING CONFIGURATIONS

---

Pressure testing of the 12-inch-OD cylinders required the design of end closures, feedthroughs, and end-cap joint rings. Two types of end closures were used. Titanium hemispheres were used as end closures for all tests performed at pressures up to, and including, 13,000 psi. Flat-steel end plates were used as end closures for all pressure tests run at pressures greater than 13,000 psi. Titanium hemispheres were the end closure of choice for pressure testing, but could not be used for tests at greater pressures because of the potential for failure due to elastic instability. Additionally, two types of Naval Ocean Systems Center

(NOSC)<sup>2</sup> Mod 1 (hereafter called Mod 1) end-cap joint rings were used for the pressure testing, depending on the duration of each test. Mod 1, Type 1 end-cap joint rings were used for short-term pressure tests. Mod 1, Type 2 end-cap joint rings were used for all long-term pressure tests. This test hardware was configured in three basic test assemblies that were used for evaluating the structural performance of the 12-inch-OD alumina cylinders for this study.

The test assembly I configuration was used for all external pressure loadings of cylinders at pressures up to, and including, 13,000 psi for determining low-cycle fatigue life and static fatigue life for long-term external pressure loading. The second configuration, test assembly II, was used for all external pressure cycling of cylinders at pressures greater than 13,000 psi for determining low-cycle fatigue life. The last configuration, test assembly III, was used for all short-term pressurization tests (single pressure cycle) for determining the buckling behavior of the ceramic cylinders.

Details of the test assembly I configuration are shown in figure 5. The bearing surfaces at each end of the ceramic cylinders were capped with titanium Mod 1, Type 2 end-cap joint rings epoxied in place per the bonding procedures listed in note 4 of figure 5. Figure 6 shows the details of the Mod 1, Type 2 end-cap joint rings used for all cyclic and long-term pressurization testing. The dimensions of the U-shaped end-cap joint rings were selected to allow for a minimum radial clearance of 0.015 of an inch between the interior and exterior surfaces of the ceramic cylinder and the end cap during bonding. A minimum axial clearance of 0.010 of an inch between the bearing surfaces at the ends of the ceramic cylinders and the seat of the U-shaped end-cap joint rings was maintained during bonding using the spacer (reference 11) shown in figure 7. Additionally, the outer flange of the end-cap joint ring was flared at a 30-degree angle to provide a circumferential gland for capturing a bead of room-temperature vulcanizing

silicone rubber (RTV) after the end-cap joint ring had been bonded in place. RTV acted to prevent water intrusion into the epoxy bond during pressure testing.

The ceramic cylinders, subjected to testing at an external pressure up to and including 13,000 psi, were closed at both ends with titanium hemispheres (figure 8). The end-cap joint-ring/hemisphere interface was sealed via a face-seal gland machined into the external flange of each end-cap joint ring for capturing the nitrile O-ring shown in figure 9. Closure of each joint interface was maintained using the V-shaped clamp bands shown in figure 10. During pressure testing of the ceramic cylinders with the titanium hemispheres, the plugs shown in figure 11 were assembled through the polar penetration of each hemisphere with the washers shown in figure 12. One end of the housing had a drain plug that could be used to check for leaks, while the plug at the opposite end was used for passing strain-gage wires and a vent line to the exterior of the pressure-vessel end closure during testing. Each ceramic cylinder that was pressure tested contained five water-proofed biaxial strain-gage rosettes uniformly spaced about the ID of the cylinder at mid bay for reading axial and hoop strains. The strain gages used were 0.250-inch, 120-Ohm resistance gages (part number CEA-06-250UT-120) manufactured by Micro-Measurements Division. Pressure testing was performed at Southwest Research Institute in San Antonio, Texas. A wooden plug (figure 13) was placed inside each test assembly I configuration to minimize damage to the titanium hemispheres that could occur if the ceramic cylinders failed catastrophically during testing.

Titanium hemispheres were used when possible for cyclic testing because they represented a more likely end-closure configuration than flat-bulkhead end closures for future ceramic housings designed to provide optimum buoyancy and withstand a large number of external pressure cycles. The titanium hemispheres (figure 8) were designed to allow for cycling the ceramic cylinders to external pressures as high as 13,000 psi. Additionally, these hemispheres were designed to be robust enough to withstand damage associated with failure of the ceramic cylinders during testing. Since

<sup>2</sup>NOSC is now the Naval Command, Control and Ocean Surveillance Center (NCCOSC) RDT&E Division (NRaD).

the hemispheres were to be used over a range of external pressures and reusable even after a catastrophic cylinder failure, they do not represent an optimized end-closure design for a ceramic pressure housing which is intended to operate to any one specific service depth. In order to pressure test the ceramic cylinders at external pressures greater than 13,000 psi, the titanium hemispheres were replaced with flat-steel end closures (figure 14) for test assembly II. Details of the flat-steel end plates that were used for this configuration are shown in figure 15.

The test assembly III configuration used for short-term pressurization of the ceramic cylinders to 20,000 psi or until failure by general instability is shown in figure 16. The titanium Mod 1, Type 1 end-cap joint rings and epoxy bonding procedures used for the short-term tests were similar to those used for test assemblies I and II. The Mod 1, Type 1 end-cap joint rings (figure 17) contain slightly looser radial clearances with the ceramic cylinders and do not have the RTV gland for sealing the epoxy bond from water intrusion. These simplifications were considered acceptable, given the brief submersion time that would be experienced by the short-term test assemblies during their single pressurization. The test assembly III configuration had the same massive flat-steel end plates used on test assembly II (figure 15). These end plates were designed to be stout enough to withstand the tremendous release of energy associated with implosion of the ceramic cylinders by buckling.

Sealing of the end-cap joint-ring/flat end-plate joint interface was accomplished with the identical face-seal configuration used for the test assemblies described previously. Closure between the cylindrical assembly and end plates was maintained by using four external tie rods (figure 18). Wire leads from the five strain gages located on the ID of the ceramic cylinders at mid bay were passed to the exterior of the test assembly and through the pressure vessel lid using feedthroughs (figure 19) potted with epoxy and urethane. Additionally, the wooden plugs shown in figure 20 were placed in the interiors of test assemblies II and III prior to pressurization to minimize damage of the flat steel

plates in case of collapse of the ceramic cylinder. As with the titanium hemispheres used for the test assembly I configuration, the design of the flat-steel end plates was driven by survivability during testing as opposed to being an optimized end closure for a ceramic underwater pressure housing.

## FABRICATION

### BACKGROUND

Figure 21 shows the details of the 12-inch-OD alumina cylinders that were tested. The dimensions of these cylinders were kept the same as the alumina-ceramic cylinders that were procured for a prior NReD program (reference 20) to allow for the option of using existing fabrication tooling. The length-to-outer-diameter ratio ( $L/OD = 1.50$ ) and thickness-to-outer-diameter ratio ( $t/OD = 0.034$ ) of these alumina-ceramic cylinders was originally selected to construct underwater pressure housings capable of operating at ocean depths of 20,000 feet (9,030 psi external pressure) with a minimum factor of safety (SF) of 2.0 on stress (compressive strength of alumina/minimum principal stress) and a minimum SF of 1.5 on buckling when capped with hemispherical end closures. The weight of the 12-inch-OD 96-percent alumina-ceramic cylinder with titanium Mod 1, Type 2 end-cap joint rings was 42 pounds, of which 5 pounds was contributed by the end-cap joint rings. This cylindrical assembly has a W/D ratio of 0.55 when submerged in water.

### MANUFACTURING

Alumina (aluminum oxide) is a general term to describe a group of ceramic materials composed of between 85- and 99.9-percent aluminum-oxide crystals. The remaining portion of the alumina body consists of binders that are added to assist the bonding of alumina grains during fabrication. Commercially available aluminas are composed of crystalline grains that can vary in size from a few microns to several-hundred microns. Alumina hull pressure housings that have been designed and tested by NReD have either 94- or 96-percent alumina compositions since they proved the best tradeoff between mechanical properties and the

capacity to be fabricated in useful shapes for pressure-housing components. Alumina housing components are typically formed by isostatic pressing techniques prior to being sintered and ground to final dimensions.

A total of 10 alumina-ceramic cylinders used for this testing program were manufactured by WESGO, Inc., (477 Harbor Blvd. Belmont, CA 94002) using their alumina-ceramic composition AL-600 which consists of 96-percent alumina (aluminum oxide) crystals with an average grain size of eight microns. The remaining 4 percent of the alumina body consists of additives that aid in bonding the aluminum oxide crystals together. These binders are primarily oxides of silicon, calcium, and magnesium. Table 1 compares the properties of AL-600 with other alumina compositions available from WESGO, Inc. Figure 22 shows manufacturing methods that are applicable to the fabrication of structural parts made with alumina ceramic. The path indicated by the dashed line shows the steps that were taken to fabricate the isostatically pressed alumina cylinders that were tested for this report.

The 12-inch-OD by 0.412-inch-thick wall by 18.00-inch-length alumina cylinders were fabricated by means of isostatic pressing (reference 16). The first step of this process is the alumina powder preparation where alumina particles, binders, and water are milled together to create a well-blended slurry. A spray dryer is then used to atomize the slurry to create uniform, free-flowing powder agglomerates consisting of spherical particles of alumina and binders. This agglomerate is then screened for the desired particle size and the resulting material is referred to as the processed alumina powder.

The next step in the fabrication of the alumina cylinders is to transform the processed alumina powder into a green body (green compact) by forming the powder with isostatic pressing. Isostatic pressing involves filling a mold with processed alumina powder and applying uniform external pressure to the mold in a hydrostatic pressure chamber. The isostatic pressing mold consists of a lubricated internal steel mandrel and outer flexible elasto-

meric bag (isobag) with accessory hardware for sealing and handling the mold during pressing.

Once inside the chamber, the mold assembly is slowly pressurized to a maximum pressure of 10,000 psi, held for a period of 10- to 20-minutes and, then, gradually decompressed. Compacting of the alumina powder using the isostatic pressing process was selected over alternative forming methods such as slip casting and extrusion because of the size limitations associated with these techniques. Additionally, the uniform compaction associated with isostatic pressing results in finished parts that have more reliable material properties than obtainable from these alternative forming techniques. After the isostatic pressing is completed, the mold is removed from the pressure vessel, the isobag is removed, and the green body is slid off the lubricated steel mandrel. At this point, the green body is ready to be transported for green machining.

Pre-sinter machining (green machining) is performed on each of the green bodies after pressing to remove excess material from the forming process. Material removal is more easily done when the ceramic body is in the green state than after it has been fired. After each part is green machined, it is ready to be fired (sintered) in a kiln. Sintering the green body results in consolidation of the ceramic body to achieve the physical and mechanical properties of the finished part. This consolidation process results in net shrinkage of the ceramic body by 15 to 20 percent. This requires special care in handling the ceramic cylinders during firing to minimize distortion and residual stress.

After the ceramic parts have been fired, machining of the part to its finished dimensions is performed by diamond grinding. Diamond grinding wheels used for this purpose consist of a metallic wheel with diamond grit embedded on its surface with a soft metal or organic matrix. The parameters involved in diamond grinding such as infeed rate, wheel speed, coolant type, grit size, and concentration are critical to achieving the desired surface finish with a minimum amount of subsurface damage. Extrinsic flaws, and surface residual compressive stresses introduced during surface finishing can have a substantial effect on parameters

such as flexural strength and Weibull Modulus for the finished component (references 7 and 15). Rougher grinding procedures introduce greater surface compression, which effectively increases the strength of the ceramic body, but also can generate more severe surface damage. This implies that an optimum grinding procedure should exist that provides the best tradeoff between the amount of surface compression and surface damage that is introduced.

The following list defines the grinding procedures used by WESGO, Inc., to finish the 12-inch-OD cylinders tested for this report. The finish grinding of the cylinders used 180 grit on all circumferential surfaces, and 320 grit on all bearing surfaces at the ends.

Item	Roughing Parameters	Finishing Parameters
Material Removal	to 1 inch	0.010 to 0.020 inch
Infeed Rate (in)	0.0005 to 0.001	0.0005 to 0.001
Wheel Surface Speed	4,000 fpm	4,000 fpm
Coolant	water-base lubricant, sprayed, filtered	water-base lubricant, sprayed, filtered
Wheel Type	metal-bonded diamond	resin-bonded diamond
Grit Size	100	180 to 320
Concentration (%)	75 to 100	75 to 100

## INSPECTION

After fabrication of the isostatically pressed alumina-ceramic cylinders, a nondestructive evaluation (NDE) of each part was carried out. This inspection involved a complete dimensional comparison of each cylinder to the dimensions and tolerances specified in the engineering drawing shown in figure 21. In addition, both surface and volumetric inspection techniques were employed to detect the presence of any flaws or defects that could adversely effect the performance of each cylinder during pressure testing.

The dimensional inspection data form for cylinder part # 001 is included in appendix A as an example of the tolerances that can be achieved for diamond-ground isostatically pressed alumina-ceramic cylinders. The final dimensions and surface finishes obtained through diamond grinding exceeded those that were specified on the engineering drawing. The range in measured outer diameter and wall thickness was 0.002-inch or less. Bearing surfaces at the ends of each cylinder were flat within 0.001 of an inch and the surface finish ranged between 6 and 14 microinches. A visual inspection of all the surfaces on each part was performed with the aid of dye penetrant to detect the presence of surface defects such as cracks, blisters, holes, porous areas or inclusions. In addition, the isostatically pressed alumina-ceramic cylinders were visually inspected to ensure that all surfaces of each part were uniform in color and texture and free of any adherent foreign substances.

In order to inspect each alumina cylinder for internal flaws, an NDE plan was devised using ultrasonic techniques (reference 13). Witness (calibration) standards used for calibrating ultrasonic equipment for inspection of the 12-inch cylinders were procured from WESGO, Inc. The engineering drawing used to fabricate these standards is shown in figure 23. Each standard is fabricated from the same 96-percent alumina composition (AL-600) used to fabricate the isostatically pressed alumina cylinders. Controlled flaws were introduced into these standards by placing pore-forming materials into the processed alumina powder prior to isostatic pressing. Pore-forming materials such as sugar, nylon, and polyethylene were selected because, during sintering of the standards, the pore-forming material would pyrolyze and leave an internal cavity of known size, shape, and location.

These witness standards were then mounted in the fixture shown in figure 24. The entire calibration standard assembly is shown in figure 25. This assembly was mounted on a turn table in an ultrasonic inspection tank for calibrating equipment settings to detect the presence of the known pores in the witness standards. Ultrasonic equipment was calibrated using the 0.030 pore-calibration

standard SK9402-093-C2 in order to generate a pulse-echo longitudinal-wave C-scan for each of the 10 cylinders based on a 0.010-inch scanning index. Table 2 lists the quantity and size of internal indications that were detected in each part. Size of each defect is indicated by a percentage of the average amplitude of reflection from a 0.030 void as detected in the SK9402-093-C2 calibration standard. Depth of each defect is measured in inches from the OD of the cylinder. The NDE results presented in table 2 indicate that all of the internal voids that were detected were less than 0.030 of an inch in size. Based on these findings, the alumina cylinders were considered acceptable for pressure testing.

The use of a maximum 0.030-inch pore size as an acceptance criteria for the 12-inch-OD cylinders is based on quality control experience with engineering ceramics and not based on a critical flaw size in the structural performance of alumina ceramic. Manufacturers of structural ceramic components procured by NRD have repeatedly demonstrated their ability to fabricate parts which do not contain internal flaws exceeding 0.030 of an inch. It is worth noting that there has never been any connection between the failure of an alumina-ceramic part and defects that were detected in that part during pre-service ultrasonic inspection. As mentioned previously, brittle failure of alumina housings that have been pressure cycled is believed to originate due to stress concentrations around micro pores located near the bearing surfaces of alumina hull components. These micro pores can not be detected with the standard NDE procedures described above, but can only be detected with the aid of more advanced techniques such as optical and scanning electron microscopy (SEM) methods (references 2 and 15) and surface-wave ultrasonic inspection.

## MATERIAL PROPERTIES

Alumina exhibits linear elastic stress-strain behavior until failure occurs by fracture. The shortcoming of alumina as a structural material is that it is susceptible to brittle failure. Brittle behavior in alumina and most other ceramics is attributable to these materials' lack of ductility. The low fracture tough-

ness, low strain tolerance, and substantial scatter in measured strengths for most brittle materials is due to the inability to yield in the presence of inherent microscopic flaws when subjected to external loading. Localized flaws such as micro cracks or pores can act as severe stress concentrators from which additional cracks can initiate and propagate in regions where tensile loading exists. Conversely, compressive loads can be more easily supported across such defects without necessarily degrading the materials' structural properties. This brittle behavior accounts for the fact that the compressive strength of alumina ceramic is approximately an order of magnitude greater than its flexural strength.

Microscopic flaws in alumina can be present as both volume flaws (intrinsic) or surface flaws (extrinsic). Intrinsic flaws are typically introduced during material processing of the alumina body as a result of raw material impurities. Extrinsic flaws can be introduced during surface grinding after the green body has been fired or during assembly and handling of the finished alumina housing hull components. If a wide variation in the shape and size of flaws exists, then the measured strength for alumina also can be expected to vary greatly. Since alumina is susceptible to the presence of pre-existing flaws, it can be expected that the greater the size of an alumina body, the lower the average strength will be for that component. With greater component volume and surface area comes the increased likelihood that a weaker flaw will exist.

All strength data that is reported for ceramics such as alumina are mean-strength values typically based on failing a number of compressive, or flexural, test specimens. Ideally, strength data used for designing pressure housing components should be based on measurements made with test specimens that are co-processed with the housing components from the same powder lot and finished with the same grinding procedures. A statistical parameter for quantifying the dispersion in strength data in brittle materials like alumina is the Weibull Modulus. Since failure of brittle materials is most often associated with the presence of tensile loading, the Weibull Modulus is generated by fracturing an appropriate number of flexural test

specimens and plotting the results on a frequency-of-failure versus flexural-strength plot. When this data is plotted as a cumulative probability of failure versus the log of the flexural stress at failure, an approximately linear relationship is revealed. The slope of this curve is called the Weibull Modulus. The Weibull Modulus is a significant means for characterizing the structural performance for materials such as alumina ceramic.

The higher the value of the Weibull Modulus, the more narrowly distributed the range of flexural strengths measured from test coupons. Additionally, the greater the value of the Weibull Modulus, the less the effect of increased volume and surface area will have on degrading the average strength of the material. A high Weibull Modulus is obtained by careful processing of the alumina-ceramic material through each step of manufacturing to control the size and distribution of flaws in the final part. Weibull Modulus values ranging from 5 to 15 are typical for many engineering ceramics.

Mechanical and physical properties for the isostatically pressed isotropic alumina parts tested for this report were determined from tests performed with material specimens co-processed with the cylinders. The alumina cylinders were fabricated in three lots. Lot 1 contained cylinders #1 through #4, lot 2 contained cylinders #5 and #6, and lot 3 contained cylinders #7 through #10. Strength data was generated by breaking a minimum of three flexural-test (modulus-of-rupture) specimens and three compressive-test specimens for each lot. Weibull Modulus was determined from flexural-strength results for each lot. Results of each of these tests are presented in Appendix A, while average strength values for each lot are presented below:

Lot	Cylinder #	Flexural Strength (psi)	Weibull Modulus	Compressive Strength (psi)	Density (g/cc)
1	1-4	47,700	33.8	417,200	3.729
2	5,6	50,900	38.5	432,100	3.745
3	7-10	53,000	23.2	358,400	3.742

Fracture toughness of the 96-percent alumina cylinders was measured by testing three material specimens from each of the three lots in accordance with ASTM B771-87 (reference 18). Fracture toughness was determined through application of an opening load to a material specimen that contained a chevron-shaped slot. Two unloading/reloading cycles were performed during each test to measure the effects of any residual stress which may have been present. Of the nine specimens that were tested, only two specimens survived the two unloading-reloading cycles intact. The fracture toughness measured for these two specimens was  $K_{IC}=2.50 \text{ ksi(in)}^{1/2}$  (from lot 1) and  $K_{IC}=2.96 \text{ ksi(in)}^{1/2}$  (from lot 3).

## TESTING

### PLAN

After inspection of the isostatically pressed alumina cylinders, they were delivered to NRD to be prepared for pressure testing. Figure 26 shows cylinders #1 through #6 being assembled with titanium end-cap joint rings. Figures 27 and 28 show an alumina cylinder with Mod 1, Type 2 end-cap joint rings bonded in place. Table 3 describes the pressure-testing plan for each of the ten cylinders. Pressure tests 1 to 7 were structured to provide data on the cyclic fatigue life of isostatically pressed alumina-ceramic cylinders subjected to external pressure cycles. Data on fatigue life was obtained from tests 1 to 7 by pressurizing alumina cylinders either to failure or for a fixed number of cycles and subsequently performing NDE inspection to determine the extent of sub-critical crack growth that occurred. Instability of monocoque alumina-ceramic cylinders was studied through pressure tests 8 and 9. The effects of long-term static loading on the structural performance of alumina-ceramic cylinders was explored through test 10 by submersing a test assembly I configuration for a period of 1,000 hours at an external pressure of 11,000 psi.

All pressure testing was performed in tap water at ambient room temperature at Southwest Research Institute (SWRI) in San Antonio, Texas. Each pressure test was preceded by a proof test to 10,000 psi. An approximate pressurization rate during the



proof test of 1,000 psi/minute was used, followed by a 60-minute hold at 10,000 psi. The depressurization rate back to 0 psi was not to exceed 10,000 psi/minute. The test configuration column of table 3 defines the end-cap joint ring/end-closure test configuration used for each test. All cyclic testing was performed using external pressure cycles from 50 psi to the peak pressure listed in the test-pressure column of table 3 and then back to 50 psi. The peak pressure was maintained during each cycle for less than one minute. Pressurization and depressurization rates were not to exceed 10,000 psi/minute during testing.

During the first cycle of tests 1 through 7, strains were recorded from the five biaxial strain gages at 1,000-psi increments up to the peak pressure and were recorded again after depressurization to measure any residual strains. The number of cycles performed for tests 1 through 7 is specified in the test-plan column of table 3 unless the cylinder catastrophically failed prior to reaching the target number of cycles. Cylinders that survived the specified number of test cycles were inspected using ultrasonic NDE techniques to determine the level of sub-critical crack growth that occurred during pressure testing.

After a proof test to 10,000 psi, the cylinder assemblies for tests 8 and 9 were pressurized to 20,000 psi. Strains were recorded from the five biaxial strain gages at 1,000-psi increments up to 18,000 psi and at 500-psi increments thereafter. After a 60-minute hold at 20,000 psi, the strains were recorded and then recorded once more for residual strains after depressurization at a rate not exceeding 10,000 psi/minute. Test assembly 9 was subsequently pressurized until catastrophic failure, reading the strains at 1,000-psi increments up to 18,000 psi and at 500-psi increments thereafter. Test 10 pressurized a test assembly I configuration at a rate not exceeding 1,000 psi/minute to a pressure of 11,000 psi. After reaching 11,000 psi, the cylinder assembly was held for 1,000 hours and then depressurized at a rate not exceeding 1,000 psi/minute.

Figures 29 and 30 show a test assembly I configuration as it is being prepared for pressure testing.

Figure 31 shows a test assembly II configuration being lowered into a pressure vessel for testing.

## STRUCTURAL ANALYSIS

Finite-element analysis (FEA) was performed to calculate the stresses that would exist in the ceramic cylinders during the ten pressure tests described above. All the values of stresses used in the curves presented in this report for pressure test results are based on FEA calculations that were checked by hand calculations where possible.

Axisymmetric models of the three different test assemblies were constructed using the structural analysis software ANSYS-PC, revision 4.4A, a product of Swanson Analysis Systems, Inc. Figure 32 shows a plot of the axisymmetric solid model used to calculate stresses during pressure testing of test assembly I configuration using titanium hemispherical end closures. All test-assembly components were modeled using STIF82 2-D, eight-node quadrilateral solid elements with the following linear elastic-isotropic material properties:

96-percent alumina ceramic (AL-600)  
(reference 8):  $E=47e6$  psi  
 $\nu=.23$

Ti-6Al-4V titanium (reference 6):  $E=16.4e6$  psi  
 $\nu=.31$

Epoxy (reference 11):  $E=300e3$  psi  
 $\nu=.40$

where  $E$  is the elastic modulus and  $\nu$  is the Poisson's Ratio of each material. A fine element mesh was required in the cylinder end-cap joint region in order to model the relatively thin layer of epoxy used to bond the cylinder end cap to the alumina-ceramic cylinder with elements of reasonable aspect ratio (3 to 1). STIF12 2-D gap elements were used to model the joint interface between the cylinder end-cap joint ring and the hemispherical end closure. STIF12 elements are capable of only supporting compressive loads normal to the contact surfaces. These elements allow adjacent surfaces to maintain or break physical contact and allow one surface to slide relative to the other surface. The use of gap elements introduces nonlinearities into the stress analysis and, therefore,

requires that an iterative solution be used when running the FEA model.

A number of failure criteria exist for performing structural analysis of brittle materials like alumina ceramic. In general, these failure criteria are based on the principal stresses that are calculated to exist in the ceramic body under load. Principal stresses are used because they indicate the orientation in which the stresses act, tensile or compressive, as opposed to a stress component like the equivalent stress (von Mises stress) used to predict failure of ductile materials. Orientation of stress is important since ceramic materials are typically observed to fail by fracture due to the presence of tensile loading. The stress analysis calculations presented for the externally pressurized alumina cylinders are shown as radial, axial, and hoop stress plots. Stress analysis results are plotted in this manner for easier correlation with strain gage data, easier visualization of the stress state in the cylinders, and, because in the regions of primary interest, the hoop, axial, and radial stresses will be the principal stresses. The tensile stresses of greatest magnitude (highest maximum principal stresses greater than zero) are radially oriented and occur at the bearing surface at the ceramic cylinder ends. The compressive stresses of greatest magnitude (lowest minimum principal stress less than zero) are circumferentially oriented (hoop) and occur at the inner surface of the cylinder away from the end closure joint region.

Figure 33 shows the radial stresses that exist in the alumina cylinder as predicted by the ANSYS model for test assembly I subjected to an external pressure of 9,000 psi. For the majority of the cylinder, the radial stress varies from a stress of 9,000 psi at the cylinder's outer radius to a pressure 0 psi at the cylinder's inner radius. This radial stress pattern changes at the cylinder interface with the hemispherical end closure as shown in detail in figure 34. The variations in stresses at the cylinder end are due to the material and geometric discontinuities that are present at the cylinder/end-cap joint ring/hemispherical end-closure interface. Most notably, a peak tensile stress of 14,406 psi is calculated to exist at the bearing surface of the alumina cylinder. This stress distribution is signifi-

cant since it is known that the cyclic life of ceramic underwater pressure-resistant housings can be limited by cracks which originate from the bearing surface of ceramic cylinders where tensile stresses are calculated to exist.

Figure 35 shows the axial stresses that are calculated to exist in the test assembly I alumina cylinder at an external pressure of 9,000 psi. A uniform axial membrane stress of -66,620 psi occurs in the cylinder away from the joint interface. In the region of the cylinder/hemisphere interface, the axial stresses in the cylinder varies from -28,563 psi to -90,679 psi because of bending due to the presence of the encapsulating cylinder end-cap joint ring with its external flange, and the interface with the end closure.

Figure 36 shows the hoop-stress contour plot for the alumina cylinder in the test assembly I at an external pressure of 9,000 psi. The hoop stress varies from a peak level of -133,498 psi at the inner radius of the ceramic cylinder away from the hemispherical end-closure interface to a value of -109,684 psi at the outer radius of the cylinder in the region of cylinder end-cap encapsulation. The variation in stresses that are calculated to exist in the alumina-ceramic cylinder in test assembly I for external pressures ranging from 9,000 psi to 13,000 psi are summarized in table 4.

Figure 37 shows a plot of the FEA solid axisymmetric model used to calculate stresses in test assembly II subjected to external hydrostatic pressure cycles. All housing components were modeled using STIF82 2-D eight-node quadrilateral solid elements with the same material properties used for test assembly I FEA model with the addition of the following properties for the flat steel plate end closure:

4340 steel (reference 6):  $E=29e6$  psi  
 $\nu=.32$

Again, STIF12 gap elements were used for the interface between the titanium end cap and the flat-steel plate end closure. Figure 38 shows a detailed view of the solid model at the alumina cylinder/end-cap joint ring/flat-steel bulkhead end closure interface. The alumina cylinder appears aqua, the epoxy bond appears red, the titanium joint ring

appears purple, and the end closure appears royal blue.

Tensile radial stresses are also predicted to occur at the bearing surface of the alumina cylinder of test assembly II. Figure 39 shows a detail of the radial-stress contour plot in the alumina cylinder end at an external pressure of 15,000 psi. A peak tensile radial stress of 20,945 psi is calculated to exist at the bearing surface at the alumina cylinder end. Table 5 summarizes the stresses that are calculated to exist in the alumina cylinder tested in the test assembly II configuration for external pressures of 14,000 psi, 15,000 psi, and 18,000 psi. Stress levels in the alumina cylinder of test assembly III also are reported in table 5 at an external pressure of 20,000 psi. The FEA models for each of the test assemblies were used additionally to ensure that the titanium end-cap joint rings and end closures were adequately designed for the full range of test pressures that were used on the alumina cylinders.

Buckling analysis of all test configurations subjected to uniform external pressure was performed using computer-aided analysis and hand calculations. The wall thickness of the titanium hemispherical end closures used in test assembly I was sized, in part, to ensure that the alumina cylinders could be safely cycled at external pressures up to 13,000 psi. The test assembly I configuration was predicted to buckle due to general instability with three circumferential lobes forming ( $N=3$ ) at a pressure of 15,128 psi using the BOSOR4 computer program (references 4 and 5) and with three lobes forming at a critical pressure of 15,536 psi based on hand calculations. BOSOR4 is a structural analysis computer program developed by David Bushnell at Lockheed Missiles and Space Co., Inc. that can be used to predict buckling of complex shells of revolution. The meridian of the shell is modeled using a number of segments with material, geometric, and end-constraint conditions representative of the actual structure. Buckling calculations are based on finite difference energy minimization and can be computed for a range of circumferential wave numbers.

Three segments were used to generate a half-symmetry model of the ceramic cylinder capped by

a hemispherical end closure. Two segments were used to model the titanium hemisphere to account for varying wall thicknesses, and a single segment was used to model the ceramic cylinder with a symmetry boundary condition at midbay. The BOSOR4 model was constructed to allow for meridional rotations at the short-lap joint between the titanium hemisphere and the ceramic cylinder. The end-cap joint ring was not incorporated into the BOSOR4 model since its presence had little effect on the general instability of the test assembly I housing.

Hand calculations were performed using equation 15.3 of reference 1 derived for closed-ended housings under uniform external pressure where the ends of the cylinder are assumed to be simply supported. To account for hemispherical end closures, the effective length of the cylindrical hull section was increased by one third the depth of each hemisphere:

$$L = 18.00 + 2(0.09) + 2(5.794/3) = 22.043$$

where 18.00 = cylinder length, and 0.09 = bearing thickness of the end-cap joint rings, and 5.794 = mean radius of the hemispherical end closures.

Buckling analysis of the test assembly III configuration with the BOSOR4 computer program indicates that general instability failure will occur with three lobes forming at an external pressure of 25,340 psi. Two segments were used to model the test assembly III configuration. One segment was used to model the flat-steel plate end closure, and one segment was used to model the ceramic cylinder with a symmetry condition at midbay.

Buckling analysis of the test assembly III configuration with flat-bulkhead end closures was checked using hand calculations and predicted to buckle due to a general instability with three lobes forming at an external pressure of 19,713 psi (i.e., hand calculations predict that the use of the more-rigid flat-steel plate end supports increases the collapse pressure of the alumina cylinder by approximately 4,000 psi as compared to when the cylinder is supported by the test assembly I titanium hemispherical end closures). The effective simply supported length used in equation 15.3 from reference 1 was 16.82 inches:

$$L = 18.00 + 2(0.09) - 2(0.68)$$

where 0.68 equals the engagement length of the cylinder with the flat-steel end closure. The use of simply supported boundary conditions as assumed with equation 15.3 would lead to more conservative results, although additional boundary conditions at the cylinder end have little effect on the collapse pressure unless the length of the cylinder is relatively short.

## TEST RESULTS

The results of the ten pressure tests performed for this report are listed in table 6. Cylinder test 1 completed 3,500 cycles to an external pressure of 9,000 psi without any visual signs of structural degradation. Figure 40 shows a plot of the strains recorded during the first pressure cycle to 9,000 psi. As expected, the strains increase linearly through the entire pressurization. No significant residual strains were detected after depressurization of the cylinder for the first cycle. Slight tensile residual strains (typically on the order of 20 microinches/inch) existed for each strain gage after the first pressure cycle indicating that the gages may have slipped during pressurization. After completion of all pressure testing, cylinder test 1 was shipped back to NRC where the titanium end-cap joint ring was removed from one end of the alumina cylinder. The bearing surface at the end of the cylinder was cleaned and dye penetrant was applied to detect the presence of any cracks that developed during cyclic testing. Figure 41 shows a close up view of two short circumferential cracks that were found on the cylinder end bearing surface. A number of these cracks were detected with the aid of dye penetrant randomly distributed around the circumference of the bearing surface near the midplane of the cylinder shell wall.

The exposed end of alumina cylinder from test 1 was then ultrasonically inspected to determine the depth of sub critical cracks that had been previously detected with dye penetrant. Figure 42 shows an ultrasonic C-scan of the entire circumference of the test 1 alumina cylinder to a length of 0.75 inches from the bearing surface end based on a 0.030 scanning index. The end of the cylinder where cracks were found with dye penetrant is the top edge of the C-scan shown in figure 42. Most of

the C-scan is dark, indicating that no internal discontinuities exist at that location. The white patches extending from the top edge of the cylinder in the C-scan indicate regions where internal cracks were detected. These cracks appear randomly scattered around the circumference of the bearing surface with the longest crack penetrating to a depth of 0.40 inch from the bearing surface.

As long as the depth of crack penetration does not extend beyond the bond length of the end-cap joint ring (bond length equal 1.31 inches for Mod 1 end-cap joint rings used in this report), these internal cracks pose no threat to the structural performance of the ceramic cylinder housing. Only when these cracks penetrate beyond the encapsulating flanges of the end-cap joint ring does the potential for spalling of the ceramic cylinder exist. In some instances, internal cracks have been observed to propagate as far as 4 inches beyond the termination of the end-cap flanges without the occurrence of spalling or any signs of degradation in structural performance (reference 23). In other cases, cylinders have been observed to spall, but still were able to withstand additional pressure cycles. Because of this observed variation in crack penetration required to cause actual failure of the ceramic cylinder assembly, the number of pressure cycles required to catastrophically fatigue ceramic cylinders can be expected to vary from case to case. Ideally, ceramic pressure housings should be inspected periodically with ultrasonics or similar NDE techniques to check for internal subcritical crack growth. Once internal cracks are detected to penetrate beyond the encapsulating end-cap joint ring flanges, the cylinder should be removed from service. Since the test 1 alumina cylinder had subcritical crack growth that had only penetrated to a depth of 0.40 inch from the bearing surface after 3,000 cycles to a peak pressure of 9,000 psi, the actual fatigue life for this housing configuration and load case would be much greater than 3,000 cycles.

Figure 43 through 48 show strains measured during the initial pressure cycle of tests 2 through 7 also performed to study the fatigue life of alumina-ceramic external pressure housings. Comparison of the slopes of the pressure-strain plots indicates that the material properties of the AL-600 cylinders

tested for this study are consistent. Specifically, the elastic constants, the Poisson's ratio, and the elastic modulus of the alumina cylinders varies little from cylinder to cylinder. This consistency in properties is by no means typical for all ceramic materials, but, rather, indicates WESGO, Inc.'s substantial experience in fabricating large pressure-hull components from their alumina-ceramic composition AL-600. Several of the pressure-strain plots show some minor variation in slope from gage to gage, as, for example, the hoop strains recorded during the initial cycle of test 3 to 11,000 psi. This is likely due to the fact that since the gages were bonded to the cylinder surface by hand, slight variations in gage orientation exist. In other instances, such as with one of the axial strain gages used for test 7 to 15,000 psi, the erratic strain measurements are probably attributable to a faulty gage and/or gage slippage on the cylinder surface. Consistent strain measurements at midbay of all the test cases confirms that the type of end closure used only affects the local deformation of the alumina cylinder in the region of the joint interface. After completion of 1,380 cycles to 11,000 psi without failure for test 2, the alumina cylinder was returned to NRD where the end-cap joint ring was removed from one end and NDE for subcritical crack growth was performed. The C-scan from the ultrasonic inspection indicated that no internal cracking had occurred in the cylinder after 1,380 cycles. The intent in limiting the number of cycles of test 2 (i.e., not cycling all the way to failure) was to ensure that at least one of the cylinders would survive testing to investigate the nature of the subcritical crack growth behavior in 96-percent alumina using NDE techniques. The fact that the test 2 cylinder bearing surface was free of cracks after being subjected to over 1,000 cycles to 11,000 psi external pressure exceeded all expectations for the structural performance of this particular alumina-ceramic cylinder.

Of the test cases that were pressure cycled, tests 3 through 7 were cycled until they failed catastrophically. The test 3 cylinder withstood 2,969 cycles to 11,000 psi before failing. The test 4 cylinder withstood 1,065 cycles to 12,000 psi before failing. The test 5 cylinder withstood 762 cycles to

13,000 psi before failing. The test 6 cylinder withstood 214 cycles to 14,000 psi before failing. And the test 7 cylinder withstood 707 cycles to 15,000 psi before failing. Figure 49 shows the remains of the cylindrical assembly for test 3 after it failed on cycle 2,969 to a peak pressure of 11,000 psi. Figure 50 shows the remains of the titanium end-cap joint rings from test 7 after failure on cycle 707 to a peak pressure of 15,000 psi.

Inspection of the failed end-cap joint rings shows evidence of a consistent failure mode when the cylinders are cycled to failure. Through repeated pressure cycles, subcritical crack growth initiates from the bearing surfaces at the ceramic ends and penetrates meridionally into the shell wall. Once these cracks have extended beyond the flanges of the end-cap joint ring, flakes of the ceramic wall spall off. This spalling may lead not only to leakage through the pressure housing wall, but will also reduce the amount of shell wall that can bear the pressure-induced loads. Once spalling has reached a critical level, further external pressurization leads to pushthrough of the housing wall and subsequent collapse of the entire cylindrical assembly. Study of the joint rings in figures 49 and 50 shows locations of each joint ring where the inner titanium flange has been driven inward in the location where spalling had reached a critical-enough state for the ceramic wall to implode. Figure 50 shows that the fragments of the ceramic cylinder that remain embedded in the titanium end cap are a fine grit in the region where the inner titanium flange has deformed inward, but are larger pieces elsewhere in the joint ring.

Figures 51 and 52 show pressure-strain plots of tests 8 and 9 performed to evaluate the short-term pressurization of alumina-ceramic cylinders with specific interest in the buckling behavior of monocoque alumina cylinders. Acoustic emissions were recorded during pressure testing of test 9 cylinder assembly. During the initial proofing to 10,000 psi, test 9 was quiet up to 3,000 psi, followed by a burst of 72 acoustic events between 3,000 psi and 6,000 psi, and was quiet again up to the peak pressure of 10,000 psi. On the second proof test to 20,000 psi, the cylinder was quiet up to an external pressure of 7,000 psi, followed by a total of

158 acoustic events between 10,000 psi and 11,000 psi, and was essentially quiet thereafter.

Figure 52 is of most interest because the strain plot clearly indicates the onset of buckling before the eventual implosion of the cylinder at an external pressure of 23,730 psi for test 9. After the external pressure exceeded 21,000 psi, the strains recorded began to diverge from their linear course in a dramatic fashion, most notably, for the hoop strains. Initiation of this nonlinear behavior indicates that circumferential lobes or waves have begun to form (three lobes were predicted to occur as discussed previously in the structural analysis section). The bending of the cylindrical shell associated with the formation of lobes either acts to increase or decrease the measured strains, depending on the gage location with respect to the waves that form. Monocoque cylindrical housings subjected to external hydrostatic pressure have general instability failure modes characterized by long axial wavelengths and a relatively few number of circumferential wavelengths. The relatively longer axial wavelengths explain why the axial strains shown in figure 52 do not deviate as much as the hoop strains during the onset of buckling. The appearance of lobe formation at approximately 90 percent of the final collapse pressure is typical of other ceramic pressure housings that have undergone a short-term pressurization test to failure by buckling (reference 9).

The alumina cylinder assembly used in test 10 survived long-term pressurization to 11,000 psi for 1,000 hours without any visual signs of structural degradation. Upon completion of the pressure test, the cylinder was returned to NRC, where the titanium end-cap joint ring was removed from one end and the bearing surface was inspected with the aid of both dye penetrant and a pulse-echo ultrasonic C-scan. Both tests did not indicate the presence of any subcritical crack growth in the alumina-ceramic cylinder.

## FINDINGS

The cyclic performance of the 12-inch-OD AL-600 alumina cylinders assembled with Mod 1 titanium end-cap joint rings surpassed all initial expecta-

tions of the material. The use of NOSC-developed end-cap joint rings and bonding procedures, along with WESGO, Inc. experience in fabricating large alumina cylinders, resulted in an alumina-ceramic pressure housing capable of withstanding nearly 3,000 pressure cycles (test 3) with the presence of hoop stresses exceeding 160,000 psi during each cycle. Since this high number of dive cycles would more than likely exceed the requirements of the vast majority of ocean engineering pressure housings, the reliable structural performance of alumina-ceramic housings for operational use would seem assured. Figure 53 shows a semi-log plot of the results from cyclic pressure tests 1 through 7. The log of the number cycles is plotted versus the peak external pressure for each test. The results of tests 1 and 2 are plotted and labeled as non-failure points since these particular tests were terminated before catastrophic failure of the alumina cylinder assembly.

Figure 54 shows a plot of cyclic test data, again with the log of the number of cycles completed plotted against the maximum tensile bearing surface stress calculated to exist at the ends of the alumina cylinder during each cycle. An additional data point corresponding to the proof test to 20,000 psi (test 8) was added to this graph as a non-failure point. The tensile stresses used for figure 54 are based on the finite element models described previously for the various test configurations as tabulated in tables 4 and 5. The level of pressure-induced tensile loading that exists at the cylinder end-bearing surface largely dictates the structural performance of pressure housings constructed from brittle materials like alumina. Failure of ceramic materials by fracture is most often associated with the presence of tensile forces on the ceramic body.

Undoubtedly, the values of peak tensile stress are somewhat sensitive to the modeling techniques and assumptions that were used in the FEA described previously. The level of tensile stress that exists at the cylinder ends is dependent on a number of joint ring design variables (references 9 and 10), but also likely increases proportionally with the magnitude of compressive membrane stresses that exist in the shell wall under depth load. For this reason, the results of the cyclic tests

(figure 55) are also presented as the number of dive cycles completed, versus the more routinely calculated maximum hoop stress that exists in the alumina cylinder at the peak pressure loading during each cycle. The maximum calculated hoop stress occurs at the inner surface of the alumina cylinder away from the joint interface region with the end closure. The maximum calculated hoop stresses as a function of the peak cyclic pressure are tabulated in tables 4 and 5.

Based on cyclic tests 1 through 7 results, a design curve for AL-600 alumina-ceramic external pressure housings is presented in figure 56. For example, 12-inch-OD or similar sized AL-600 alumina hull components intended to withstand a total of 1,000 dive cycles, should be designed so that the compressive membrane stress does not exceed 160,000 psi during each cycle. Again, it is essential to recognize that this design curve is based on housings assembled with Mod 1 type joint rings (reference 24) and NRaD bonding procedures. It is the joint ring configuration that determines the level of tensile loading that will exist in the cylinder bearing surface region and, thus, controls the fatigue life of the housing assembly. If different joint rings and bonding procedures are used and extensive pressure testing cannot be performed, then a detailed stress analysis of the joint region is required to ensure that tensile stress levels don't exceed those that existed in the test housings from which the design curve in figure 56 was generated. In general, the magnitude of tensile stress (maximum principal stress greater than zero) should not exceed 1/10 of the magnitude of the maximum compressive stress (minimum principal stress less than zero).

It is also important to note that all the results reported in this study refer specifically to AL-600 96-percent alumina-ceramic pressure housings fabricated by WESGO, Inc. and should not be inferred to apply to alumina-ceramic housing components of different compositions or of different manufacturers. Variations in material properties are common in ceramic materials because of their sensitivity to numerous processing variables that exist during manufacture. Each ceramic manufacturer has developed processing techniques that

they feel gives them the best product. WESGO, Inc.'s alumina cylinders were evaluated in this report based on a competitive procurement for a quantity of ten 12-inch-OD alumina cylinders that they won over other manufacturers capable of fabricating the same part.

The collapse of the test 9 cylinder by buckling at an external pressure of 23,730 psi compared well with both hand and computer-aided calculations discussed previously. Predictions based on hand calculations (19,713 psi) were roughly 17 percent low of the tested result. Predictions generated using the BOSOR4 computer program (25,340 psi) were approximately 7 percent high. The accuracy of both these predictions is due largely to minimal amount of geometric imperfection that existed in the finished cylinders (see dimensional data form in Appendix A). In general, a 1.50 SF (BOSOR4 predicted collapse pressure/maximum operational service pressure) is considered adequate by NRaD for the design of alumina-ceramic pressure housings. This margin covers uncertainties brought about by looser dimensional tolerance and variations in material properties.

The required wall t/OD ratios of submerged alumina monocoque cylindrical housings capped with hemispherical bulkheads and designed for 1,000 dive cycles are shown in figure 57 for external pressures to 16,000 psi and various L/OD ratios. These t/OD curves are based on sizing the wall thickness to ensure that the nominal hoop stresses in the cylinder wall at midbay do not exceed 160,000 psi (based on design curve shown in figure 56) and that the wall thickness is adequate to resist failure by buckling (using equation 15.3 of reference 1) with an SF of 1.5 at design pressure. For example, for an alumina cylinder with an L/OD ratio of 1.5 designed for 1,000 cycles to 9,000 psi external pressure, the required t/OD ratio would be about 0.032. As seen in figure 57, all the various L/OD curves converge or near convergence on a straight line corresponding to the wall thickness for which the hoop stresses equal  $\sim 160,000$  psi. The design pressure varies as a linear function of t/OD for the stress criteria, but varies as a nonlinear (approximately cubic) function of t/OD for the buckling criteria. Before the various L/OD curves converge on this straight line, the required wall

thickness of the  $t/OD$  ratio is driven by meeting the buckling requirement (1.5 SF against collapse by general instability). The point of convergence between the nonlinear and linear portions of each  $L/OD$  curve represents an optimized wall thickness which identically satisfies the design criteria for stress and buckling. For 9,000 psi external pressure, an optimized pressure housing design with respect to minimum weight would have an  $L/OD$  ratio of 1.0 or less. At external pressures less than 9,000 psi, the wall thickness of an  $L/OD$  1.0 housing is dictated by meeting the buckling criteria, and consequently is under stressed, i.e., the magnitude of the nominal hoop stresses are less than 160,000 psi. At external pressures greater than 9,000 psi, the wall thickness of an  $L/OD$  1.0 housing is driven by the maximum hoop stress criteria, and, consequently, the housing is over designed with respect to the selected buckling criteria.

The curves in figure 57 can be replotted as shown in figure 58 to show the calculated  $W/D$  ratios in sea water of the various  $L/OD$  housings over the same range of design pressures. The  $W/D$  ratios presented are for the ceramic cylinder only and do not include the weight of joint rings or any other hardware used to construct the cylindrical portion of the housing. For a monocoque alumina cylinder with an  $L/OD$  ratio of 1.5 designed for 1,000 cycles to 9,000 psi external pressure ( $t/OD$  0.032), the resulting  $W/D$  ratio would be about 0.47. For this example, the potential housing payload capacity would be roughly equal to the dry weight of the alumina cylindrical housing in order to maintain neutral buoyancy.

While monocoque cylindrical housing assemblies are certainly the simplest and lowest cost means of constructing alumina-ceramic pressure housings, a monocoque cylinder design does not always represent an optimum pressure-housing design when minimum dry weight and maximum in-service buoyancy are design requirements. Monocoque cylindrical assemblies with higher values of  $L/OD$  are driven solely by meeting the buckling criteria and are, consequently, well under stressed (below 160,000 psi). For example, the

required wall  $t/OD$  ratio of a  $L/OD$  3.0 monocoque cylinder is 0.04 for 8,000 psi external design pressure (figure 57). At this design pressure and wall thickness, the maximum hoop stress in the alumina hull wall is 100,000 psi. This low stress level does not utilize the excellent compressive strength of 96-percent alumina which motivates the use of different cylindrical housing designs when weight savings is a concern (references 9 and 12). Reducing the wall thickness of the alumina hull components to obtain the desired design stresses can be accomplished as long as additional means are used to stiffen the housing assembly to meet the desired buckling criteria. The use of intermittent metallic joint rings with integral stiffening ribs has been used for this purpose to decrease the  $W/D$  ratio of alumina-ceramic cylindrical pressure housings than would otherwise be obtainable with simple monocoque shell designs.

From the design curve shown in figure 56, if an alumina-ceramic cylindrical housing is being designed for a maximum number of 100 dive cycles, then a maximum compressive hoop stress of approximately 200,000 psi can be used as a stress criteria. Using this as a design stress, and a 1.50 SF for buckling, the  $t/OD$  and  $W/D$  design curves shown in figures 59 and 60 can be generated for monocoque 96-percent alumina-ceramic cylinders capped with hemispherical end closures. Similarly from figure 56, for a maximum number of ten dive cycles, a maximum compressive hoop stress of nearly 230,000 psi can be used as a stress criteria for monocoque 96-percent alumina-ceramic cylinders. With this selected criteria, the  $t/OD$  and  $W/D$  curves shown in figures 61 and 62 can also be created. Obviously, as the allowable stresses in the pressure housing are increased for a lower number of dive cycles, the wall thickness of monocoque cylinders is more than likely to be dictated by satisfying the stability criteria. Thus, for housings undergoing relatively few dive cycles, an optimum housing design that is driven both by stress and buckling criteria will undoubtedly require the use of intermittent stiffening rings to minimize dry weight and to maximize buoyancy.



## CONCLUSIONS

1. Isostatically pressed 96-percent alumina ceramic produced by WESGO, Inc. under the trade name of AL-600 has been found to be an acceptable material candidate for fabrication of external pressure housings designed for service on underwater manned or unmanned vehicles and other deep submergence ocean engineering applications. Isostatically pressed 96-percent alumina ceramic is attractive for external pressure housings owing to its high values of specific compressive strength and elastic modulus, as well as excellent corrosion resistance and thermal conductivity. The 12-inch-OD ( $L/OD=1.5$ ,  $t/OD=.034$ ) alumina cylinders tested for this report were procured for a per-item price of \$2,500.00 (1993) for a quantity of 10 cylinders. The 96-percent alumina-ceramic pressure housings represent a more economical means of fabricating deep submergence pressure housings than can be obtained using advanced composite shells or rib-stiffened titanium hulls for a given design requirement. In addition to being cost effective, 96-percent alumina housings offer improved performance in terms of minimal dry weight and maximum in-service buoyancy than can be obtained from these more traditional hull materials.
2. The cyclic fatigue life of external pressure-loaded alumina-ceramic housings is determined by the initiation and propagation of cracks that originate on the bearing surface of ceramic component ends at their interface with metallic joint rings. The fatigue life of the ceramic housings was found to depend on the magnitude of loading experienced by the housing during each dive cycle. Through extensive pressure testing, safe loading levels have been determined corresponding with the maximum number of intended dive cycles that preclude the possibility of failure by cyclic fatigue for AL-600 96-percent alumina-ceramic pressure housing components.
3. Accurate predictions of buckling failure of external pressure housings utilizing 96-percent alumina as the primary structural material can be made using both computer-aided and standard hand-calculation techniques. The linear elastic behavior of alumina coupled with outstanding dimensional tolerances that can be obtained through finish grinding allows buckling calculations to be made based on standard analysis techniques used for traditional metallic pressure housing designs.
4. The effect of static fatigue on AL-600 96-percent alumina-ceramic pressure housings is significantly less than the effect of cyclic fatigue on structural performance. Static fatigue may be disregarded in the design of ceramic housings for underwater applications that require intermittent dives.

## RECOMMENDATIONS

1. WESGO, Inc. AL-600 ceramic with 96-percent alumina composition is considered to be a cost effective material for construction of external pressure housings because of its superior structural properties and its demonstrated capability of being fabricated into relatively large cylinders and hemispheres. The following minimum-average material properties should be specified for AL-600 with suggested military or industrial specifications for measuring each property:

Property	Value	Specifications
Compressive Strength	350 kpsi	ASTM C773, Procedure B
Flexural Strength (MOR)	47 kpsi	MIL-STD-1942 or ASTM F417
Weibull Modulus	20	minimum of 12 MOR bars
Fracture Toughness ( $K_{IC}$ )	2.50 kpsi ( $\text{in}^{1/2}$ )	ASTM B771
Elastic Modulus	45E6 psi	ASTM C848

2. The bearing surfaces at the ends of the alumina hull components should be ground flat to less than 0.001 of an inch. The bearing surface should be finish ground using the grinding procedures outlined in the fabrication section of this report, resulting in a surface roughness not exceeding 16 microinches. Edges of the bearing surface should be broken with a 0.03-inch radius to reduce epoxy stresses under depth loading and to reduce the chance of damaging the edges of the bearing surface during handling of the ceramic hull prior to assembly.

3. Alumina components for external pressure hull applications should undergo thorough NDE to ensure that no gross defects such as internal or external cracks or large voids exist in the ceramic body that could affect the structural integrity of the part while in service. This NDE should include the following inspection steps at a minimum:

- a. Visual inspection of all surfaces with the aid of a dye penetrant to detect any surface discontinuities such as cracks, blisters, holes, porous areas, inclusions, or any adherent foreign particles.
- b. C-scan of the entire ceramic volume using ultrasonic pulse-echo or through-transmission techniques. Calibration of ultrasonic equipment should be performed first with the aid of a calibration-standard block of the same ceramic composition as the pressure housing hull components and with the same approximate thickness of the hull components. The calibration standard should contain a series of 0.032-, 0.063-, and 0.125-inch-diameter holes, with each diameter drilled to depths of 1/8, 1/4, 1/2, 3/4, and 7/8 of the block's thickness (reference 3).

Experience indicates that quality isostatically pressed alumina-ceramic pressure housing hulls can be fabricated which do not contain any internal discontinuities with dimensions exceeding 10% of the ceramic shell wall

thickness. If further clarification of internal defects is needed beyond information obtained through an ultrasonic C-scan, a digital or film radiography inspection can further determine the defect's size and shape.

4. The bearing-surface ends of alumina external pressure housing components should be assembled with NOSC Mod 1, Type 2 metallic joint rings that are adhesively bonded using NRaD procedures. The important design features of this joint interface are

- a. the length of the encapsulating joint ring flanges should be a minimum of  $2.5t$ , where  $t$  is the thickness of the alumina shell wall at the bearing surface.
- b. the thickness of the encapsulating joint ring flanges should be the minimum that stress analysis allows, the epoxy adhesive-filled radial clearance between the flanges of the joint ring and the alumina hull OD and ID should be  $1/1,000$  of the hull OD.
- c. the epoxy adhesive-filled axial clearance between the bearing surface of the alumina hull component and the seat of the metallic joint ring should be 0.010 of an inch. Control of the axial clearance during assembly can be achieved using an annular 0.010-inch-thick manila gasket.
- d. water intrusion into the epoxy bond between the OD of the hull and the outer flange of the joint ring should be prevented with a sealant such as FTV.
- e. all localized loads associated with the handling, sealing, maintaining closure, and mounting of external and internal pressure housing hardware (fairings, payload rails, etc.) should be directed onto the metallic joint rings and not onto the ceramic hull components.

5. Stress criteria used to design AL-600 ceramic pressure housing components up to a 12-inch OD should be based on the expected maximum number of dive cycles (figure 56). Housings designed to perform up

to 1,000 cycles at design depth or to sustain submergence for up to 1,000 hours should be sized such that the maximum nominal compressive membrane hoop stresses in the shell wall do not exceed 160,000 psi under depth loading in any dive cycle.

6. Because of the potential effect of component size on strength properties, the design of external pressure housings fabricated from AL-600 larger than 12 inches in OD may require a "knockdown" factor with the design stress criteria suggested in this report. Current efforts to design, fabricate, assemble, and pressure test larger AL-600 pressure housings (references 8 and 12) should help determine the structural capability of large (up to 32-inch-OD) alumina-ceramic pressure housings for deep submergence applications.

#### ADDENDUM

Subsequent to the completion of this report, three of the cylinders that survived the original test program intact were subjected to additional cyclic testing as follows:

Cylinder #	Original Pressure Test	Additional Pressure Test
5	proof test to 20,000 psi	3,000 cycles to 14,000 psi without failure
6	1,000 hour hold at 11,000 psi	failed on cycle 1,019 to 16,000 psi
10	1,380 cycles to 11,000 psi	failed after 864 additional cycles to 11,000 psi

The retesting of these three cylinders is significant because the test results support the original data used to construct the design curves for AL-600 monocoque cylinders recommended in this report. The result of the retest of cylinder 5 is important because it indicates that the original proof test to 20,000 psi had no deleterious effect on the cyclic life of the cylinder to lower peak external pressures (14,000 psi). The additional pressure cycles performed on cylinder 6 after an original hold for 1,000 hours at 11,000 psi support the conclusion that the effect of static fatigue on AL-600 monocoque cylinders is significantly less than the effect of cyclic fatigue on the structural performance of the material. Cylinder 10 completed a total of 2,244 cycles to a pressure of 11,000 psi, generating a peak compressive membrane hoop stress of 160,000 psi during each cycle. This test supports the recommendation that this stress level be used as a maximum stress criteria for AL-600 cylinders intended to perform up to 1,000 dive cycles.

## REFERENCES

1. Bickell, M. B. and C. Ruiz, "Pressure Vessel Design and Analysis," St. Martin's Press.
2. Burke, M. A., W. H. Gordon. 1993. "A Fractographic Study of the Spalling Failure of a Compressively Loaded Adhesive Bonded Ceramic/Composite Gasket/Metal Joint Structure," The Marine Technology Society MTS '93 Conference, Long Beach, CA, (Sep).
3. Burke, M. A., W. H. Gordon. 1993. "A Study of Load Transfer Materials for Compressively Loaded Ceramic to Metal Joints," The Marine Technology Society MTS '93 Conference, Long Beach, CA, (Sep).
4. Bushnell, David, "BOSOR4 User's Manual," Lockheed Missiles & Space Co., Inc.
5. Bushnell, David, "Buckling of Shells—Pitfalls for Designers," AIAA Journal, vol. 19, Sep 1981, pg. 1183.
6. Department of Defense, "Metallic Materials and Elements for Aerospace Vehicle Structures," MIL-HDBK-5E, Washington, D.C., June 1, 1987.
7. Gordon, W. H. 1993. "Investigation of Spalling in a Cylindrical Alumina Deep Submergence Pressure Vessel," The Marine Technology Society MTS '93 Conference, Long Beach, CA, (Sep).
8. Johnson, R. P., R. R. Kurkchubasche, J. D. Stachiw. 1993. "Evaluation of Alumina Ceramic Housings for Deep Submergence Service—Fifth Generation Housings - Part I," NRaD TR 1584 NCCOSC RDT&E Division, San Diego, CA.
9. Johnson, R. P., R. R. Kurkchubasche, J. D. Stachiw. 1993. "Exploratory Study of Joint Rings for Ceramic Underwater Pressure Housings," NRaD TR 1586 (May) NCCOSC RDT&E Division, San Diego, CA.
10. Johnson, R. P. 1993. "Structural Design Criteria for Alumina Ceramic Deep Submergence Pressure Housings," The Marine Technology Society MTS '93 Conference, Long Beach, CA, (Sep).
11. Johnson, R. P., R. R. Kurkchubasche, J. D. Stachiw. 1993. "Effect of Different Axial Bearing Supports on the Cyclic Fatigue Life of Ceramic Pressure Housings," NRaD TR 1607 (Oct) NCCOSC RDT&E Division, San Diego, CA.
12. Johnson, R. P., R. R. Kurkchubasche, J. D. Stachiw. 1993. "Design and Structural Analysis of Alumina Ceramic Housings for Deep Submergence Service—Fifth Generation Housings," NRaD TR 1583 (Mar) NCCOSC RDT&E Division, San Diego, CA.
13. Kurkchubasche, R. R., R. P. Johnson, J. D. Stachiw. 1993. "Evaluation of ND Testing Techniques for Quality Control of Alumina Ceramic Housing Components," NRaD TR 1588 (Sep) NCCOSC RDT&E Division, San Diego, CA.
14. Kurkchubasche, R. R., R. P. Johnson, J. D. Stachiw. 1993. "Application of Ceramics to Large Housings for Underwater Vehicles: Program Outline," NRaD TD 2585 (Oct) NCCOSC RDT&E Division, San Diego, CA.
15. Cox, B. L., M. K. Ferber, C. R. Hubbard, A. E. Pasto, M. L. Santella, W. A. Simpson, Jr., T. R. Watkins. 1993. "Effect of Surface Condition on Strength and Fatigue Behavior of Alumina Ceramic," work performed by ORNL, Oak Ridge, TN, under MIPR No. N66001 92NP00120, NRaD TD 2584 NCCOSC RDT&E Division, San Diego, CA.
16. Salloum, S., and P. C. Smith. 1992. "Ceramic Hull Fabrication Methods," The Intervention/ROV 92 Committee of The Marine Technology Society; Jun. San Diego, CA.
17. Salloum, S., "WESGO's AL-600 Alumina Stress Rupture Test Report," WESGO, Inc., Belmont, CA, October 22, 1991.
18. "Short Rod Fracture Toughness of Cemented Carbides," American Society for Testing Materials B771-87, 1916 Race St, Philadelphia, PA 19103.
19. Smith, P. C. 1992. "Ceramic Hull Reliability Considerations Twenty Weibulls Under the Sea," The Intervention/ROV 92 Committee of The Marine Technology Society; Jun. San Diego, CA.

20. Stachiw, J. D. 1993. "Exploratory Evaluation of Alumina Ceramic Housings for Deep Submergence Service—Third Generation Housings," NRaD TR 1314 (Jun) NCCOSC RDT&E Division, San Diego, CA.
21. Stachiw, J. D., J. L. Held. 1987. "Exploratory Evaluation of Alumina Ceramic Cylindrical Housings for Deep Submergence Service: The Second Generation NOSC Ceramic Housings," NOSC TR 1176 (Sep), Naval Ocean Systems Center, San Diego, CA.
22. Stachiw, J. D. 1990. "Exploratory Evaluation of Alumina Ceramic Cylindrical Housings for Deep Submergence Service—Fourth Generation Housings," NOSC TR 1355 (Jun), Naval Ocean Systems Center, San Diego, CA.
23. Stachiw, J. D., R. P. Johnson, R. R. Kurkchubasche. 1993. "Evaluation of Scale Model Ceramic Housing for Deep Submergence—Fifth Generation Housings," NRaD TR 1582 (Mar) NCCOSC RDT&E Division, San Diego, CA.
24. Stachiw, J. D. 1993. "Adhesive Bonded Mod 1 Joint with Improved Cyclic Fatigue Life—Fourth Generation Housings," NRaD TR 1587 (Aug) NCCOSC RDT&E Division, San Diego, CA.
25. Swanson Analysis Systems, Inc. 1991. "ANSYS-PC Reference Manual for Revision 4.4A." (May) Houston, PA.

## **GLOSSARY**

---

FEA      finite element analysis

ID      inner diameter

L      length

L/OD      length-to-outer-diameter ratio

MOR      Modulus of rupture

NDE      nondestructive evaluation

OD      outside diameter

RTV      room-temperature vulcanizing silicone rubber

SEM      Scanning Electron Microscopy

SF      safety factor

t      ceramic shell thickness

t/OD      thickness-to-outer-diameter ratio

W/D      weight-to-displacement



Figure 1. 25-inch-OD 96-percent alumina-ceramic cylindrical assembly for ocean depth service of 20,000 feet.



Figure 2. 25-inch-OD 96-percent alumina-ceramic hemispherical end-closure assembly for ocean depth service of 20,000 feet.

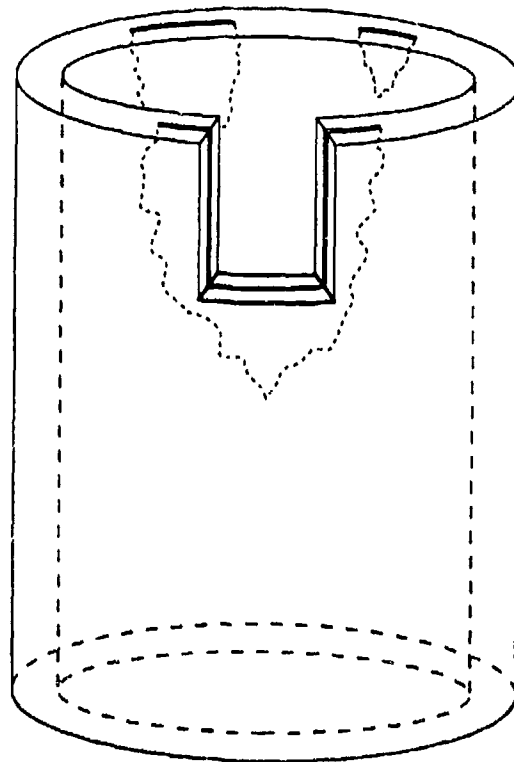


Figure 3. Sub-critical crack growth in a ceramic cylinder.

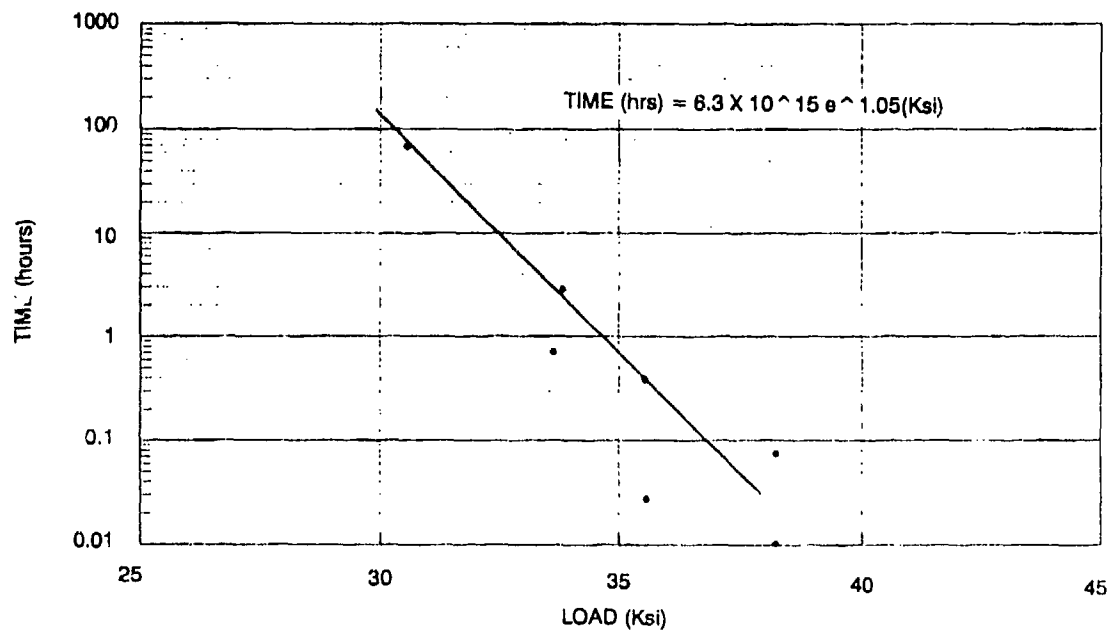


Figure 4. 96-percent alumina-ceramic AL-600 stress rupture curve.



REV	DATE	BY	DESCRIPTION	REVISIONS	DATE	BY	DESCRIPTION
1	1/1/70	1	INITIAL RELEASE AGENT	1	1/1/70	1	INITIAL RELEASE AGENT
2	2/1/70	2	ADHESIVE-SEALANTS RTV	2	2/1/70	2	ADHESIVE-SEALANTS RTV
3	3/1/70	3	SILICONE COMPOUND	3	3/1/70	3	SILICONE COMPOUND
4	4/1/70	4	PASA JELL 107	4	4/1/70	4	PASA JELL 107
5	5/1/70	5	OSMA CLUCY 283 HARDENER	5	5/1/70	5	OSMA CLUCY 283 HARDENER
6	6/1/70	6	OSMA BEGY 810 EPOXY RESIN	6	6/1/70	6	OSMA BEGY 810 EPOXY RESIN
7	7/1/70	7	NUT, HEX. CRES. 1.000-12UNF-28	7	7/1/70	7	NUT, HEX. CRES. 1.000-12UNF-28
8	8/1/70	8	O-RING	8	8/1/70	8	O-RING
9	9/1/70	9	WOOD PLUG, HEMISPHERE, 12 INCH	9	9/1/70	9	WOOD PLUG, HEMISPHERE, 12 INCH
10	10/1/70	10	PLUG, HEMISPHERE, 12 INCH	10	10/1/70	10	PLUG, HEMISPHERE, 12 INCH
11	11/1/70	11	WASHER, HEMISPHERE, 12 IN.	11	11/1/70	11	WASHER, HEMISPHERE, 12 IN.
12	12/1/70	12	CLAMP BAND, HEMISPHERE, 12 INCH	12	12/1/70	12	CLAMP BAND, HEMISPHERE, 12 INCH
13	13/1/70	13	END CAP, WOOD 1, TYPE 2, 12 IN. CYL.	13	13/1/70	13	END CAP, WOOD 1, TYPE 2, 12 IN. CYL.
14	14/1/70	14	HEMISPHERE, 12 INCH	14	14/1/70	14	HEMISPHERE, 12 INCH
15	15/1/70	15	SPACER, 12 INCH CYLINDER	15	15/1/70	15	SPACER, 12 INCH CYLINDER
16	16/1/70	16	O-RING, END CAP, WOOD 1, 12 IN. CYL.	16	16/1/70	16	O-RING, END CAP, WOOD 1, 12 IN. CYL.
17	17/1/70	17	12 INCH CYLINDER	17	17/1/70	17	12 INCH CYLINDER

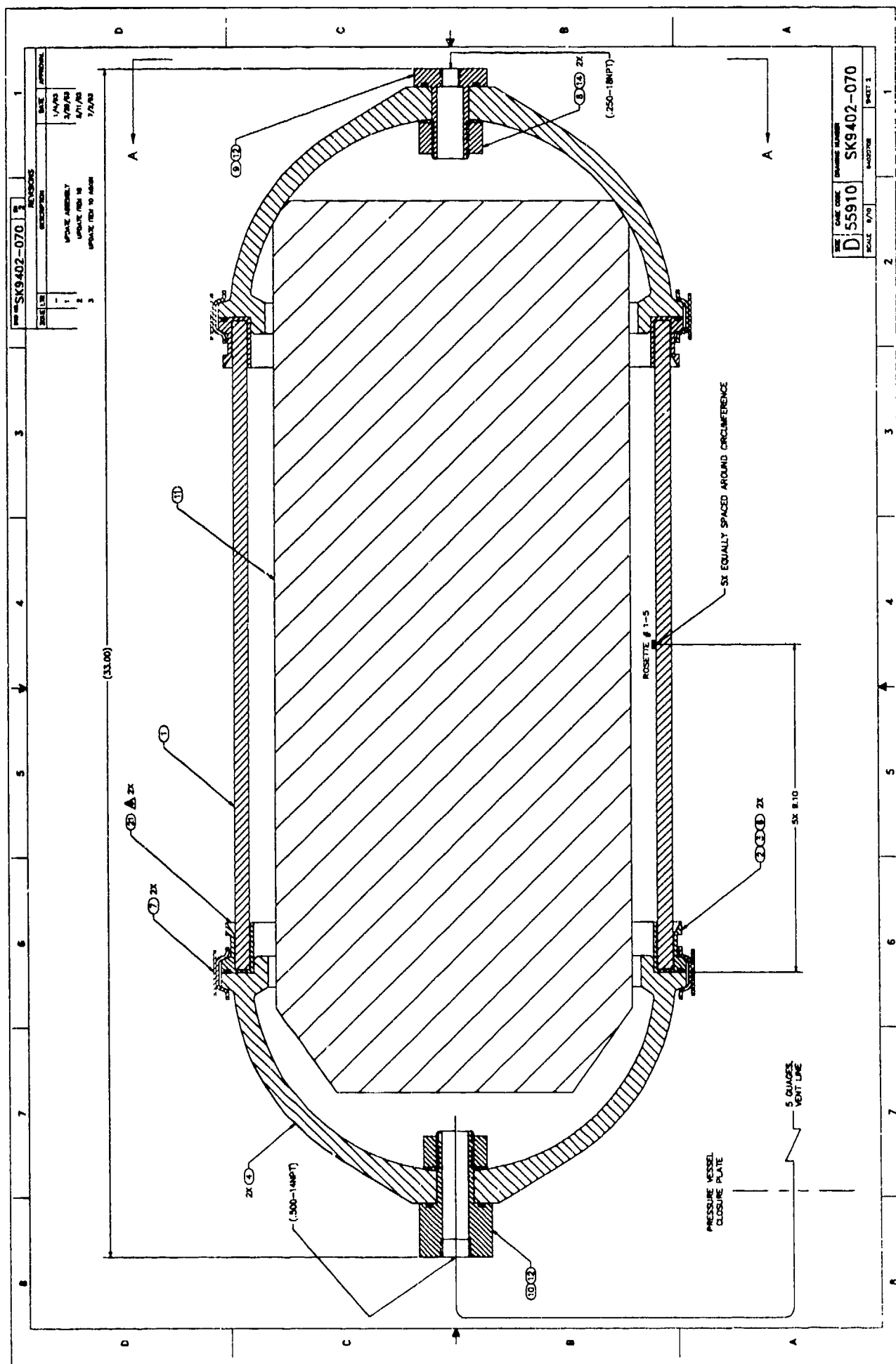
  

REV	DATE	BY	DESCRIPTION	REVISIONS	DATE	BY	DESCRIPTION
1	1/1/70	1	INITIAL RELEASE AGENT	1	1/1/70	1	INITIAL RELEASE AGENT
2	2/1/70	2	ADHESIVE-SEALANTS RTV	2	2/1/70	2	ADHESIVE-SEALANTS RTV
3	3/1/70	3	SILICONE COMPOUND	3	3/1/70	3	SILICONE COMPOUND
4	4/1/70	4	PASA JELL 107	4	4/1/70	4	PASA JELL 107
5	5/1/70	5	OSMA CLUCY 283 HARDENER	5	5/1/70	5	OSMA CLUCY 283 HARDENER
6	6/1/70	6	OSMA BEGY 810 EPOXY RESIN	6	6/1/70	6	OSMA BEGY 810 EPOXY RESIN
7	7/1/70	7	NUT, HEX. CRES. 1.000-12UNF-28	7	7/1/70	7	NUT, HEX. CRES. 1.000-12UNF-28
8	8/1/70	8	O-RING	8	8/1/70	8	O-RING
9	9/1/70	9	WOOD PLUG, HEMISPHERE, 12 INCH	9	9/1/70	9	WOOD PLUG, HEMISPHERE, 12 INCH
10	10/1/70	10	PLUG, HEMISPHERE, 12 INCH	10	10/1/70	10	PLUG, HEMISPHERE, 12 INCH
11	11/1/70	11	WASHER, HEMISPHERE, 12 IN.	11	11/1/70	11	WASHER, HEMISPHERE, 12 IN.
12	12/1/70	12	CLAMP BAND, HEMISPHERE, 12 INCH	12	12/1/70	12	CLAMP BAND, HEMISPHERE, 12 INCH
13	13/1/70	13	END CAP, WOOD 1, TYPE 2, 12 IN. CYL.	13	13/1/70	13	END CAP, WOOD 1, TYPE 2, 12 IN. CYL.
14	14/1/70	14	HEMISPHERE, 12 INCH	14	14/1/70	14	HEMISPHERE, 12 INCH
15	15/1/70	15	SPACER, 12 INCH CYLINDER	15	15/1/70	15	SPACER, 12 INCH CYLINDER
16	16/1/70	16	O-RING, END CAP, WOOD 1, 12 IN. CYL.	16	16/1/70	16	O-RING, END CAP, WOOD 1, 12 IN. CYL.
17	17/1/70	17	12 INCH CYLINDER	17	17/1/70	17	12 INCH CYLINDER

REV	DATE	BY	DESCRIPTION	REVISIONS	DATE	BY	DESCRIPTION
1	1/1/70	1	INITIAL RELEASE AGENT	1	1/1/70	1	INITIAL RELEASE AGENT
2	2/1/70	2	ADHESIVE-SEALANTS RTV	2	2/1/70	2	ADHESIVE-SEALANTS RTV
3	3/1/70	3	SILICONE COMPOUND	3	3/1/70	3	SILICONE COMPOUND
4	4/1/70	4	PASA JELL 107	4	4/1/70	4	PASA JELL 107
5	5/1/70	5	OSMA CLUCY 283 HARDENER	5	5/1/70	5	OSMA CLUCY 283 HARDENER
6	6/1/70	6	OSMA BEGY 810 EPOXY RESIN	6	6/1/70	6	OSMA BEGY

Figure 5. 12-inch cylinder test assembly I configuration, Sheet 1.



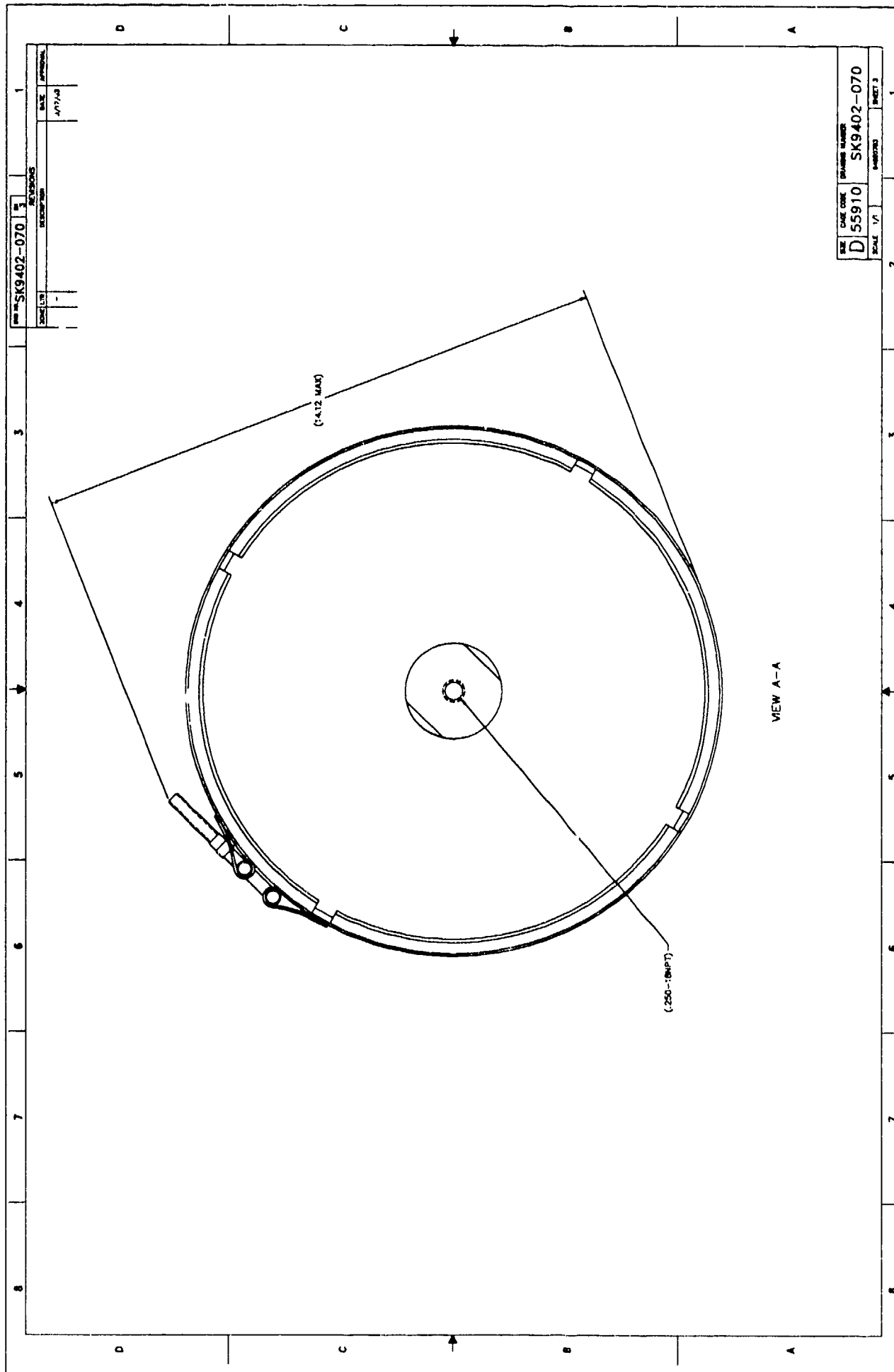
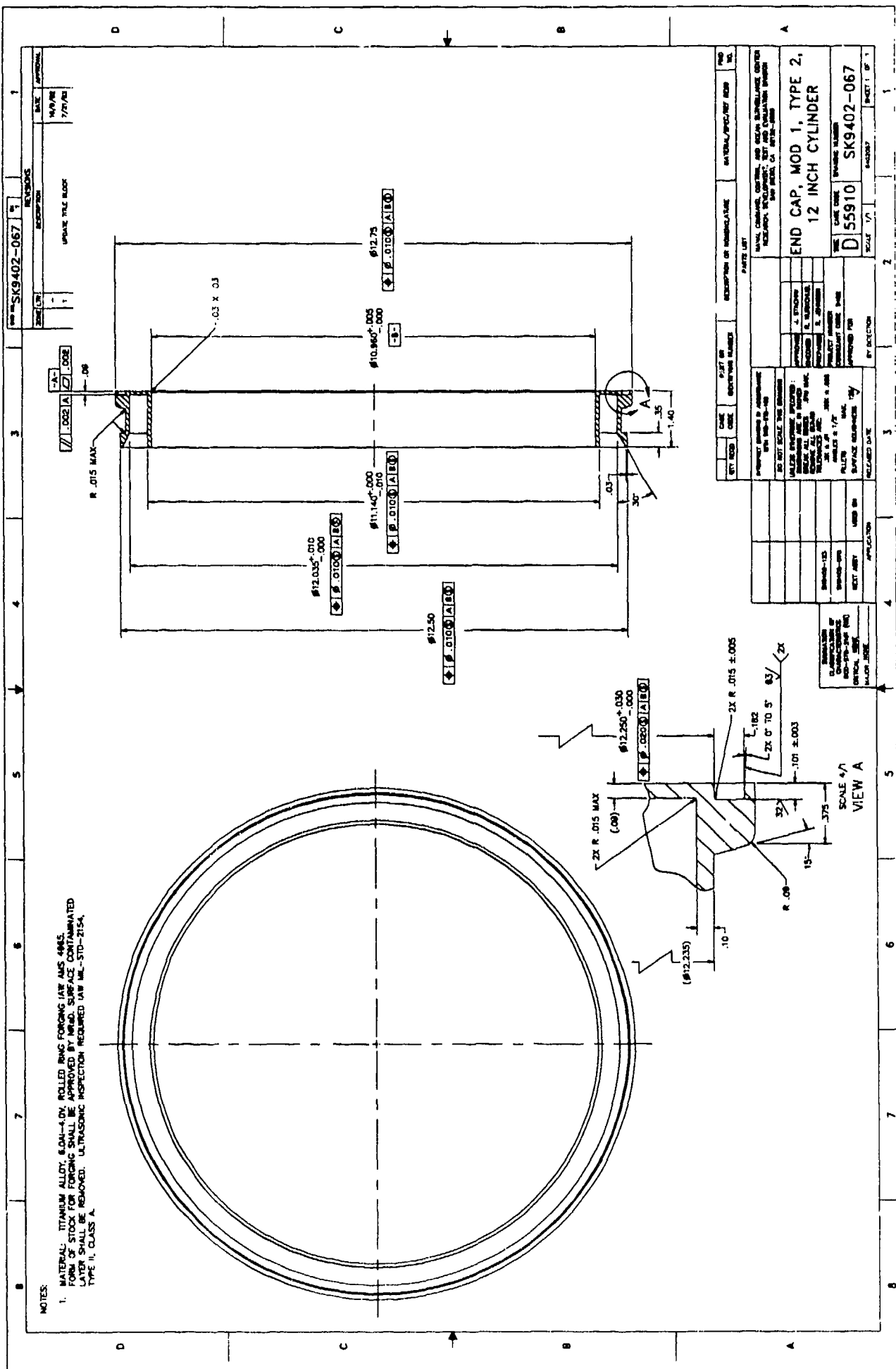


Figure 5. 12-inch cylinder test assembly I configuration, Sheet 3.







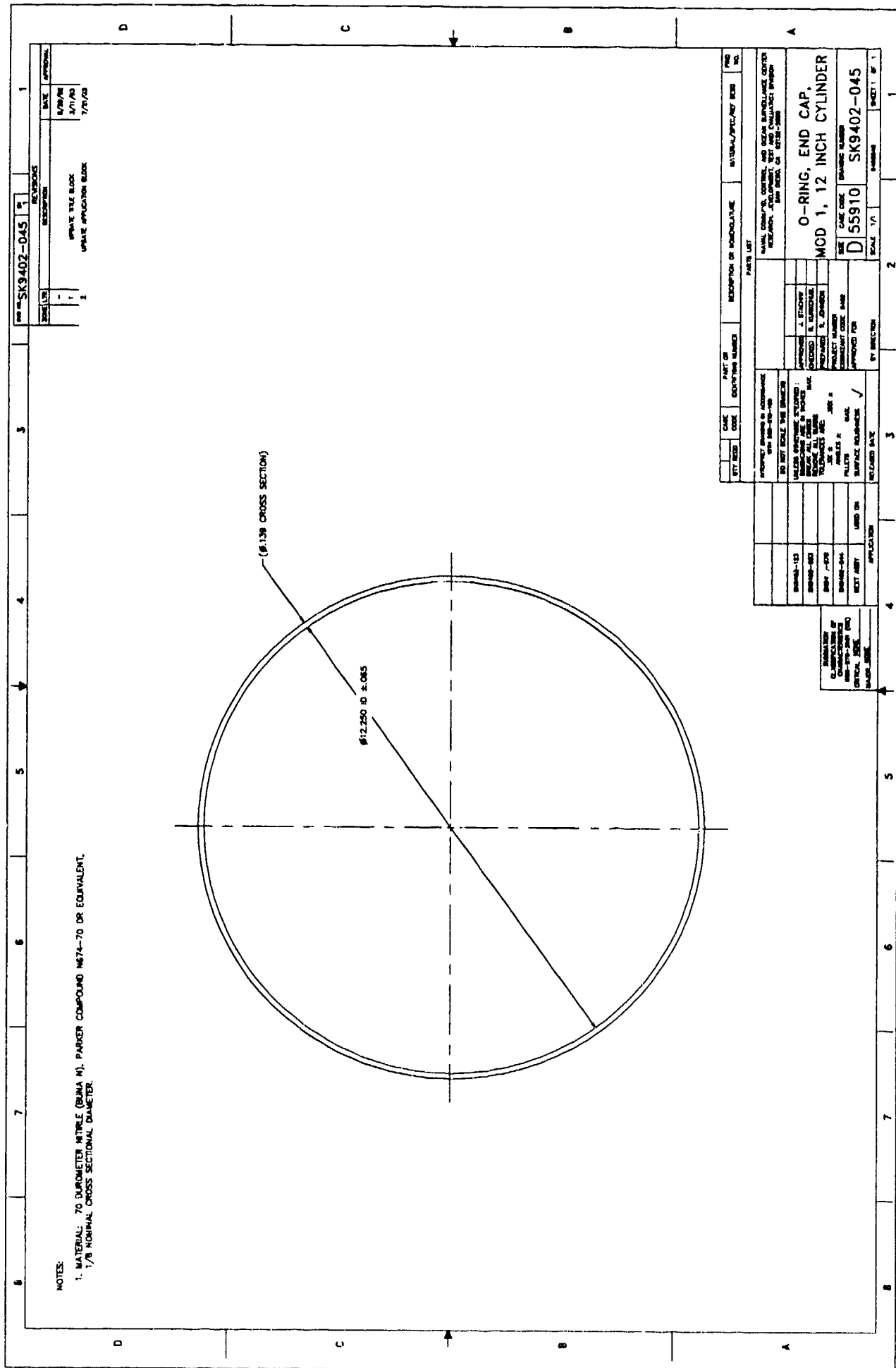


Figure 9. 12-inch cylinder Mod 1 end-cap joint ring O-ring.

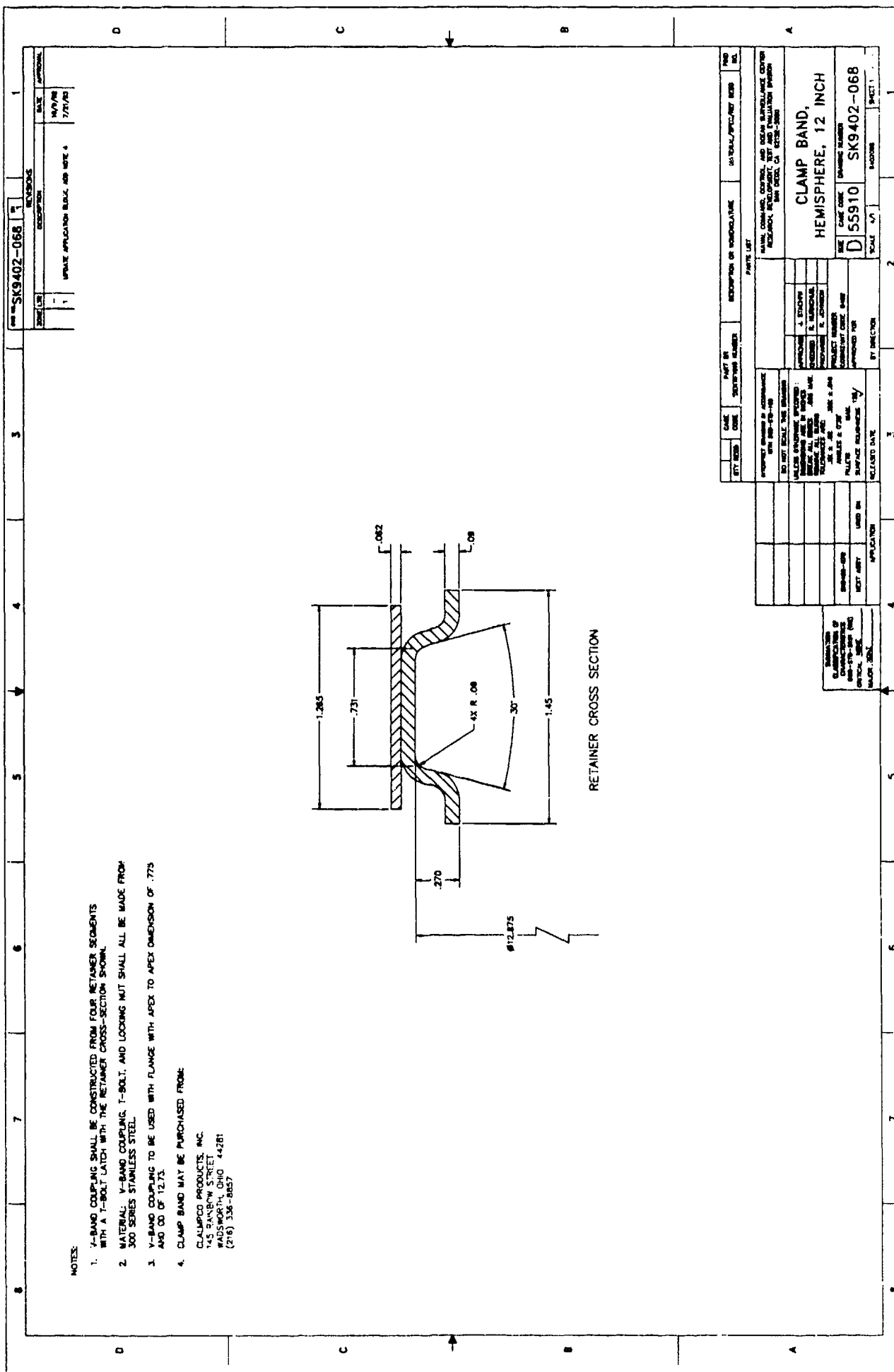


Figure 10. 12-inch hemisphere clamp band.



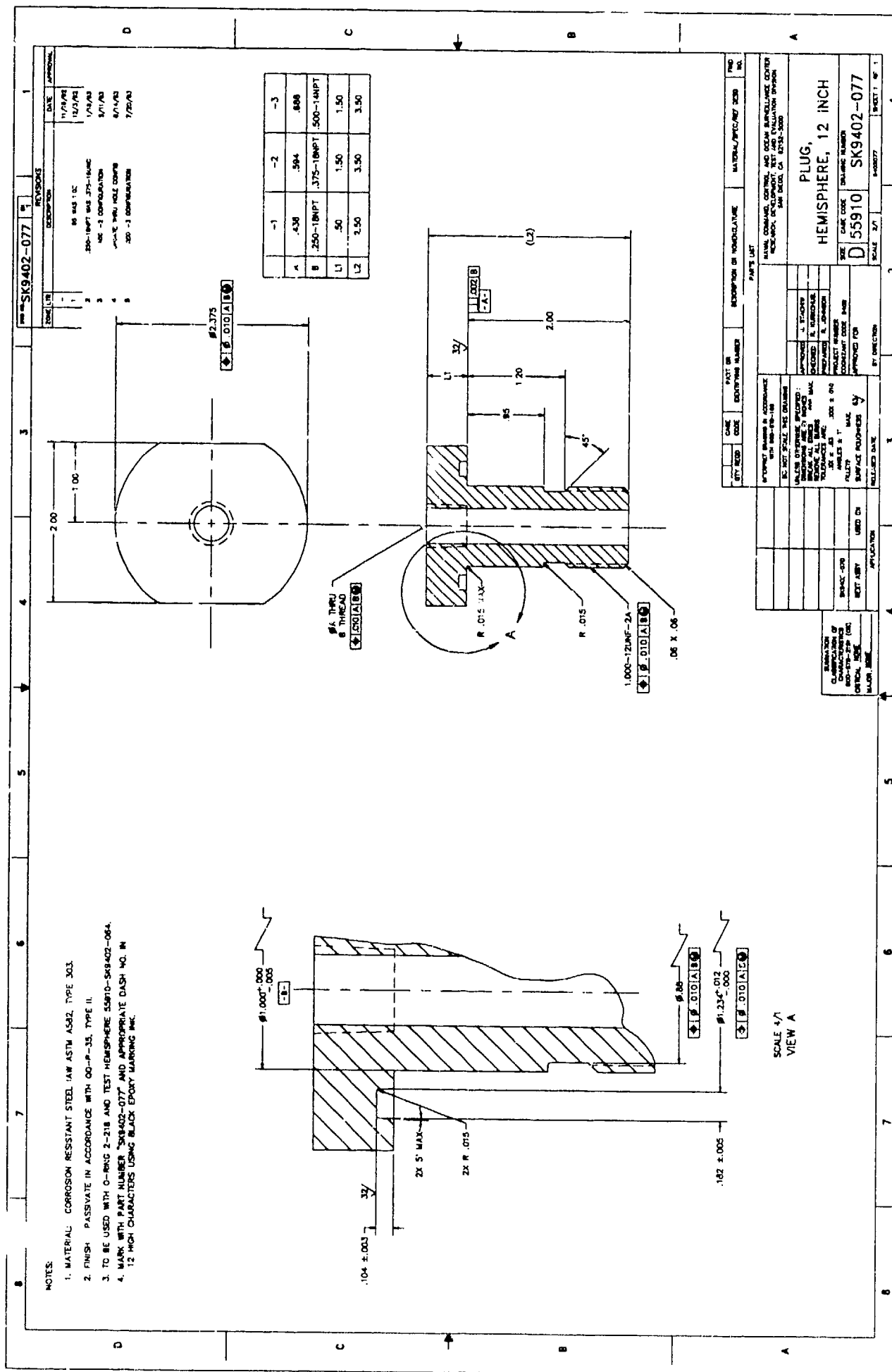
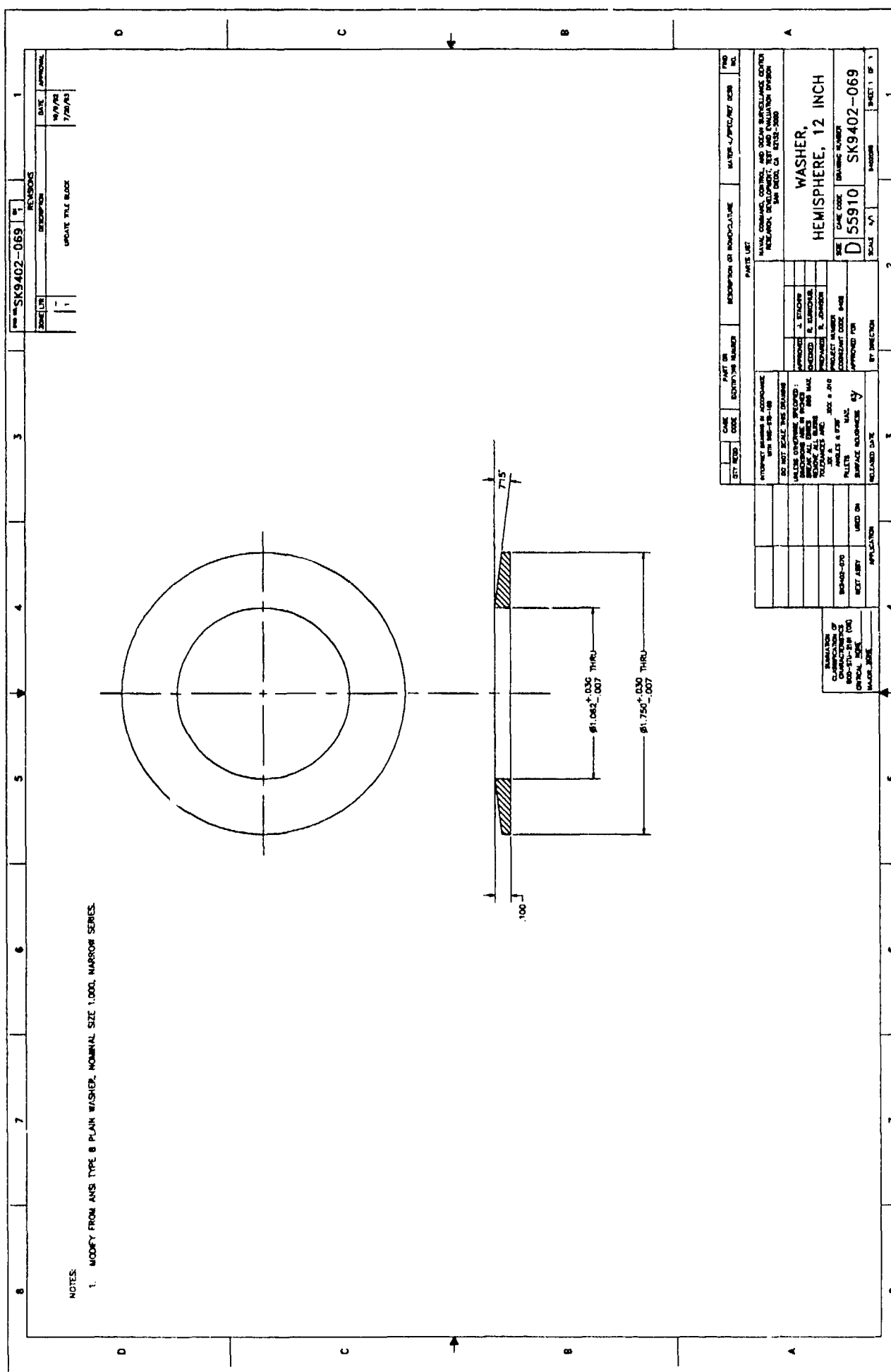


Figure 11. 12-inch hemisphere plug.



**Figure 12. 12-inch hemisphere washer.**

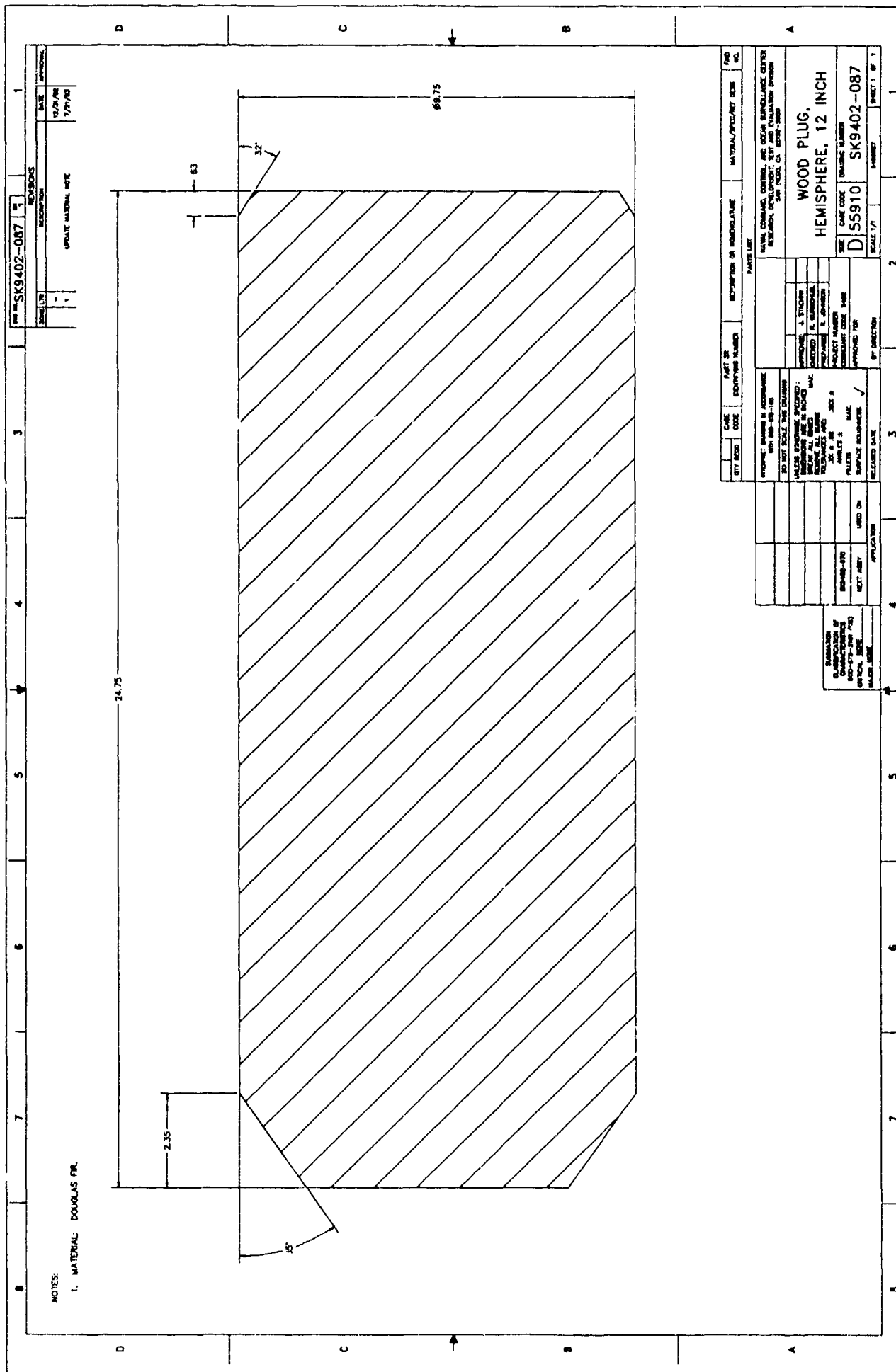


Figure 13. 12-inch hemisphere wood plug.

1	2	3	4	5	6	7	8	9	10	11	12	13	14	15	16	17	18	19	20	21	22
<p>ADHESIVE-SEALANTS, RTV MIL-A-46148</p>																					
<p>DEVCON LIQUID RELEASE AGENT A</p>																					
<p>SILICONE COMPOUND MIL-S-8660</p>																					
<p>PASA JELL 107 A</p>																					
<p>OBIA DEGT 283 HARDENER A</p>																					
<p>OBIA DEGT 6010 EPOXY RESIN A</p>																					
<p>MUT. HCL. CRES. 500-1310C-28</p>																					
<p>WASHER, LOCK. CRES. #500 NOM</p>																					
<p>WASHER, F.L.T. CRES. #531 D</p>																					
<p>2-218</p>																					
<p>WOOD PLUG, FLAT END PLATE, 12 INCH</p>																					
<p>TIE ROD</p>																					
<p>FEED THRU, FLAT END PLATE, 12 INCH</p>																					
<p>SPACER, 12 INCH CYLINDER</p>																					
<p>END CAP, MOD 1, TYPE 2, 12 IN. CYL</p>																					
<p>O-RING, END CAP, MOD 1, 12 IN. CYL</p>																					
<p>FLAT END PLATE, 12 INCH</p>																					
<p>FLAT END PLATE, 12 INCH</p>																					
<p>12 INCH CYLINDER</p>																					

1	2	3	4	5	6	7	8	9	10	11	12	13	14	15	16	17	18	19	20	21	22
<p>TEST ASSEMBLY II, 12 INCH CYLINDER</p>																					
<p>SK9402-123</p>																					
<p>SK9402-123</p>																					

Figure 14. 12-inch cylinder test assembly II configuration, Sheet 1.

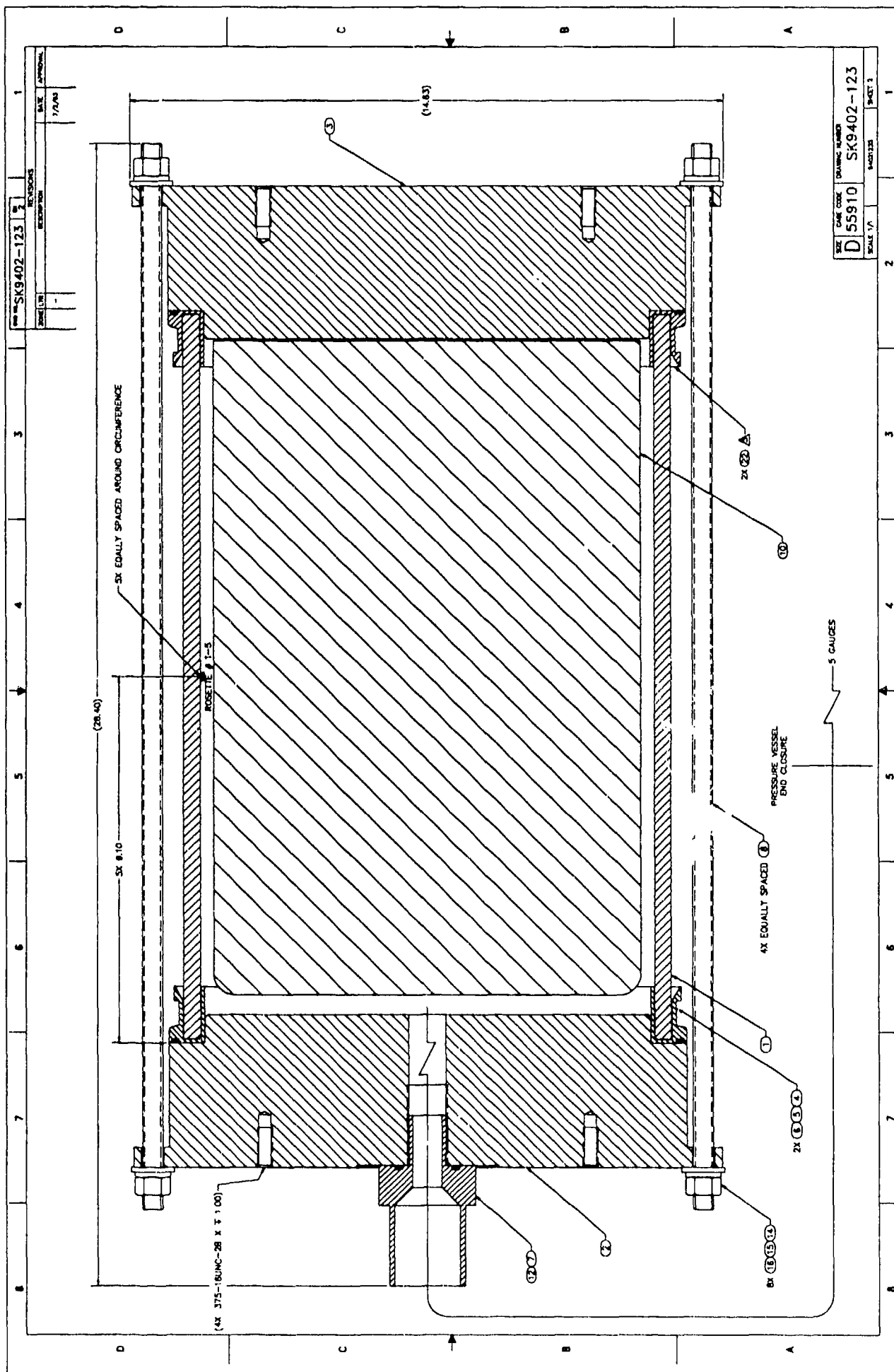
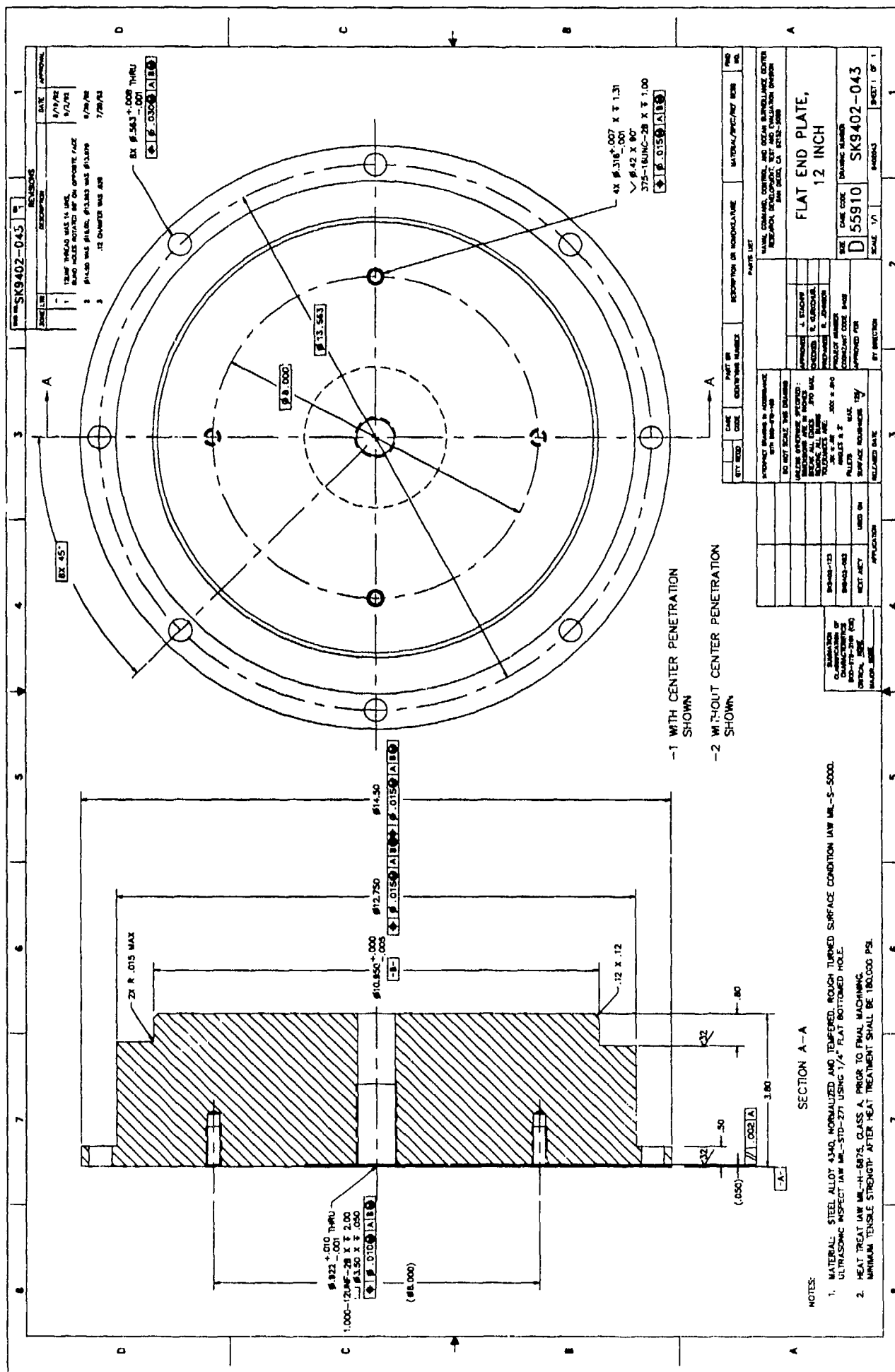


Figure 14. 12-inch cylinder test assembly II configuration, Sheet 2.



**Figure 15. 12-inch flat end plate.**

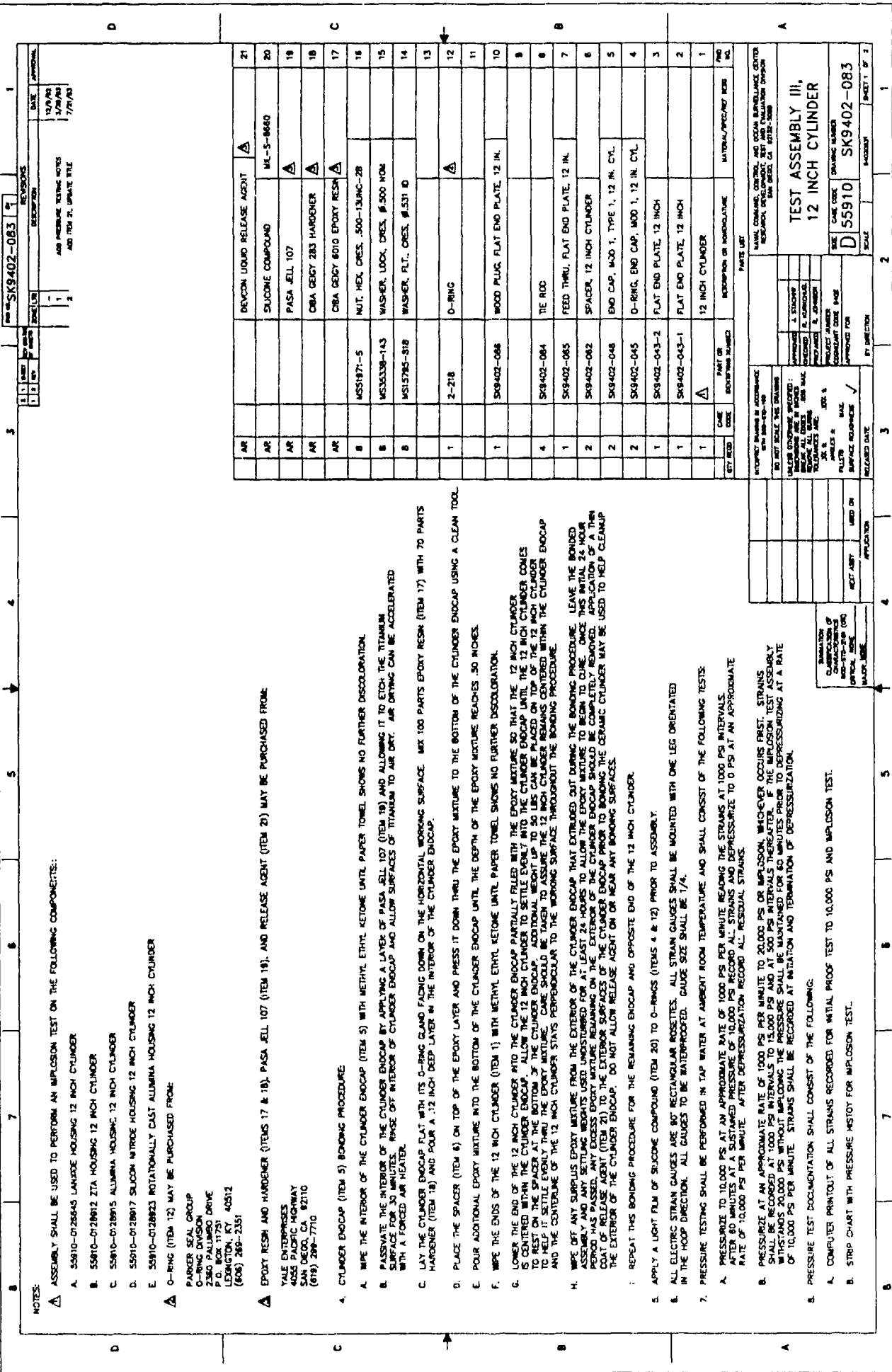


Figure 16. 12-inch cylinder test assembly III configuration, Sheet 1.

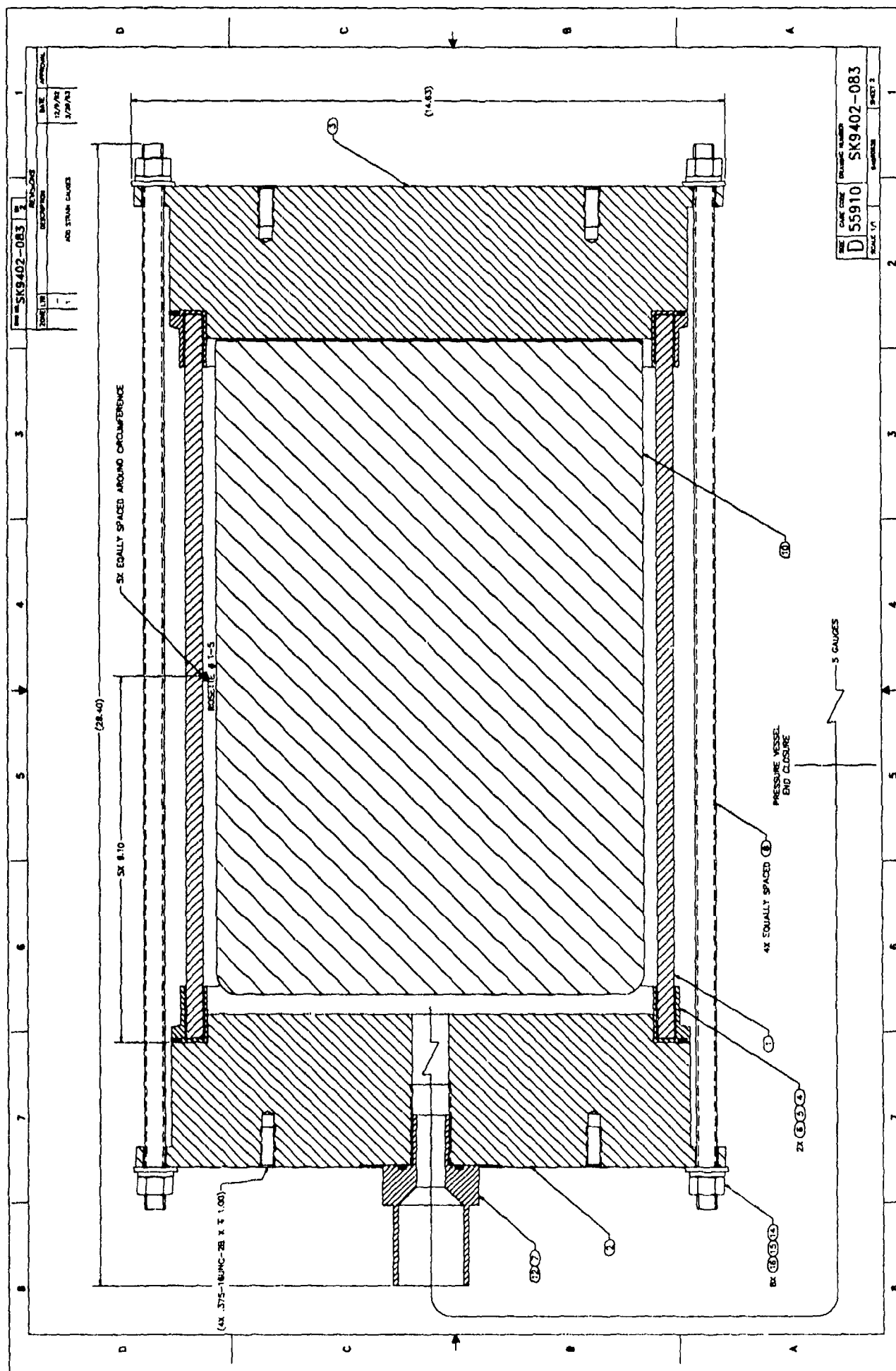
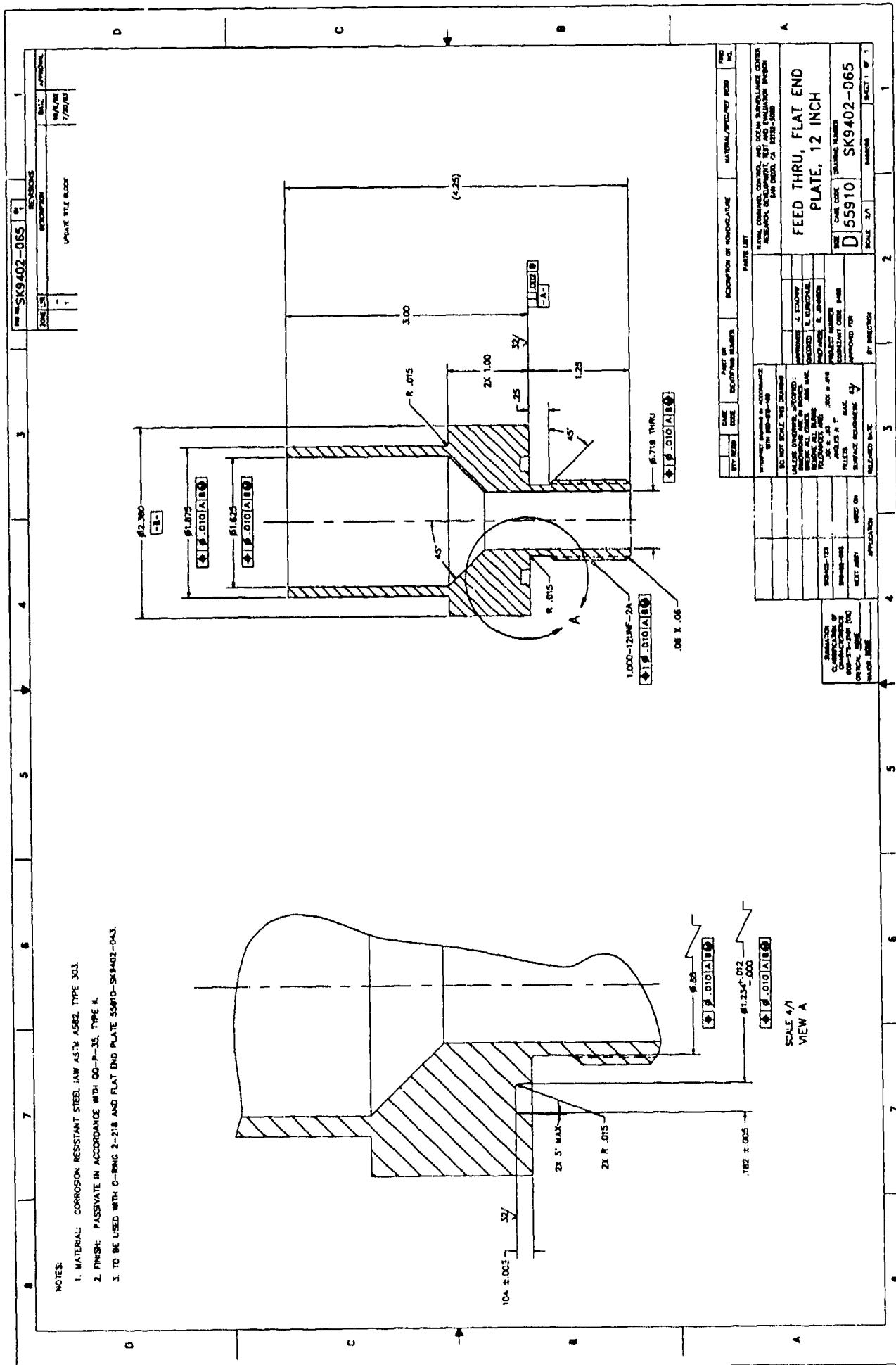


Figure 16. 12-inch cylinder test assembly III configuration, Sheet 2.









**Figure 19. 12-inch flat end-plate feed through.**



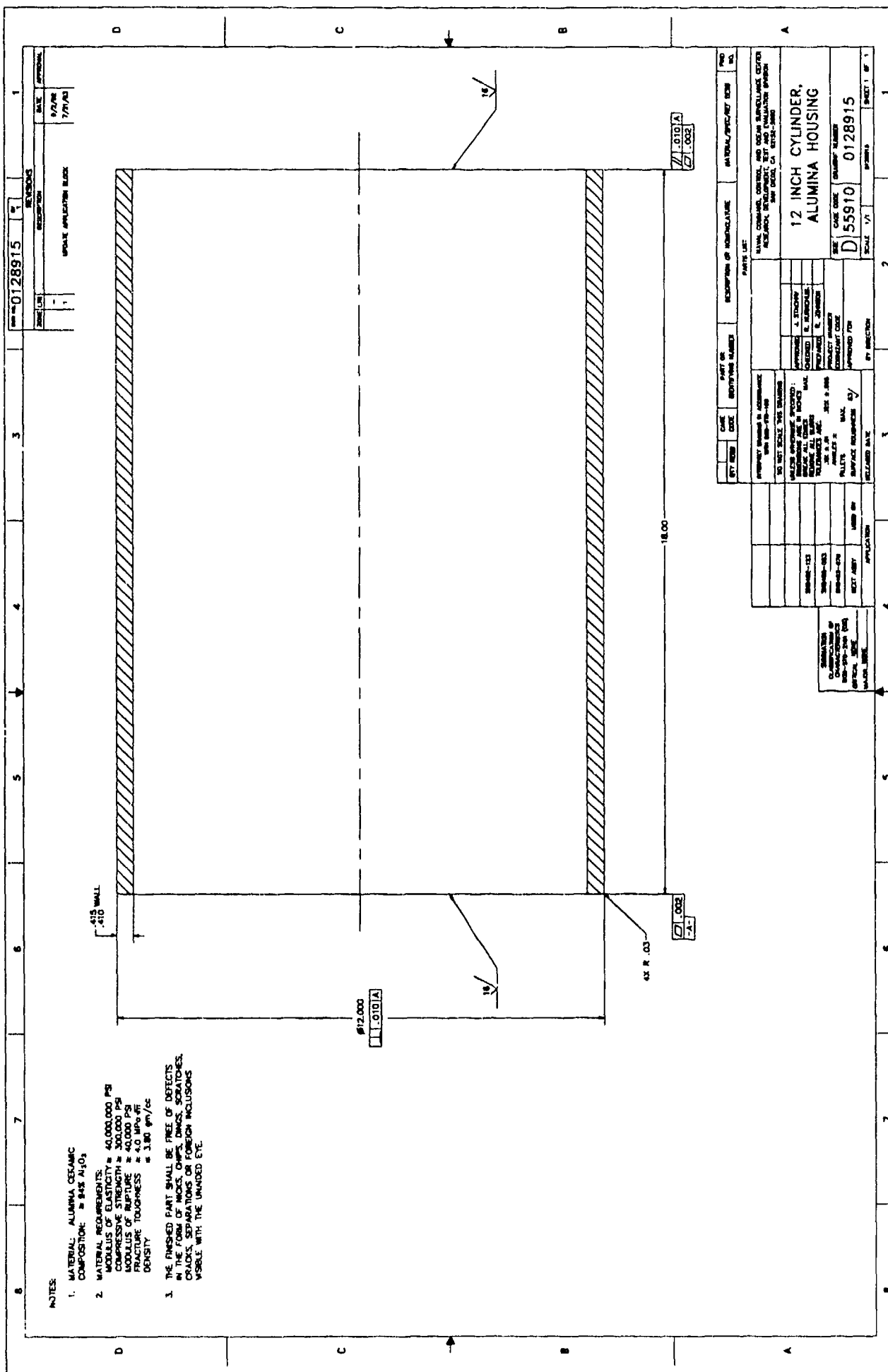


Figure 21. Alumina-ceramic 12-inch cylinder.

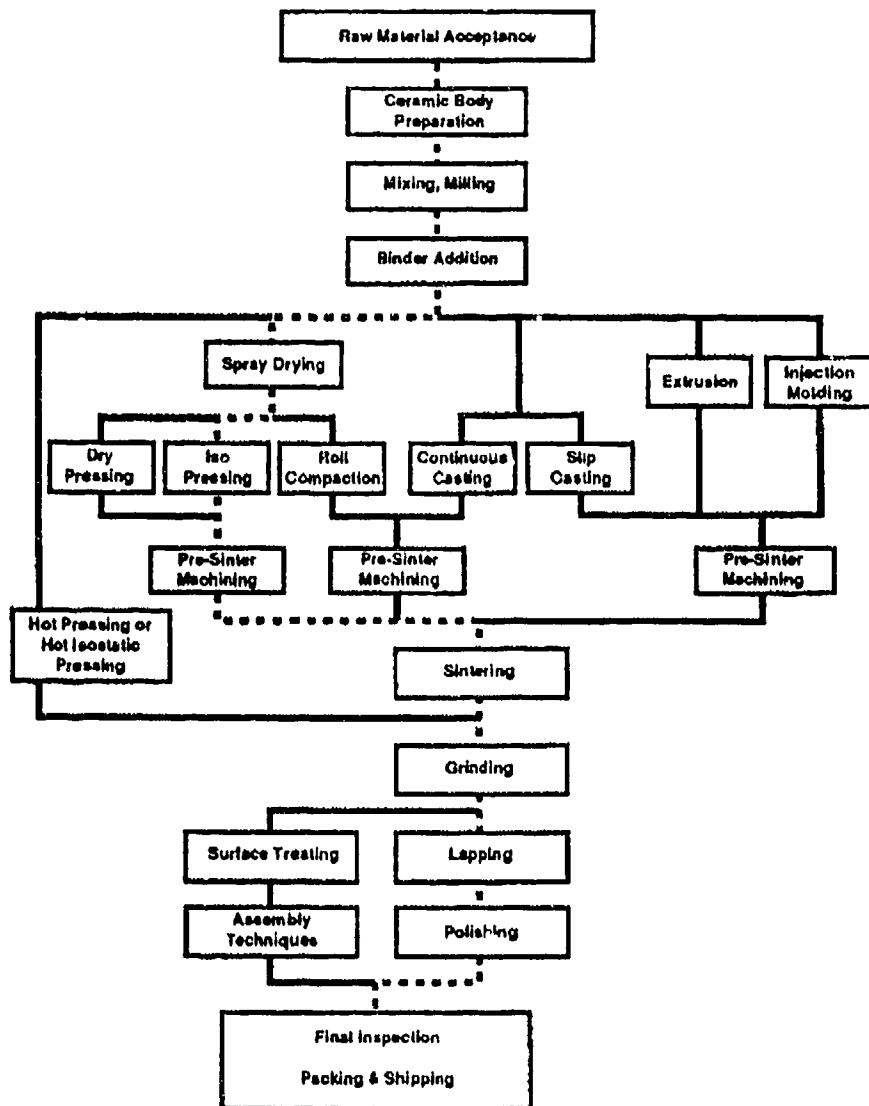


Figure 22. Alumina-ceramic manufacturing steps.











Figure 26. Bonding of Mod 1 end-cap joint rings.

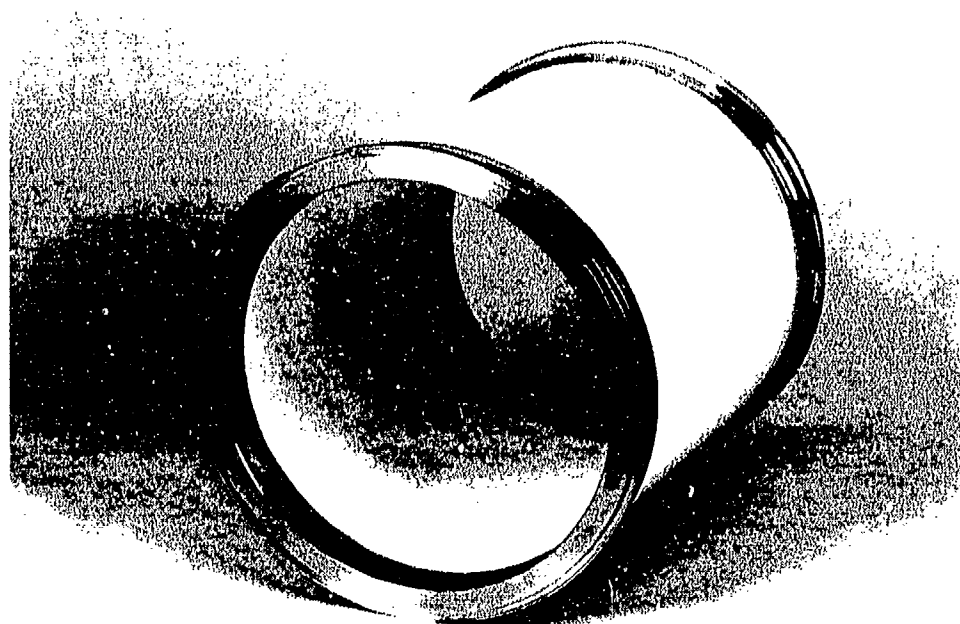


Figure 27. 12-inch alumina cylinder with Mod1, type 2 end-cap joint rings.

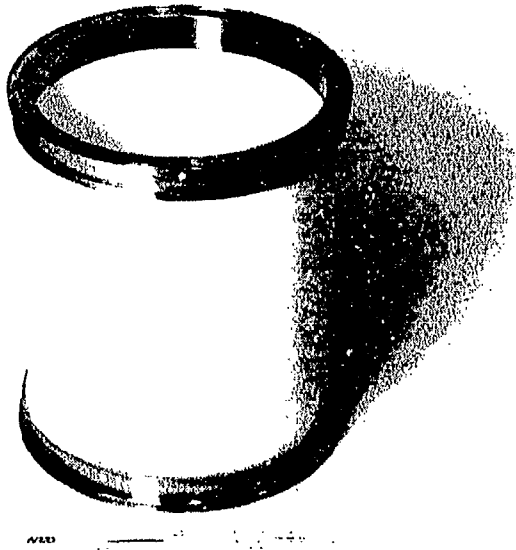


Figure 28. 12-inch alumina cylinder with Mod 1, Type 2 end-cap joint rings.



Figure 29. Test assembly I configuration.



Figure 30. Preparation of test assembly I configuration for pressure testing.

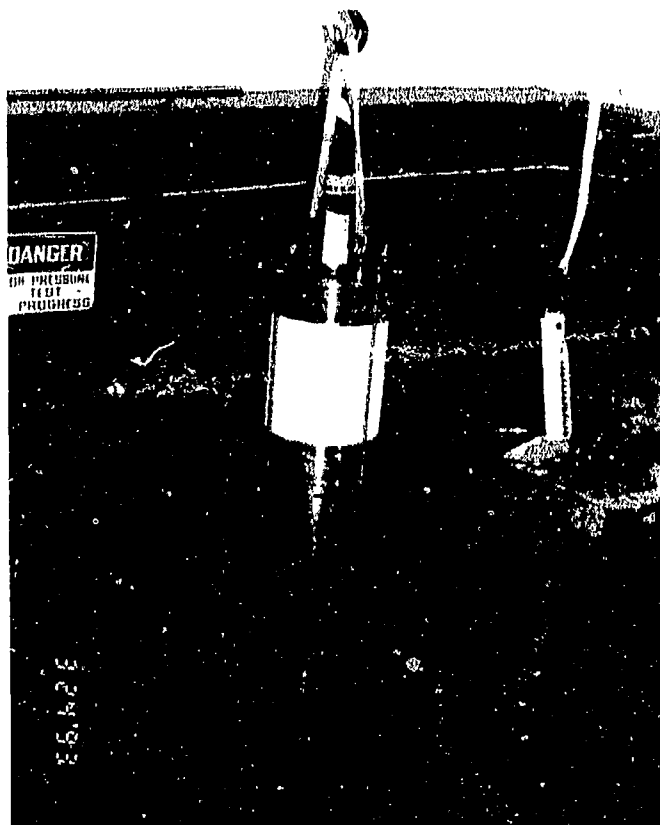


Figure 31. Preparation of test assembly II configuration for pressure testing.

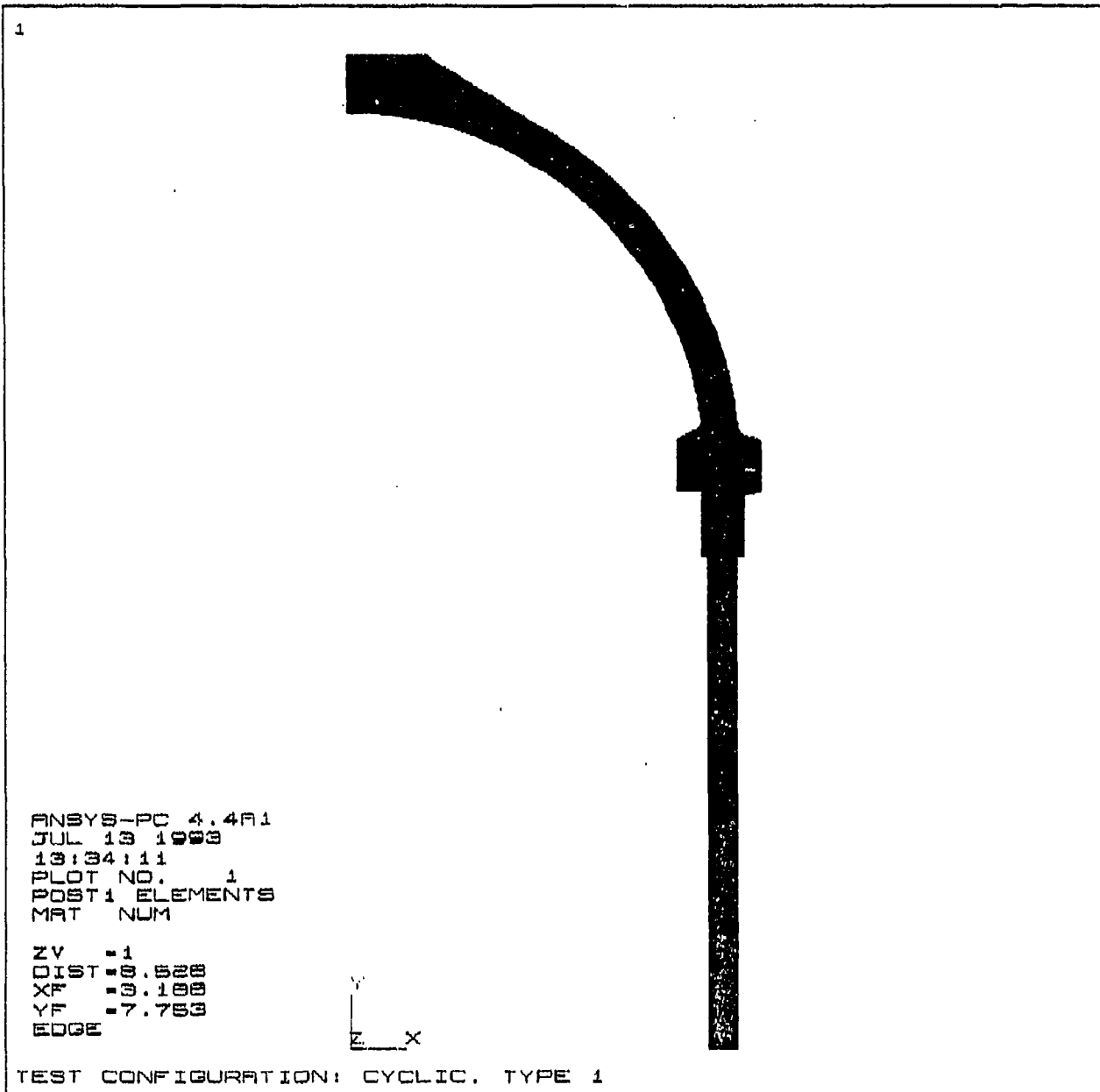


Figure 32. FEA solid model of test assembly 1 configuration.

1

ANSYS-PC 4.4A1  
 JUL 19 1993  
 13:28:44  
 PLOT NO. 1  
 POST1 STRESS  
 STEP=1  
 ITER=10  
 SX (AVG)  
 S GLOBAL  
 SMN = -10876  
 SMNB = -11627  
 SMX = 14406  
 SMXB = 14817

ZV = 1  
 XDIST = 5.206  
 XXF = 5.794  
 XYF = 4.552  
 EDGE

	-10876
	-8067
	-5258
	-2449
	360.458
	3170
	5879
	8788
	11627
	14406

CYCLIC TYPE 1. RADIAL STRESS AT 9000 PSI



Figure 33. Test assembly I radial stress plot at 9,000 psi.

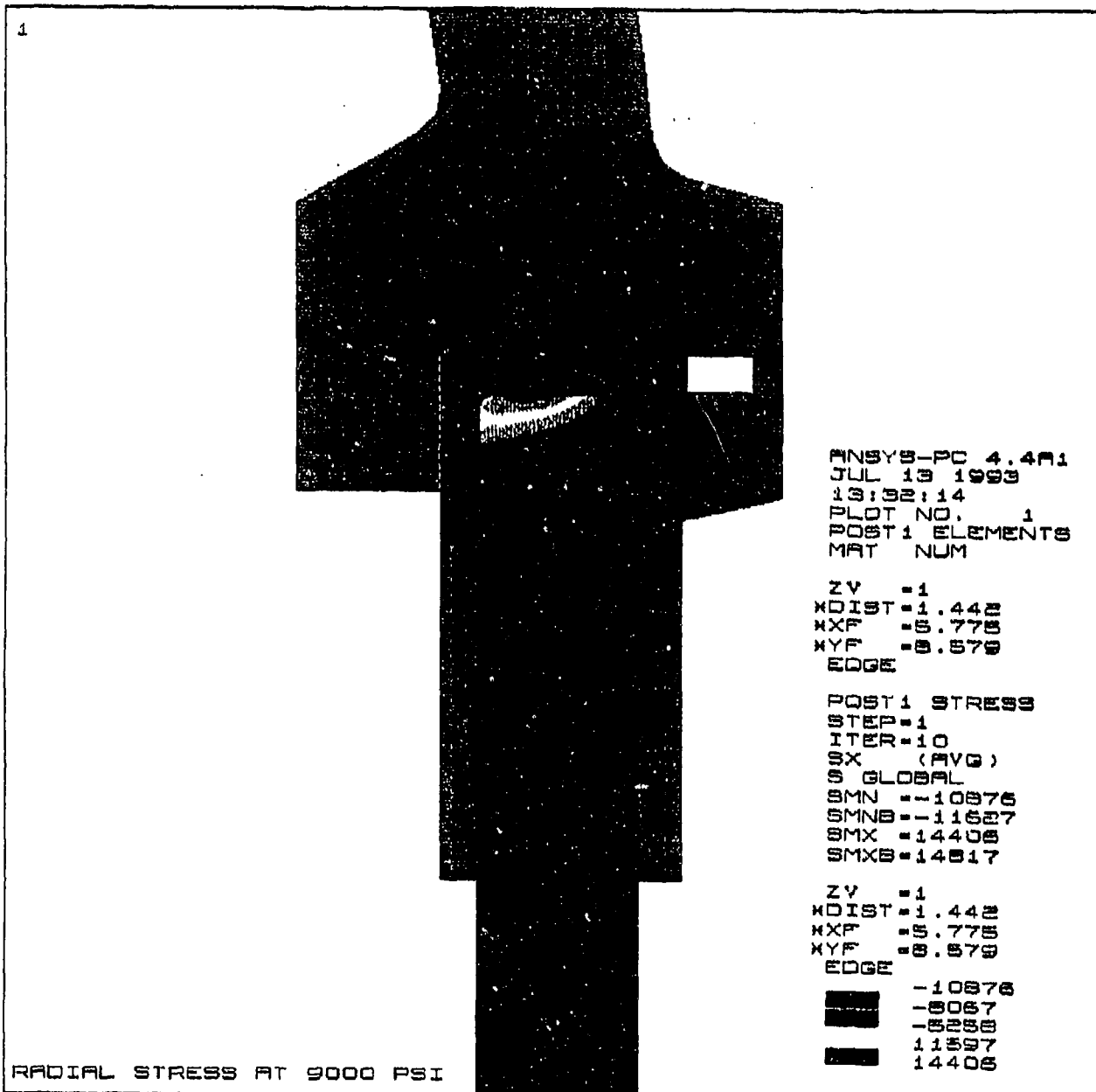


Figure 34. Detail of test assembly I radial stress plot at 9,000 psi.

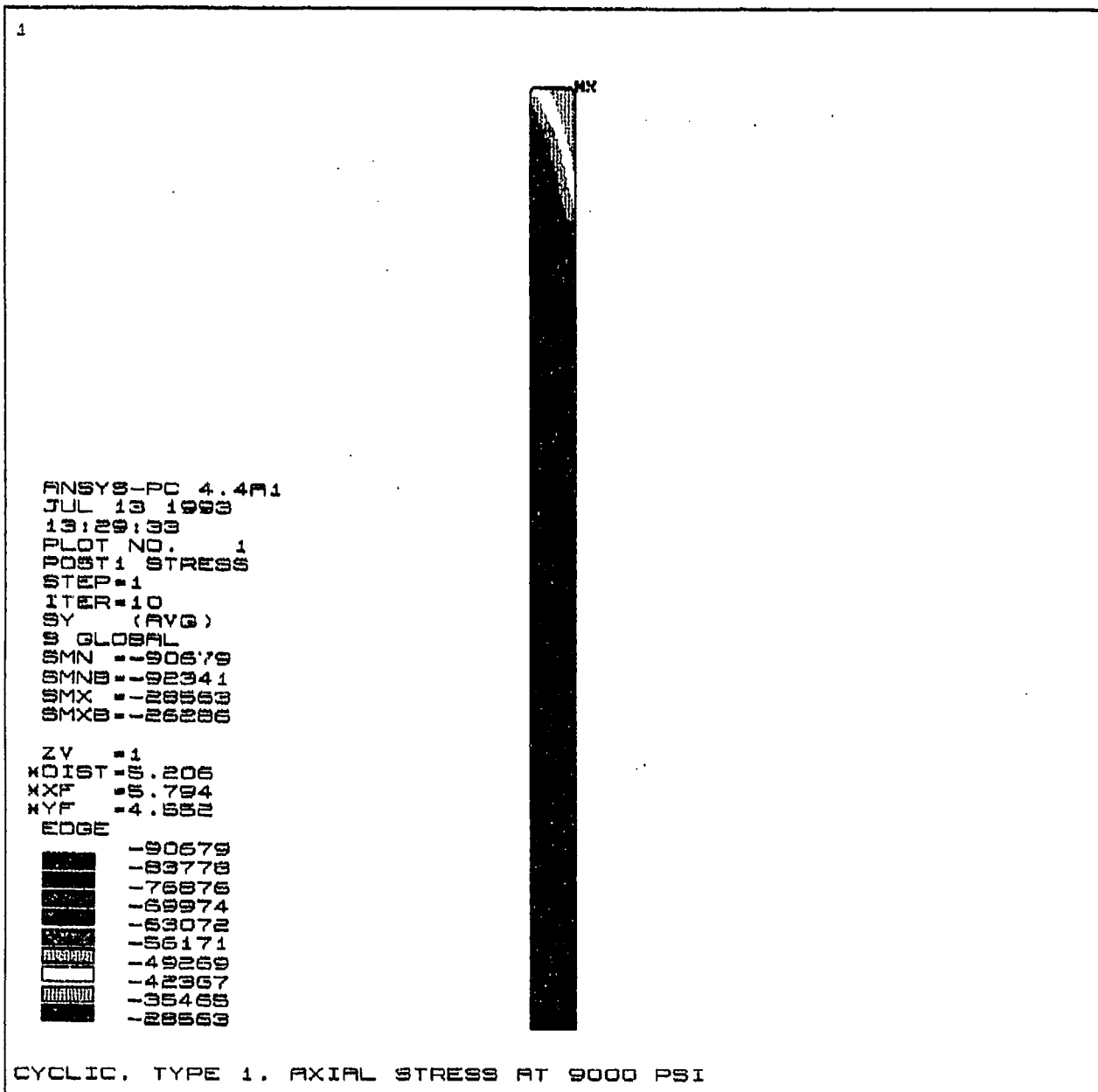


Figure 35. Test assembly I axial stress plot at 9,000 psi.



1

ANSYS-PC 4.4A1  
 JUL 13 1993  
 13:30:42  
 PLOT NO. 1  
 POST1 STRESS  
 STEP=1  
 ITER=10  
 SZ (AVG)  
 S GLOBAL  
 SMN = -133498  
 SMNB = -133502  
 SMX = -109684  
 SMXB = -109681

ZV = 1  
 XDIST = 5.206  
 XXF = 5.794  
 XYF = 4.582  
 EDGE

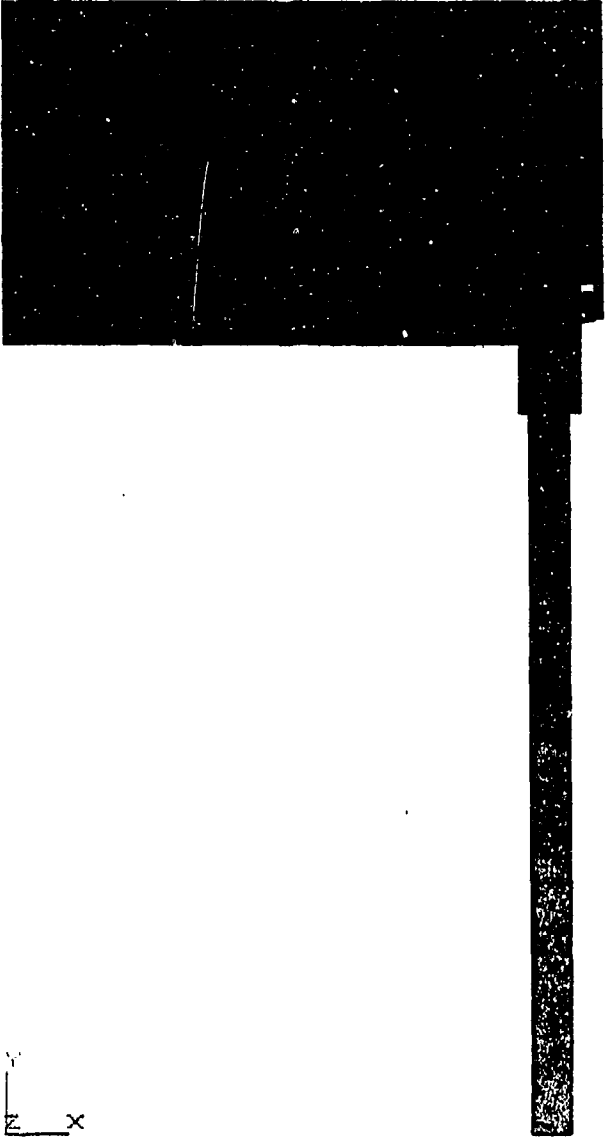
	-133498
	-130652
	-128206
	-125560
	-122914
	-120268
	-117622
	-114976
	-112330
	-109684



CYCLIC, TYPE 1, HOOP STRESS AT 9000 PSI

Figure 36. Test assembly I hoop stress plot at 9,000 psi.

1



ANSYS-PC 4.4A1  
JUL 14 1993  
8:33:19  
PLOT NO. 1  
POST1 ELEMENTS  
MAT NUM

ZV =1  
DIST=6.658  
XF =3.188  
YF =6.053  
EDGE



TEST CONFIGURATION: CYCLIC, TYPE 2

Figure 37. FEA solid model of test assembly II configuration.

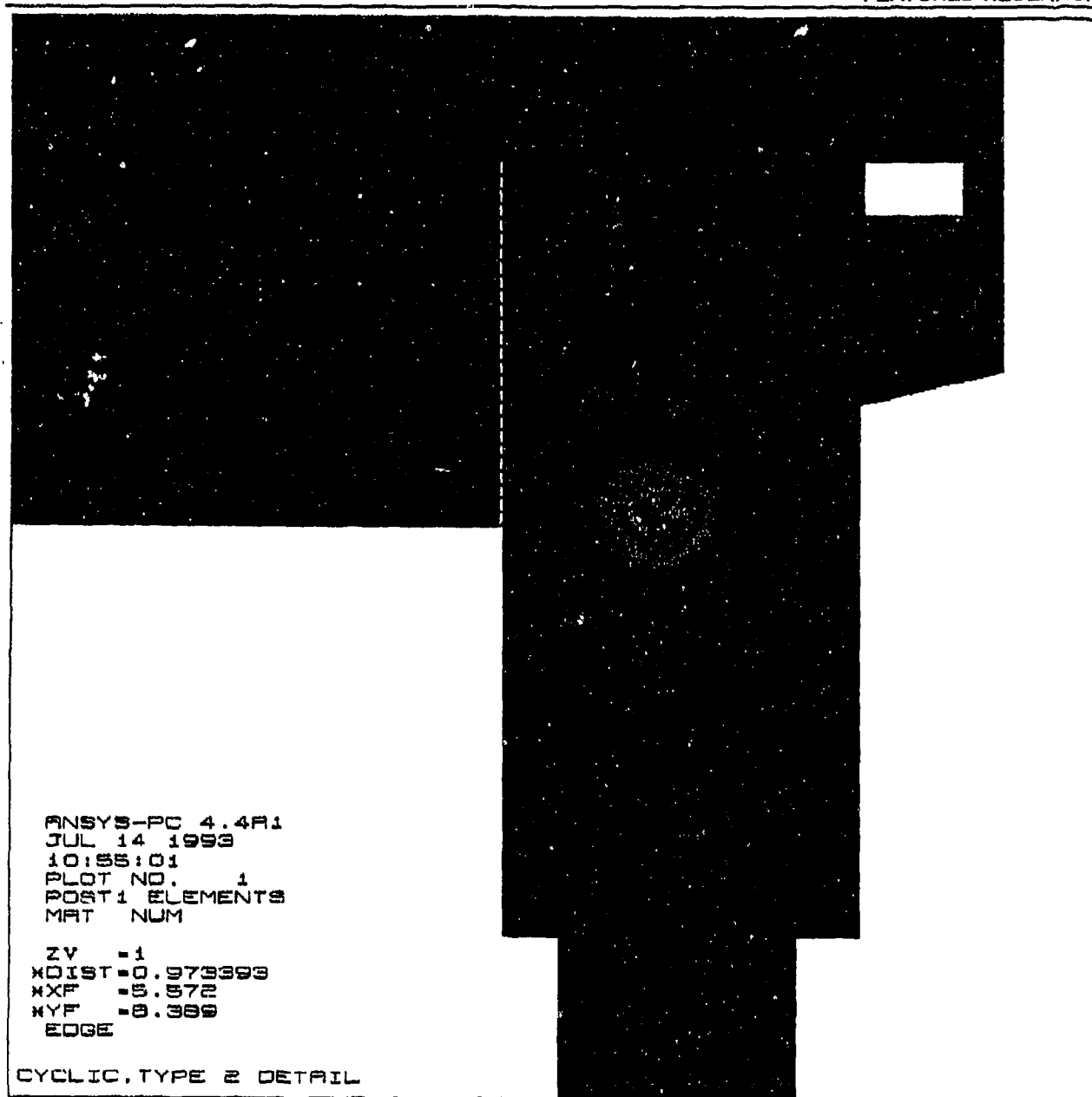


Figure 38. Detail of FEA solid model of test assembly II configuration.

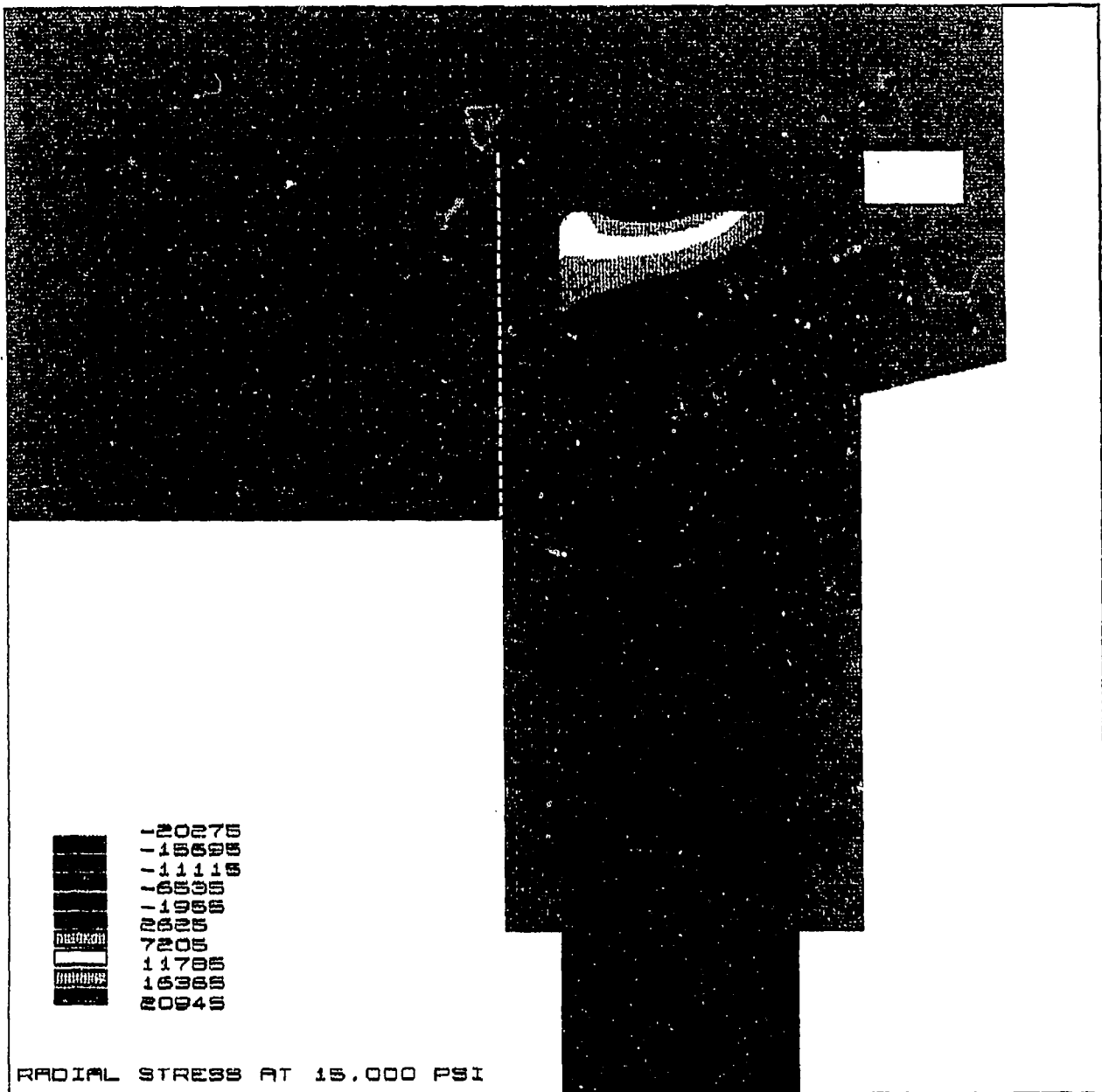


Figure 39. Test assembly II radial stress plot at 15,000 psi.

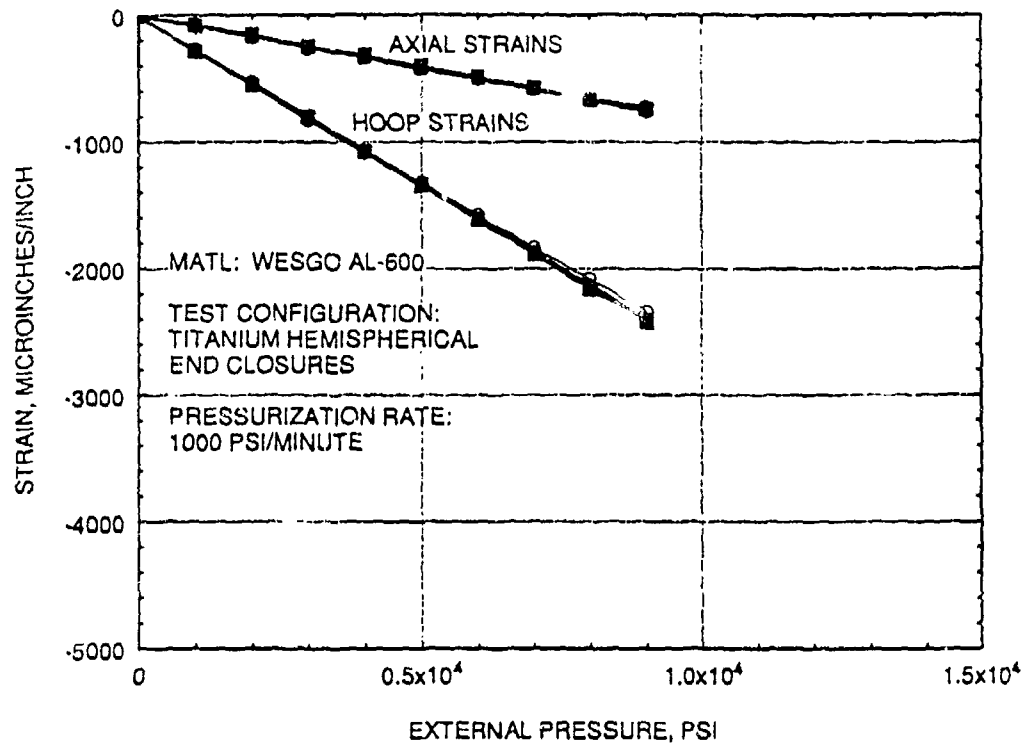


Figure 40. Plot of strains recorded during pressurization of test 1 cylinder.



Figure 41. Circumferential cracks on the bearing surface of test 1 cylinder.

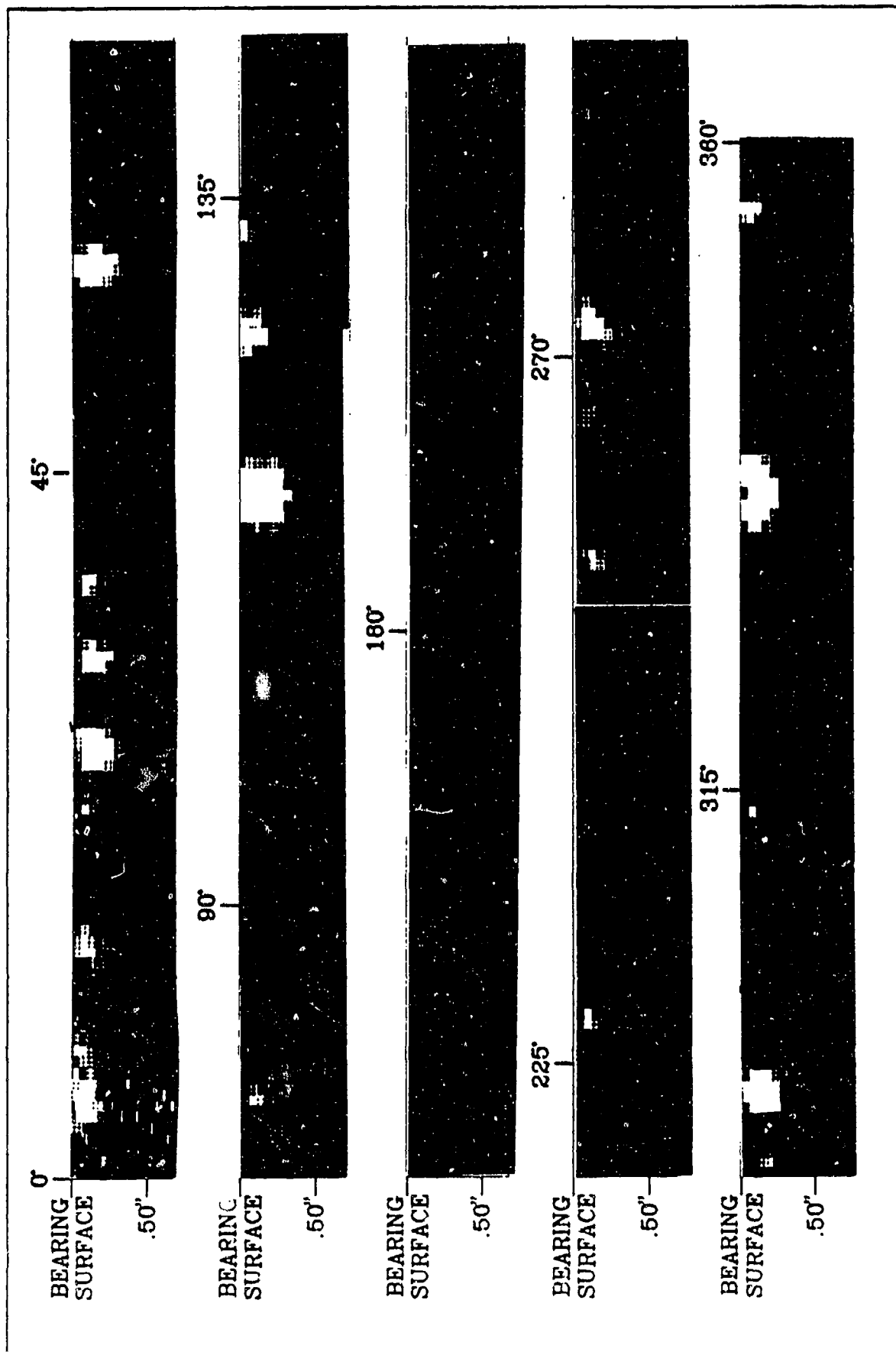


Figure 42. Ultrasonic C-scan of sub critical crack growth in test 1 cylinder.

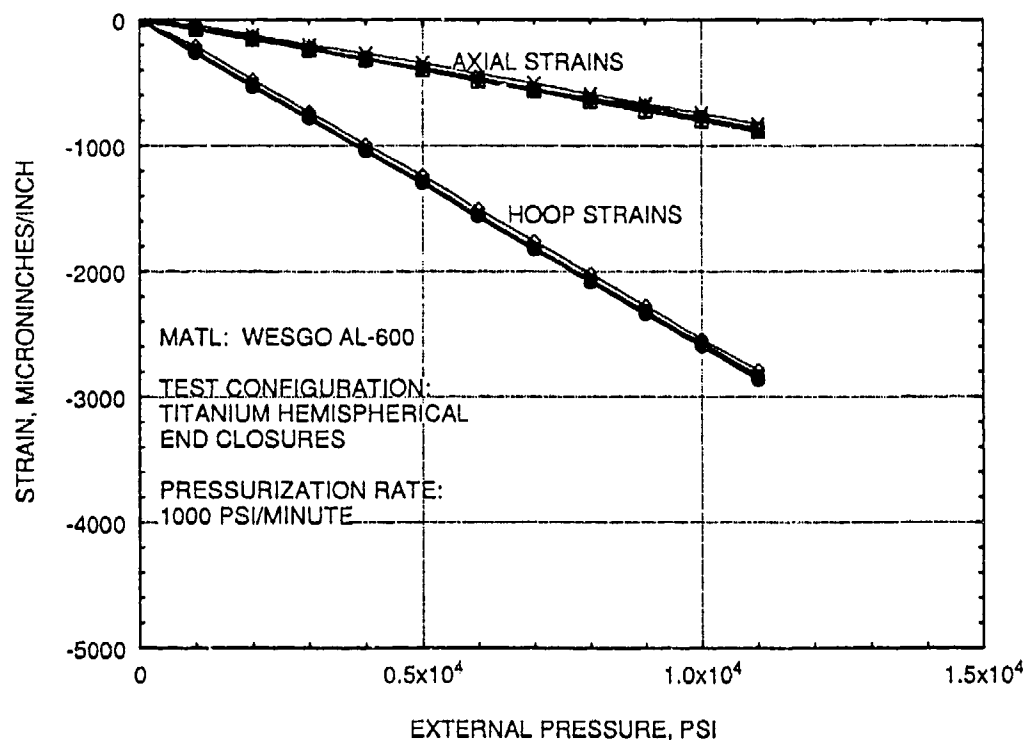


Figure 43. Plot of strains recorded during pressurization of test 2 cylinder.

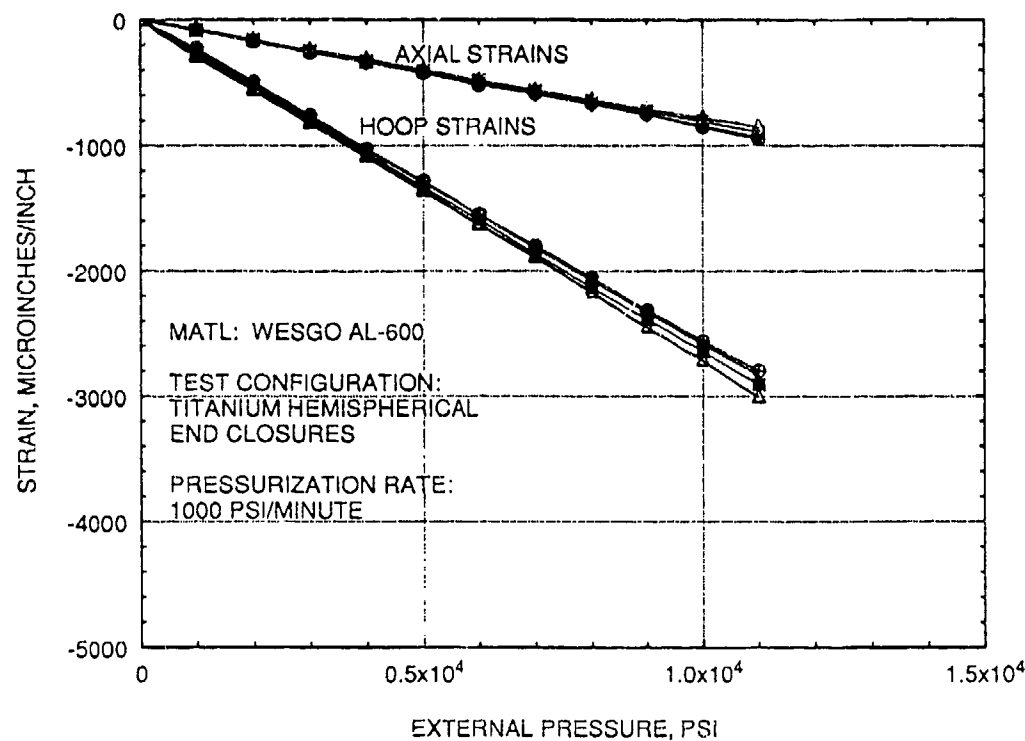


Figure 44. Plot of strains recorded during pressurization of test 3 cylinder.

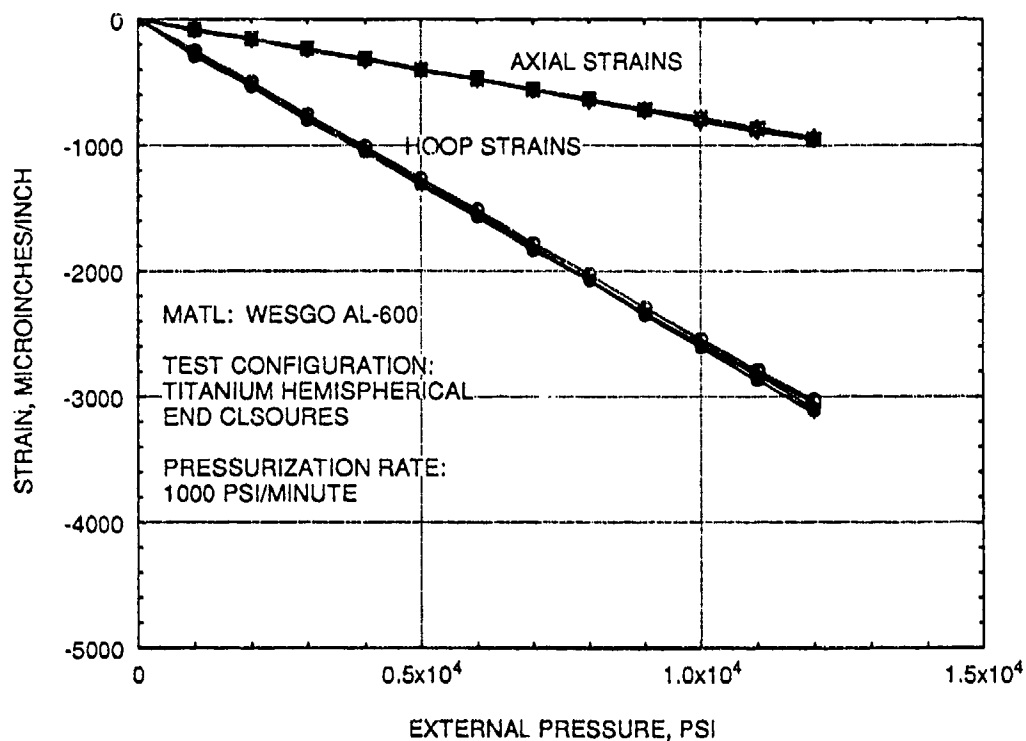


Figure 45. Plot of strains recorded during pressurization of test 4 cylinder.

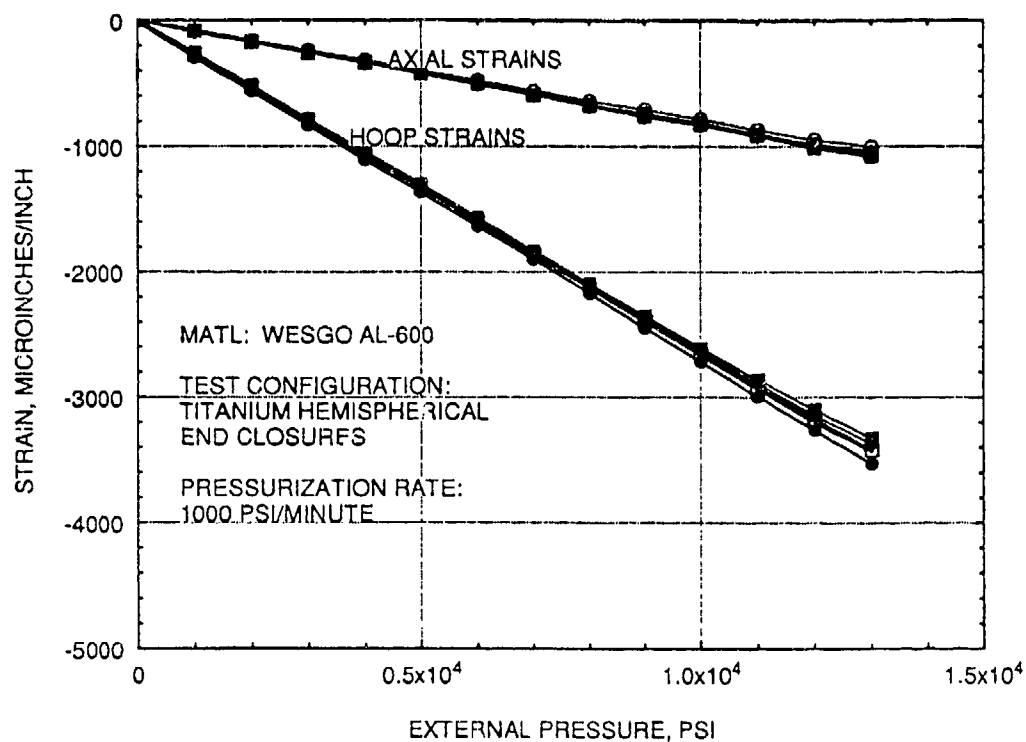


Figure 46. Plot of strains recorded during pressurization of test 5 cylinder.



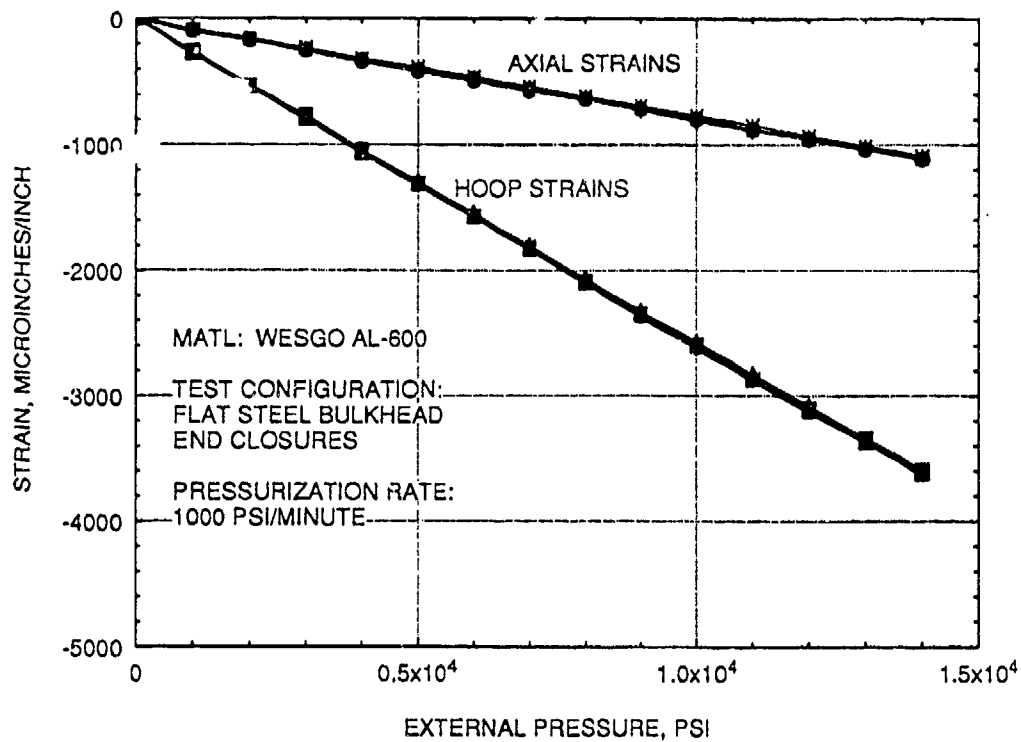


Figure 47. Plot of strains recorded during pressurization of test 6 cylinder.

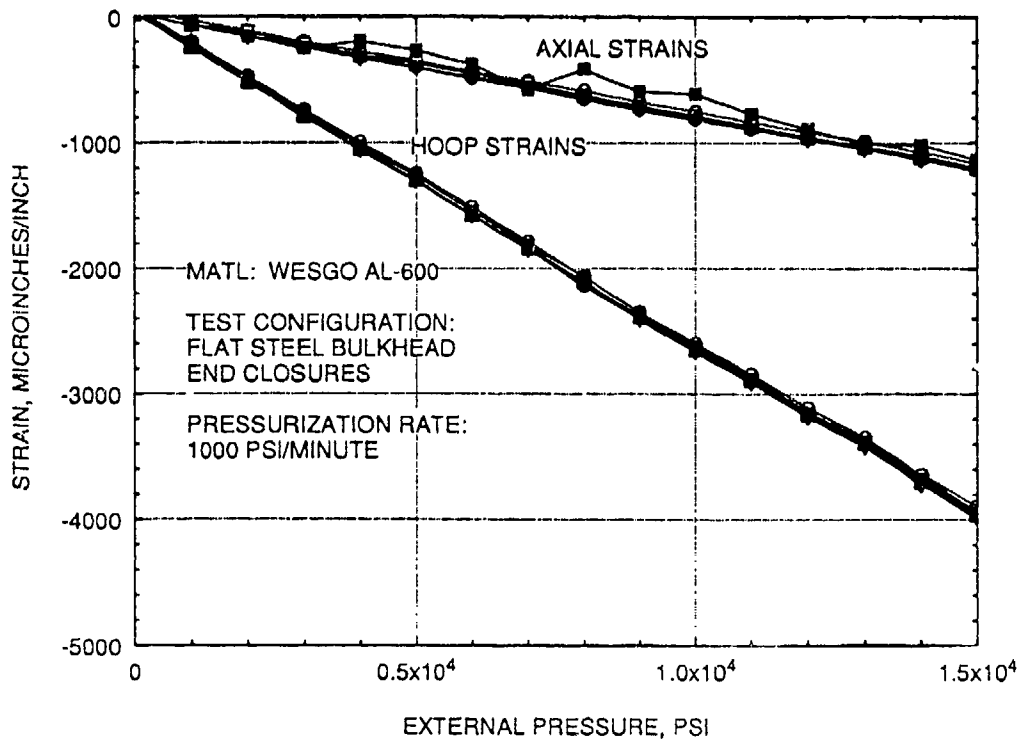


Figure 48. Plot of strains recorded during pressurization of test 7 cylinder.

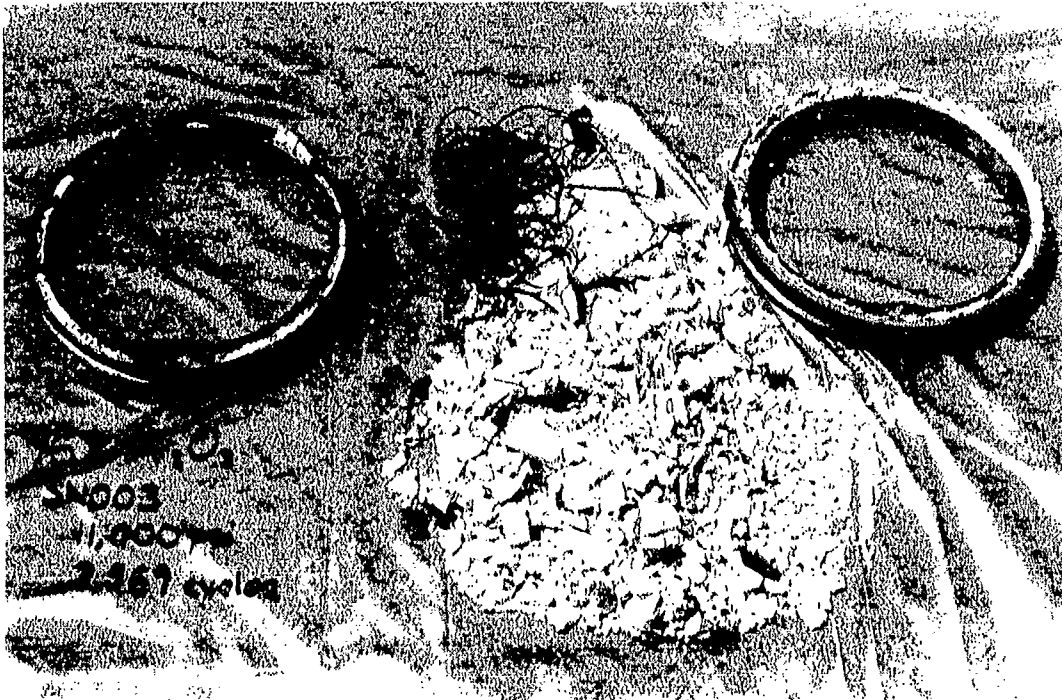


Figure 49. Remains of cylinder assembly after failure from test 3.



Figure 50. Remains of cylinder assembly after failure from test 7.

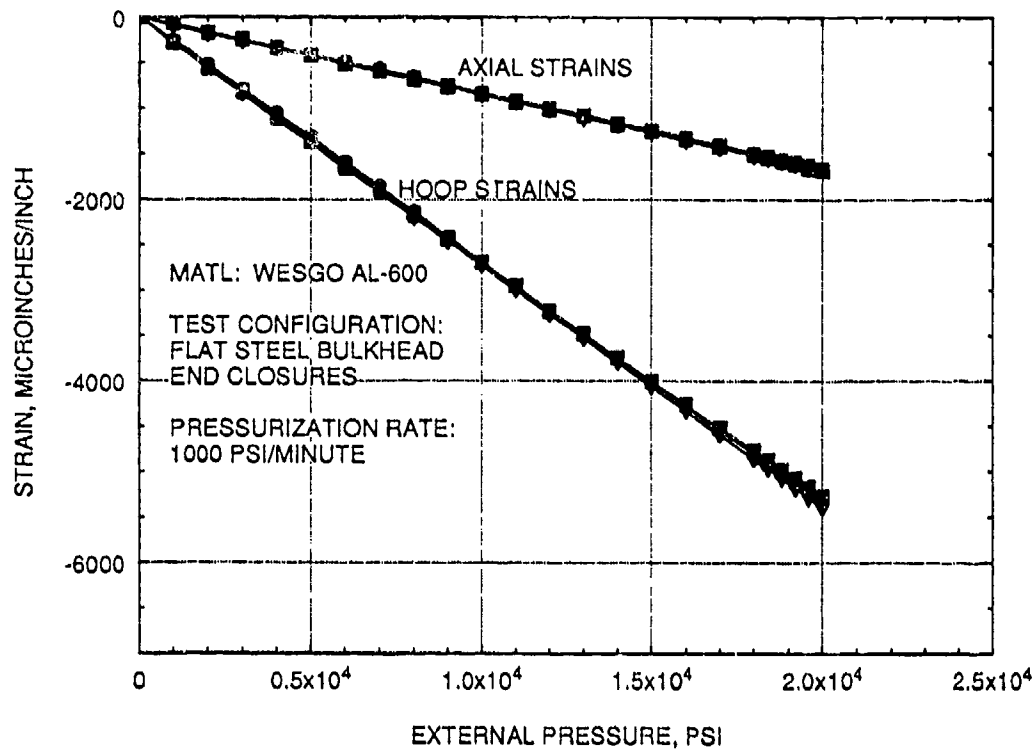


Figure 51. Plot of strains recorded during pressurization of test 8 cylinder.

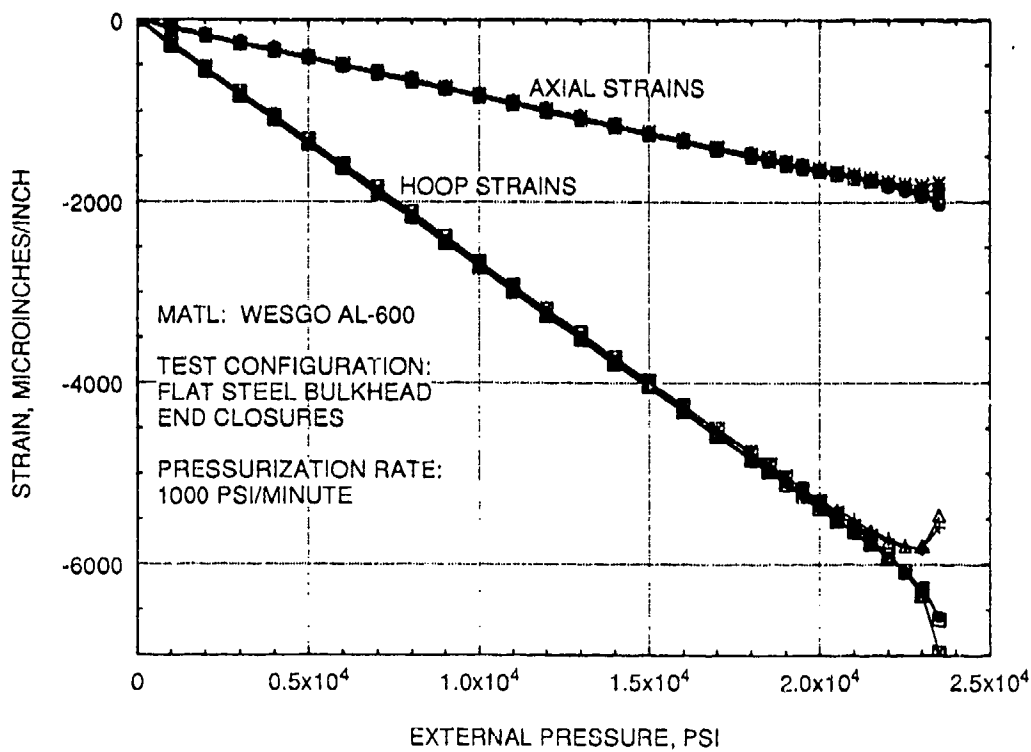


Figure 52. Plot of strains recorded during pressurization of test 9 cylinder.

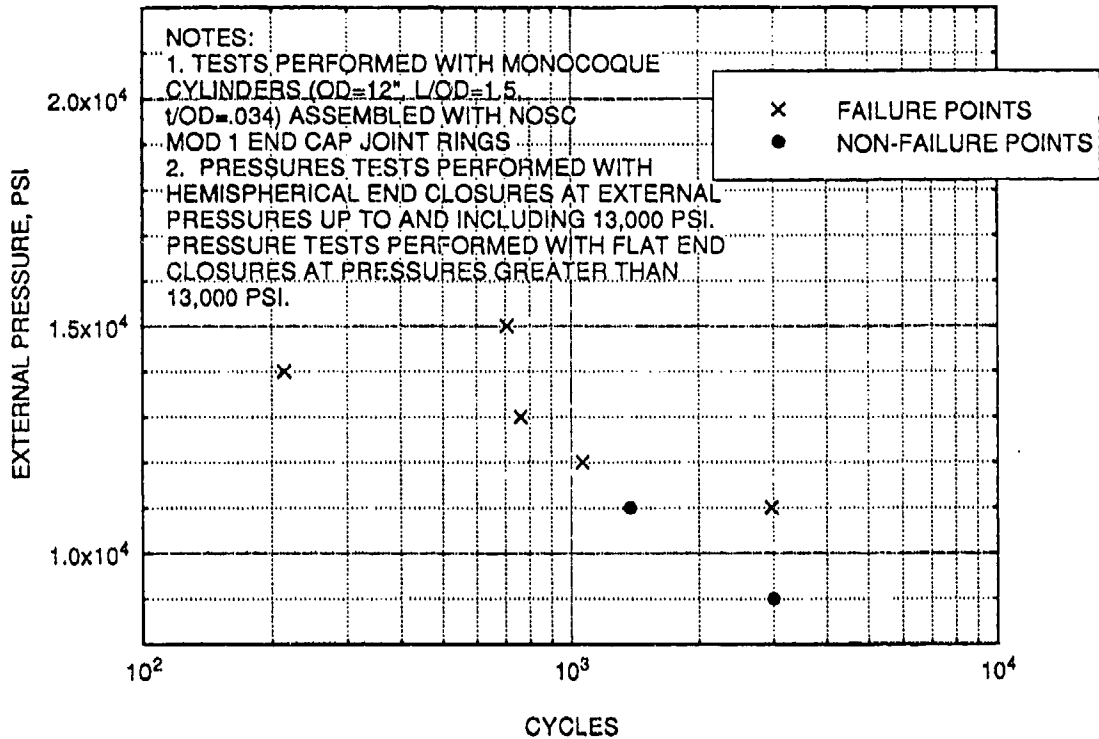


Figure 53. Cyclic external pressure loading test data for test 1 through 7 cylinders.

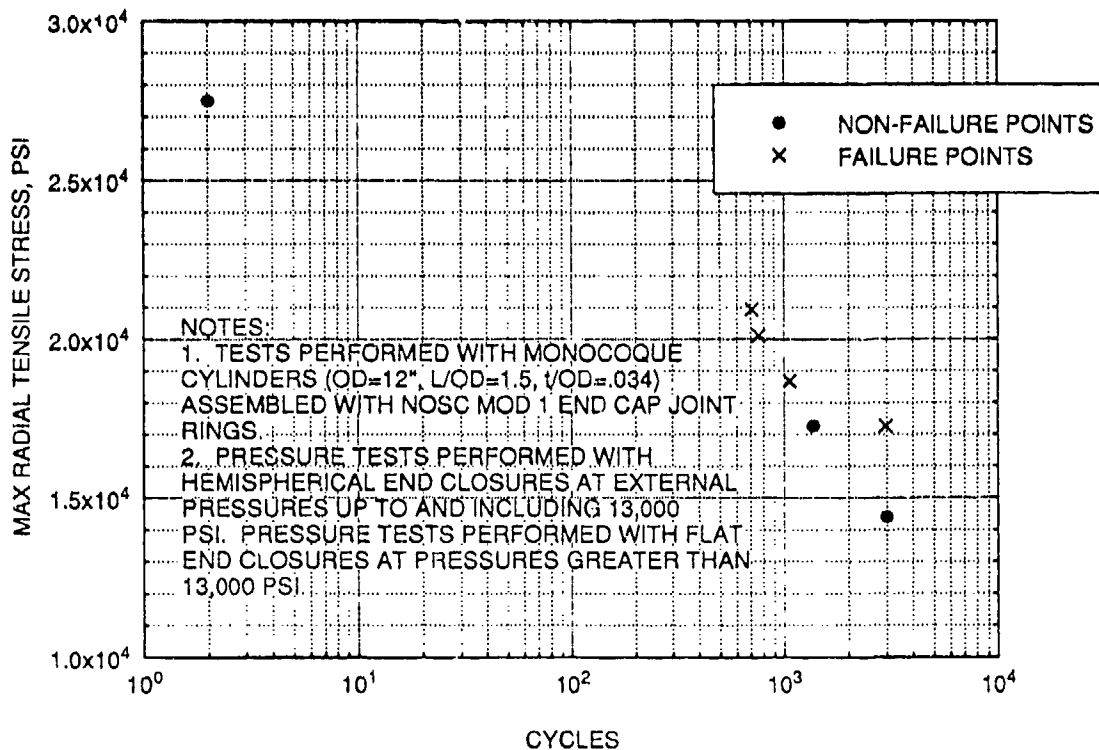


Figure 54. AL-600 alumina cyclic life versus maximum calculated tensile bearing surface stress.

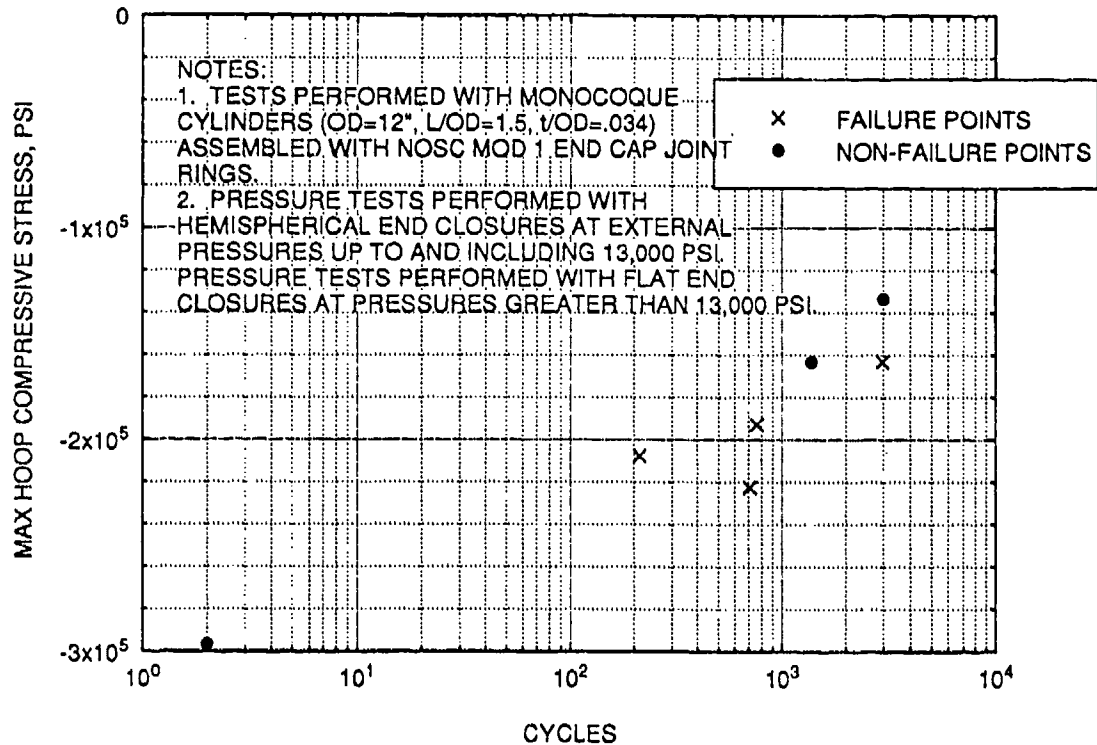


Figure 55. AL-600 alumina cyclic life versus maximum calculated compressive hoop stress.

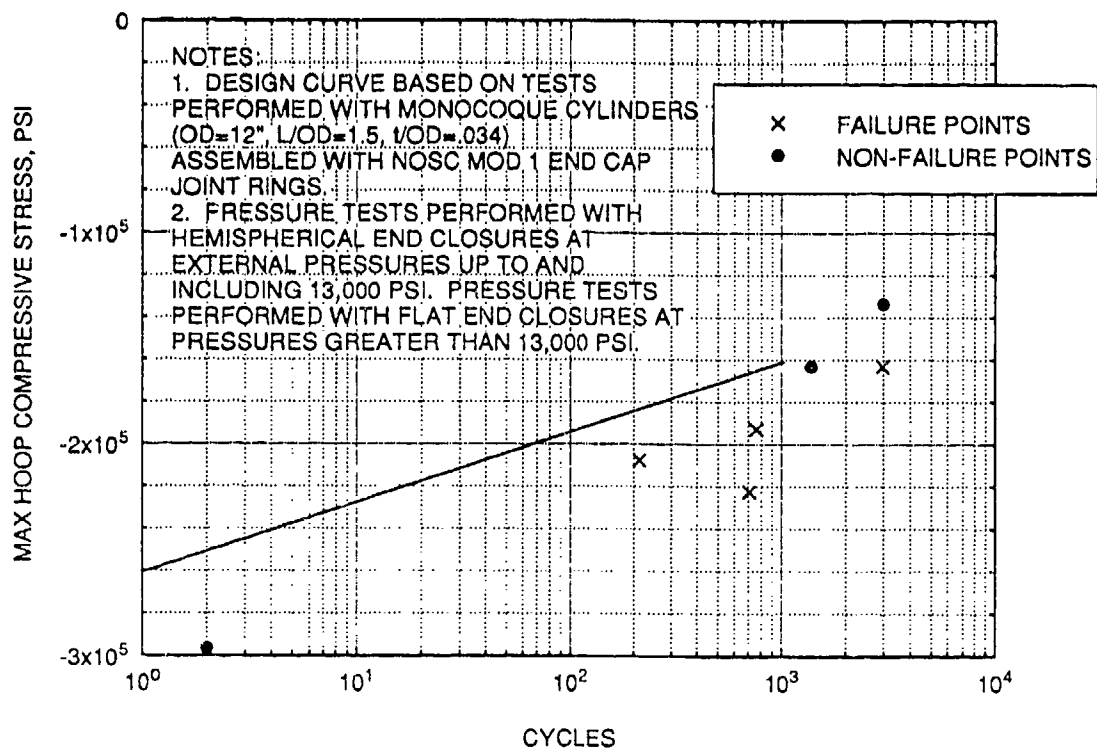


Figure 56. Design curve for external pressure cyclic loading of AL-600 alumina cylinders.

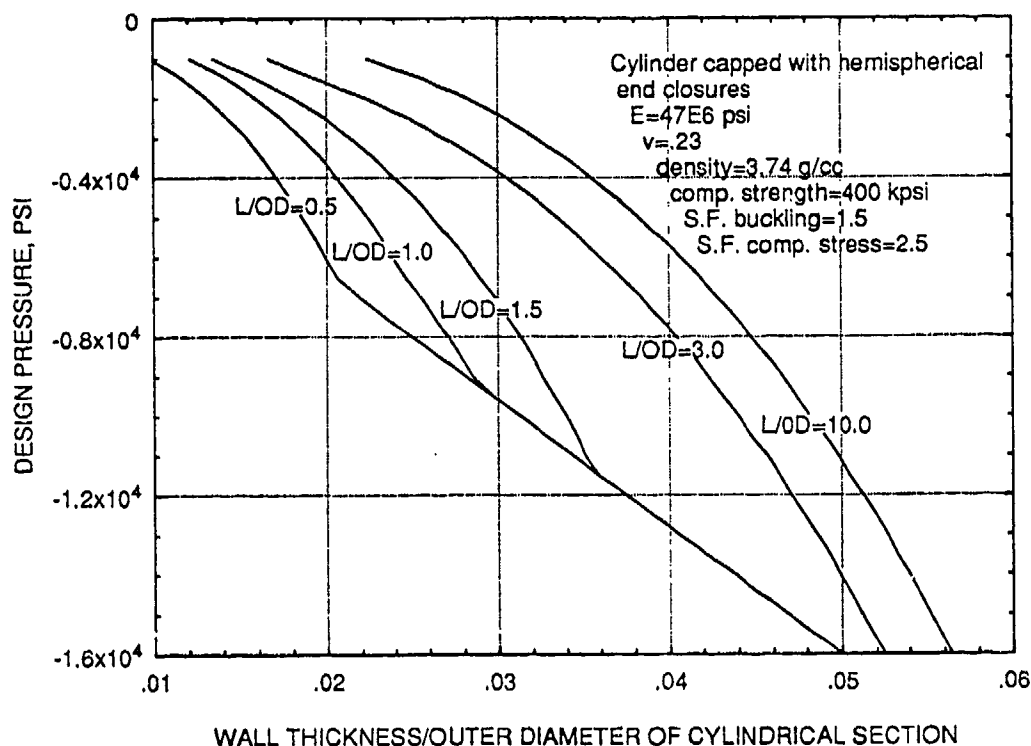


Figure 57.  $t/OD$  ratios of monocoque AL-600 alumina cylinders for 1,000 cycles to design depth.

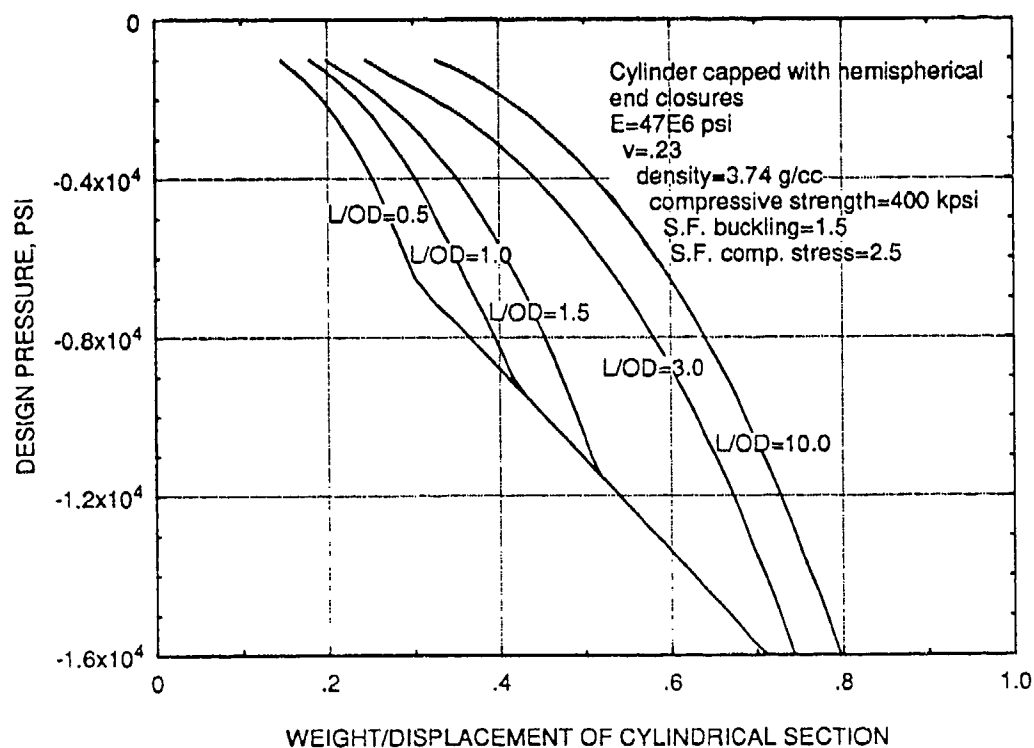


Figure 58.  $W/D$  ratios of monocoque AL-600 alumina cylinders for 1,000 cycles to design depth.

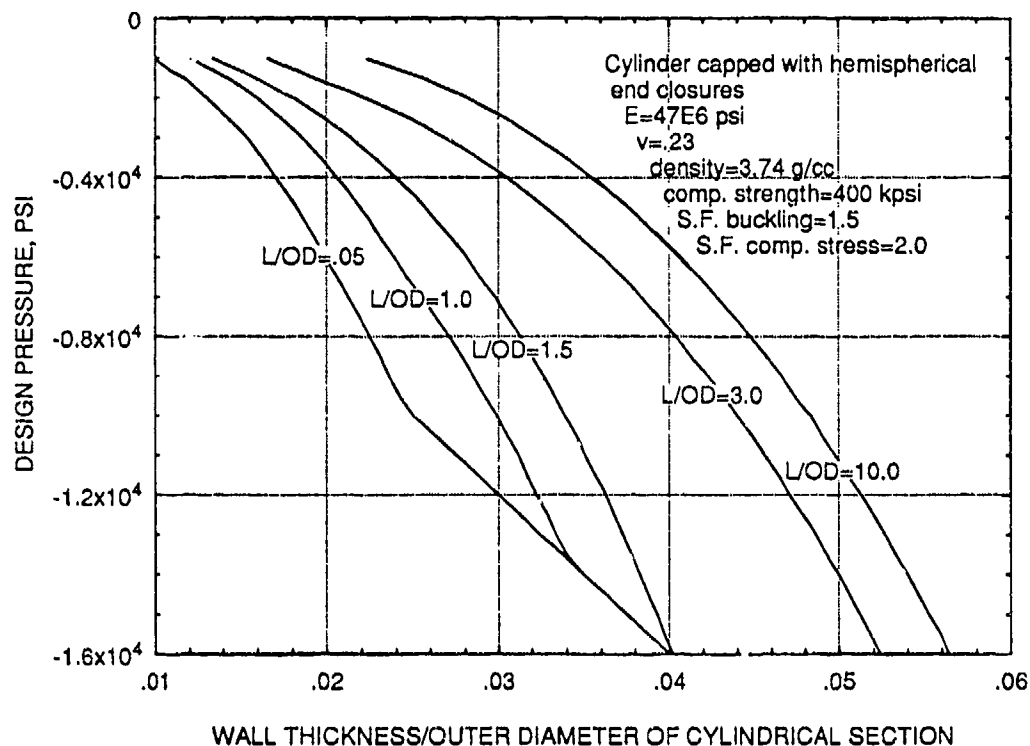


Figure 59.  $t/OD$  ratios of monocoque AL-600 alumina cylinders for 100 cycles to design depth.

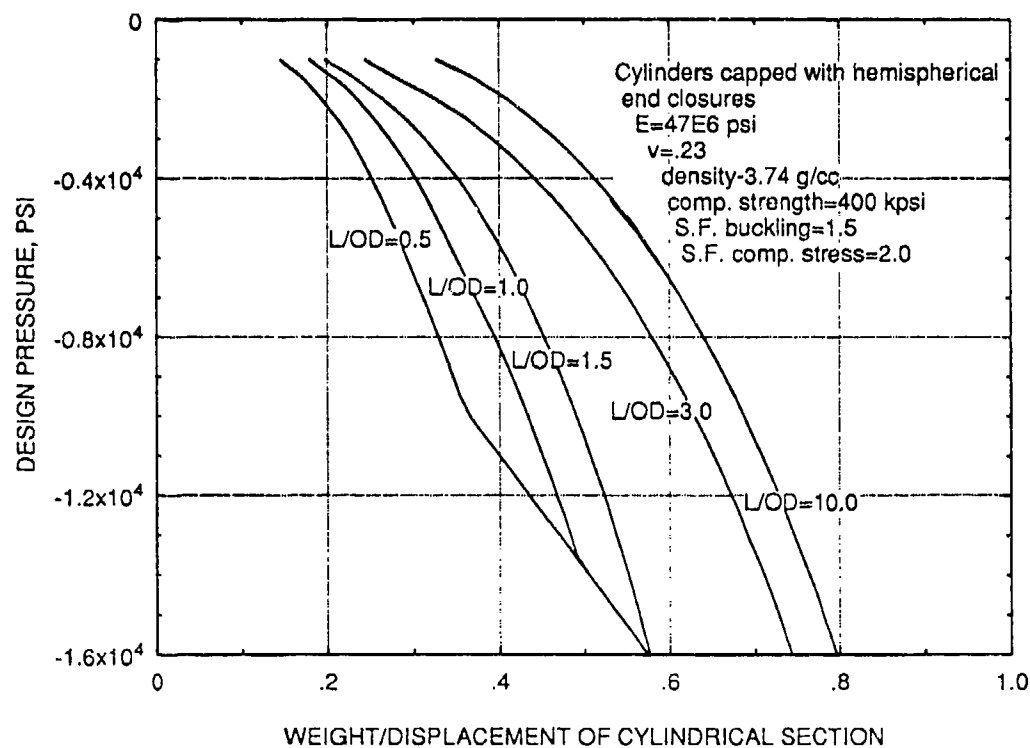


Figure 60.  $W/D$  ratios of monocoque AL-600 alumina cylinders for 100 cycles to design depth.

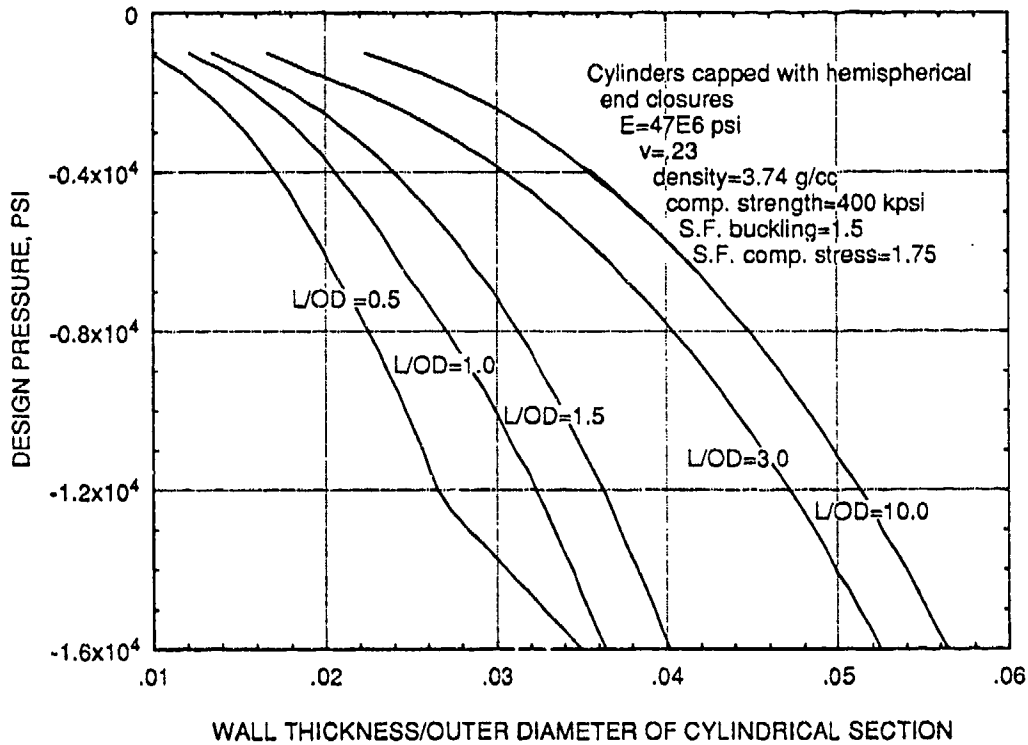


Figure 61.  $t/OD$  ratios of monocoque AL-600 alumina cylinders for 10 cycles to design depth.

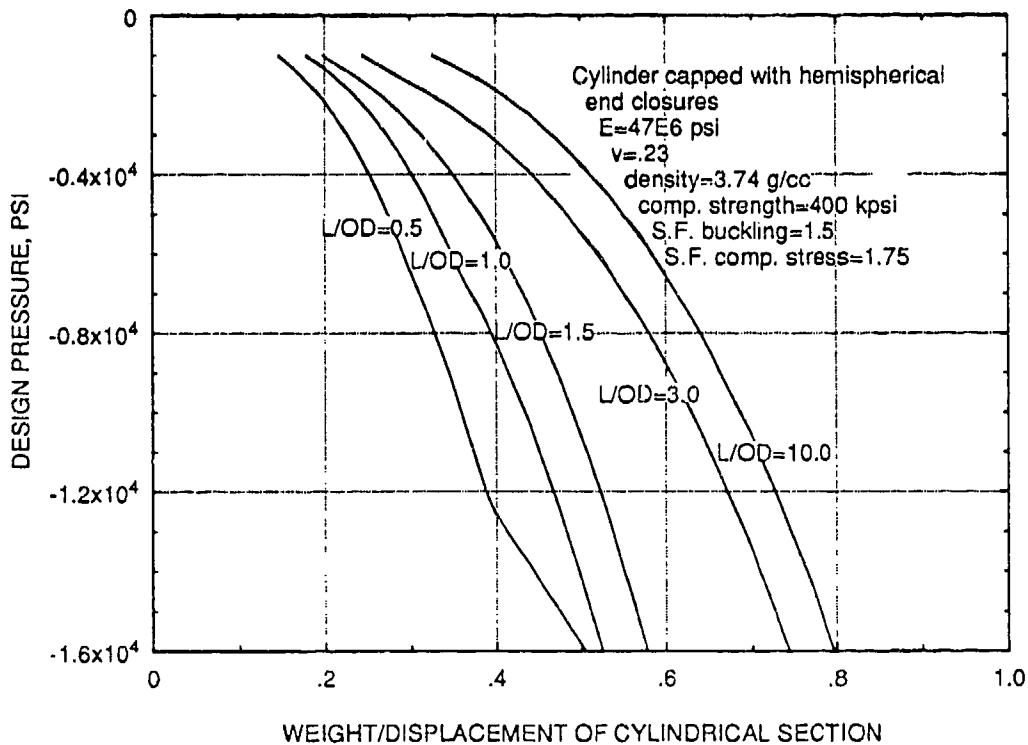


Figure 62.  $W/D$  ratios of monocoque AL-600 alumina cylinders for 10 cycles to design depth.



Table 1. Material properties for WESGO, Inc. alumina-ceramic compositions.

**WESGO**

Technical Ceramics  
and Brazing Alloys



**WESGO Dense Alumina & Properties**

Property	Unit	Temp.	AL-500*	AL-600*	AL-300*	AL-995*
Al <sub>2</sub> O <sub>3</sub> Content	%		94.0	96.0	97.6	99.5
Flexural Strength	psi	Room	50,000	53,000	43,000	45,000
	MPa	Temp. (RT)	345	365	296	310
Compressive Strength	psi		>300,000	>300,000	>250,000	>300,000
	MPa	R.T.	>2070	>2070	>1720	>2070
Density	lbs/in <sup>3</sup>		0.132	0.134	0.136	0.139
	g/cc	R.T.	3.67	3.72	3.76	3.86
Porosity	% water absorption		vacuum tight 0.00	vacuum tight 0.00	vacuum tight 0.00	vacuum tight 0.00
Color	—		white	white	white	white
Hardness	Rockwell 45N		78	79	75	81
Thermal Conductivity	BTU/ft hr °F		11.9	14.8	15.5	16.9
	W/m °K	R.T.	20.5	25.6	26.8	29.3
Coefficient of Linear Thermal Expansion	10 <sup>-6</sup> /°C	25°—200°C	6.3	6.4	6.9	6.9
		200°—400°C	7.5	7.6	7.8	7.8
		400°—600°C	8.0	8.2	8.5	8.3
		600°—800°C	8.6	8.7	8.8	9.0
		800°—1000°C	9.1	9.0	9.0	9.4
	10 <sup>-6</sup> /°F	77°—390°F	3.5	3.6	3.8	3.8
		390°—750°F	4.2	4.2	4.3	4.3
		750°—1110°F	4.4	4.6	4.7	4.6
		1110°—1470°F	4.8	4.8	4.9	5.0
		1470°—1830°F	5.1	5.0	5.0	5.2
Maximum Working Temperature	°C		1600	1620	1650	1725
	°F		2910	2950	3000	3150
Dielectric Strength (.100" thick under oil)	D.C. volts/mil	R.T.	650	675	1100	800
	D.C. kilovolts/mm		25.6	26.6	43.3	31.5
Te Value	°C		>950	>950	>1000	>975
	°F		>1740	>1740	>1800	>1790
Volume Resistivity	ohm-cm	25°C/77°F	>10 <sup>14</sup>	>10 <sup>14</sup>	>10 <sup>14</sup>	>10 <sup>14</sup>
		300°C/570°F	2.0x10 <sup>12</sup>	2.0x10 <sup>12</sup>	1.0x10 <sup>12</sup>	2.0x10 <sup>11</sup>
		600°C/1110°F	4.6x10 <sup>8</sup>	5.2x10 <sup>8</sup>	2.3x10 <sup>10</sup>	6.0x10 <sup>8</sup>
		900°C/1650°F	3.5x10 <sup>6</sup>	4.1x10 <sup>6</sup>	5.0x10 <sup>8</sup>	2.5x10 <sup>6</sup>

Property	Unit	AL-500*			AL-600*			AL-300*			AL-995*		
Dielectric Constant (K')	10MHz	25°C	300°C	500°C	25°C	300°C	500°C	25°C	300°C	500°C	25°C	300°C	500°C
	1000MHz	9.07	9.53	9.91	9.30	9.65	10.10	9.53	9.91	10.14	9.58	9.92	10.14
	8500MHz	9.04	—	—	9.20	—	—	9.00	—	—	9.30	—	—
Dissipation Factor (Tan δ)	10MHz	8.98	9.26	9.40	9.16	9.30	9.45	9.04	9.32	9.54	9.37	9.61	9.74
	1000MHz	0.00026	0.00028	0.00034	0.00030	0.00061	0.00330	0.00004	0.00016	0.00052	0.00003	0.00009	0.00014
	8500MHz	0.00062	—	—	0.00044	—	—	0.00030	—	—	0.00014	—	—
Loss Factor (K' Tan δ)	10MHz	0.00078	0.00155	0.00155	0.00062	0.00085	0.00121	0.00045	0.00040	0.00072	0.00009	0.00014	0.00014
	1000MHz	0.00236	0.00267	0.00369	0.00279	0.00588	0.03333	0.00038	0.00158	0.00527	0.00029	0.00089	0.00089
	8500MHz	0.00560	—	—	0.00405	—	—	0.00270	—	—	0.00130	—	—
		0.00700	0.01165	0.01457	0.00528	0.00719	0.01143	0.00407	0.00373	0.00687	0.00084	0.0001350	0.0001350

Table 2. Internal defects detected in alumina cylinders using ultrasonic NDE techniques.

INTERNAL DEFECTS DETECTED IN ALUMINA CYLINDERS 55910-0128915 USING ULTRASONIC NDE TECHNIQUES		
CYLINDER PART #	# OF DEFECTS	SIZE* AND DEPTH** OF DEFECTS
001	1	57% @ .250
002	1	40% @ .300
003	6	34% @ .200, 25% @ .200, 32% @ ID, 22% @ .250, 32% @ .265, 38% @ .325
004	3	35% @ .265, 45% @ .200, 35% @ .230
005	3	47% @ .200, 29% @ OD, 19% @ .300
006	4	26% @ ID, 40% @ .320, 47% @ .250, 19% @ .250
007	1	49% @ ID
008	0	NA
009	2	55% @ .206, 35% @ .206
010	2	20% @ .206, 62% @ ID

\*SIZE INDICATED BY A % OF THE AVERAGE AMPLITUDE OF REFLECTION FROM A .030 INCH VOID IN CALIBRATION STANDARD SK9402-093-C2

\*\*DEPTH OF EACH DEFECT IS MEASURED IN INCHES FROM THE OD OF THE CYLINDER

Table 3. External pressure test plan for alumina cylinders.

TEST PLAN FOR ALUMINA CYLINDERS 55910-0128915				
CYLINDER PART #	TEST #	TEST CONFIGURATION	TEST PRESSURE (psi)	TEST PLAN
001	01	TEST ASSEMBLY I	9000	3000 CYCLES OR UNTIL FAILURE
010	02	TEST ASSEMBLY I	11 000	1000 CYCLES
003	03	TEST ASSEMBLY I	11,000	3000 CYCLES OR UNTIL FAILURE
009	04	TEST ASSEMBLY I	12,000	3000 CYCLES OR UNTIL FAILURE
002	05	TEST ASSEMBLY I	13,000	1000 CYCLES OR UNTIL FAILURE
008	06	TEST ASSEMBLY II	14,000	1000 CYCLES OR UNTIL FAILURE
004	07	TEST ASSEMBLY II	15,000	1000 CYCLES OR UNTIL FAILURE
005	08	TEST ASSEMBLY III	20,000	PROOF TEST
007	09	TEST ASSEMBLY III	TBD	PRESSURIZE TO FAILURE
006	10	TEST ASSEMBLY I	11,000	1000 HOUR HOLD

TEST ASSEMBLY I: TITANIUM HEMISPHERE END CLOSURES, MOD 1, TYPE 2, END CAP JOINT RINGS  
 TEST ASSEMBLY II: FLAT STEEL PLATE END CLOSURES, MOD 1, TYPE 2, END CAP JOINT RINGS  
 TEST ASSEMBLY III: FLAT STEEL PLATE END CLOSURES, MOD 1, TYPE 1, END CAP JOINT RINGS

Table 4. Calculated stresses (psi) in alumina cylinders for test assembly I configuration.

CALCULATED STRESSES (psi) IN ALUMINA CYLINDER 55910-0128915 FOR TEST ASSEMBLY I, SK9402-070					
EXTERNAL PRESSURE	9000 psi	10,000 psi	11,000 psi	12,000 psi	13,000 psi
RADIAL STRESS					
LOCAL MAX	+14,410	+15,830	+17,260	+18,680	+20,110
AXIAL STRESS					
LOCAL MIN	-28,560	-31,700	-34,840	-37,980	-41,120
LOCAL MAX	-90,680	-100,570	-110,470	-120,360	-130,260
MAX NOMINAL MEMBRANE	-66,620	-74,020	-81,420	-88,530	-96,230
HOOP STRESS					
LOCAL MIN	-109,680	-121,880	-134,080	-146,280	-158,480
MAX NOMINAL MEMBRANE	-133,500	-148,330	-163,160	-178,000	-192,830

Table 5. Calculated stresses (psi) in alumina cylinders for test assembly II and III configurations.

CALCULATED STRESSES (psi) IN ALUMINA CYLINDER SK9402-0128915 FOR TEST ASSEMBLY II, SK9402-123. AND TEST ASSEMBLY III, SK9402-083				
	TEST ASSEMBLY II			TEST ASSEMBLY III
EXTERNAL PRESSURE	14,000 psi	15,000 psi	18,000 psi	20,000 psi
RADIAL STRESS				
LOCAL MAX	-19,630	+20,940	+24,880	+27,500
AXIAL STRESS				
LOCAL MIN	-44,190	-47,360	-56,860	-63,190
LOCAL MAX	-153,040	-163,440	-194,630	-215,430
MAX NOMINAL MEMBRANE	-103,680	-111,080	-133,290	-148,040
HOOP STRESS				
LOCAL MIN	-169,740	-181,960	-218,610	-243,040
MAX NOMINAL MEMBRANE	-207,680	-222,510	-267,000	-296,670

Table 6. External pressure test results for alumina cylinders.

TEST RESULTS FOR ALUMINA CYLINDERS 55910-0128915			
TEST #	TEST CONFIGURATION	TEST PRESSURE (psi)	TEST RESULT
01	TEST ASSEMBLY I	9000	WITHSTOOD 3000 CYCLES W/O FAILURE
02	TEST ASSEMBLY I	11,000	WITHSTOOD 1380 CYCLES W/O FAILURE
03	TEST ASSEMBLY I	11,000	FAILED ON CYCLE 2,969
04	TEST ASSEMBLY I	12,000	FAILED ON CYCLE 1065
05	TEST ASSEMBLY I	13,000	FAILED ON CYCLE 762
06	TEST ASSEMBLY II	14,000	FAILED ON CYCLE 214
07	TEST ASSEMBLY II	15,000	FAILED ON CYCLE 707
08	TEST ASSEMBLY III	20,000	WITHSTOOD PROOF TEST
09	TEST ASSEMBLY III	23,730	FAILED AT 23,730 psi
10	TEST ASSEMBLY I	11,000	WITHSTOOD 1000 HOURS W/O FAILURE

TEST ASSEMBLY I: TITANIUM HEMISPHERE END CLOSURES, MOD 1, TYPE 2, END CAP JOINT RINGS  
 TEST ASSEMBLY II: FLAT STEEL PLATE END CLOSURES, MOD 1, TYPE 2, END CAP JOINT RINGS  
 TEST ASSEMBLY III: FLAT STEEL PLATE END CLOSURES, MOD 1, TYPE 1, END CAP JOINT RINGS

**FEATURED RESEARCH**

---

**APPENDIX A: QUALITY CONTROL  
DATA**

---

## FIGURES

- A-1. Dimensional data form for cylinder part #1.
- A-2. MOR data for cylinder lot 1.
- A-3. Compressive strength data for cylinder lot 1.
- A-4. MOR data for cylinder lot 2.
- A-5. Compressive strength data for cylinder lot 2.
- A-6. MOR data for cylinder lot 3.
- A-7. Compressive strength data for cylinder lot 3.



SHEET \_\_\_\_\_ OF \_\_\_\_\_

DIMENSIONAL RANGE DATA FORM

**WESGO**

Technical Ceramics  
and Brazing Alloys



ORDER NUMBER

N66001-93-M-0044

DRAWING NUMBER (GRAPHIC)

55910-0128915

PART NAME

HOUSING CYLINDRICAL 12"

ISSUE

NO REVISION

S.O.

126260

LOT#

3A 4340 H0125

DRAWING DIMENSION OR NOTE		RANGE		SAMPLE SIZE
		MIN.	MAX.	
1. 18.00 ± .01		18.0075	18.009	
2. Ø 12.000 ± .005		12.000	12.0015	
3. <input type="checkbox"/> .010 A		Ø	<.001	
4. <input type="checkbox"/> .002 A		Ø	<.001	
5. .410 / .415 WALL		.4125	.4135	
6. 4 X R .03 ± .0±		.020	.025	
7.				
8. <input type="checkbox"/> .010 A		.0005	.001	
9. <input type="checkbox"/> .002		Ø	<.001	
10.				
11. 16 ✓		8	14	
12.				
13. SERIAL #				
14. 126915001				
15. VISUAL CLASS A	w/ Spec.			
16.				
17. CANDLING	No Visual			
18. POROSITY	Defects Observed			
19.				
20.				

REMARKS: STATEMENT OF WORK NRAD COSE 9402 REV. 2 DATED 9/2/92.

3061

INSPECTOR

(6-78)

*L. Davis*

QUALITY ASSURANCE

3/15/93

DATE COMPLETED

Figure A-1. Dimensional data form for cylinder part #1.

## FEATURED RESEARCH

### FMC Corporation

Corporate Technology Center  
1205 Coleman Avenue  
Box 580  
Santa Clara, California 95051  
408 289 2731

MATERIALS ENGINEERING  
RESULTS RECORD NO. 930590



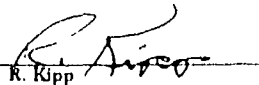
### RESULTS OF TESTING Federal Standard 1492 (4-point) FLEXURAL STRENGTH

Serial No: 4340H0125915

Specimen Number	Load at Failure (lbs)	Modulus of Rupture (psi)
1	147.52	47,229
2	154.41	49,435
3	145.40	46,550
Average		47,700
Std Deviation		1,200

Test rate - 0.02 inch/minute  
Room temperature  
Overall specimen length -  $2.000 \pm 0.050$  inch  
Specimen breadth - 0.250 inch  
Specimen depth - 0.125 inch

Tested by:

  
R. Kipp

March 24, 1993  
PA 7MM700915

1

Figure A-2. MOR data for cylinder lot 1.

## FMC Corporation

Corporate Technology Center  
1205 Coleman Avenue  
Box 580  
Santa Clara, California 95052  
408 289 2731

MATERIALS ENGINEERING  
RESULTS RECORD NO. 930590



RESULTS OF TESTING  
ASTM D695  
COMPRESSIVE STRENGTH

Serial No: 4340H0125915

Specimen Number	Ultimate Compressive Strength (lbs)	Diameter	Area	Ultimate Compressive Strength (psi)
1	17,598	0.25	0.0491	358,500
2	21,711	0.25	0.0491	442,300
3	22,129	0.25	0.0491	450,800
Average				417,200
Standard Deviation				41,700

Test rate - 10,000 pounds/minute

Room temperature

Overall specimen length - 0.500 inch; Specimen diameter - 0.250 inch

Tested by: R. Kipp

R. Kipp

March 24, 1993  
PA 7MM700915

2

Figure A-3. Compressive strength data for cylinder lot 1.

5/3/94

04:13:43 15:23

**FMC Corporation**

Corporate Technology Center  
1205 Coleman Avenue  
Box 580  
Santa Clara, California 95052  
408 289 2731

**MATERIALS ENGINEERING**  
**RESULTS RECORD NO. 93-190**



**RESULTS OF TESTING**  
**Federal Standard 1492 (4-point)**  
**FLEXURAL STRENGTH**

**Serial No: 4521F0222015**

<b>Specimen Number</b>	<b>Load at Failure (lbs)</b>	<b>Modulus of Rupture (psi)</b>
1	154	49,304
2	161	51,545
3	162	51,865
Average		50,900
Std Deviation		1,100

Figure A-4. MOR data for cylinder lot 2.

539 P07

MAR 13 '93 15:24

**FMC Corporation**

Corporate Technology Center  
1205 Coleman Avenue  
Box 580  
Santa Clara, California 95052  
408 289 2731

**MATERIALS ENGINEERING**  
**RESULTS RECORD NO. 93-190**



**RESULTS OF TESTING**  
**ACMA Test #1**  
**COMPRESSIVE STRENGTH**

Serial No: 4521F0222915

Specimen Number	Ultimate Compressive Strength (lbs)	Diameter	Area	Ultimate Compressive Strength (psi)
1	20,905	0.25	0.0491	425,900
2	20,748	0.25	0.0491	422,700
3	21,976	0.25	0.0491	447,700
Average				432,100
Standard Deviation				11,100

Figure A-5. Compressive strength data for cylinder lot 2.

**Materials Engineering Laboratories**

1205 Coleman Avenue ♦ Box 580 ♦ Santa Clara, CA 95052

**TEST REPORT**

Page 2

Federal Standard 1492 (4-point)  
**FLEXURAL STRENGTH**

Serial No: 452110519915

Specimen Number	Load at Failure (lbs)	Modulus of Rupture (psi)
1	159	50,904
2	172	55,066
3	173	55,387

Average: 53,000  
Std. Deviation: 2,000Test rate - 0.02 inch/minute  
Room temperature  
Overall specimen length -  $2.000 \pm 0.050$  inch  
Specimen breadth - 0.250 inch  
Specimen depth - 0.125 inchAnalyst: R. KiserApproved: R. Kiser

---

For more information about FMC's Materials Engineering Laboratories services, call (408) 289-0215

Figure A-6. MOR data for cylinder lot 5.

**Materials Engineering Laboratories**

1205 Coleman Avenue ♦ Box 580 ♦ Santa Clara, CA 95052

**TEST REPORT**

Page 3

ACMA Test #1  
**COMPRESSIVE STRENGTH**

Serial No: 452110519915

Specimen Number	Ultimate Compressive Load (lbs)	Diameter (in.)	Area (sq. in.)	Ultimate Compressive Strength (psi)
1	20,949	0.25	0.0491	426,800
2	17,595	0.25	0.0491	358,400
3	18,206	0.25	0.0491	370,900

Average: 385,400  
Std. Deviation: 29,700Test rate - 10,000 pounds/minute  
Room temperature  
Overall specimen length - 0.500 inch; Specimen diameter - 0.250 inchAnalyst:   
R. KoppApproved: 

For more information about FMC's Materials Engineering Laboratories services, call (408) 289-0215

Figure A-7. Compressive strength data for cylinder lot 3.

# REPORT DOCUMENTATION PAGE

Form Approved  
OMB No. 0704-0188

Public reporting burden for this collection of information is estimated to average 1 hour per response, including the time for reviewing instructions, searching existing data sources, gathering and maintaining the data needed, and completing and reviewing the collection of information. Send comments regarding this burden estimate or any other aspect of this collection of information, including suggestions for reducing this burden, to Washington Headquarters Services, Directorate for Information Operations and Reports, 1215 Jefferson Davis Highway, Suite 1204, Arlington, VA 22202-4302, and to the Office of Management and Budget, Paperwork Reduction Project (0704-0188), Washington, DC 20503.

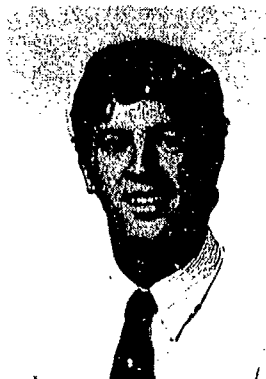
1. AGENCY USE ONLY (Leave blank)		2. REPORT DATE August 1993		3. REPORT TYPE AND DATES COVERED Final	
4. TITLE AND SUBTITLE STRUCTURAL PERFORMANCE OF CYLINDRICAL PRESSURE HOUSINGS OF DIFFERENT CERAMIC COMPOSITIONS UNDER EXTERNAL PRESSURE LOADING Part I, Isostatically Pressed Alumina Ceramic				5. FUNDING NUMBERS  PE: 0603713N PROJ: S0397 ACC: DN302232	
6. AUTHOR(S) R. P. Johnson, R. R. Kurkchubasche, J. D. Stachiw					
7. PERFORMING ORGANIZATION NAME(S) AND ADDRESS(ES) Naval Command, Control and Ocean Surveillance Center (NCCOSC) RDT&E Division San Diego, CA 92152-5001				8. PERFORMING ORGANIZATION REPORT NUMBER  TR 1590	
9. SPONSORING/MONITORING AGENCY NAME(S) AND ADDRESS(ES) Naval Sea Systems Command Washington, DC 20362				10. SPONSORING/MONITORING AGENCY REPORT NUMBER	
11. SUPPLEMENTARY NOTES					
12a. DISTRIBUTION/AVAILABILITY STATEMENT  Approved for public release; distribution is unlimited.				12b. DISTRIBUTION CODE	
13. ABSTRACT (Maximum 200 words)  Ten monocoque cylinders, 18-inches (length) by 12-inches (outer diameter, OD) by 0.412 inches (thickness), fabricated by WESGO, Inc. from 96-percent alumina ceramic were assembled into external pressure housings and experimentally evaluated under short-term, static, and cyclic pressure loadings. This study was undertaken as part of a program to promote the application of ceramics to large external pressure housings for underwater vehicles. Pressure testing was performed to generate structural performance data that could be used to establish design criteria for external pressure housings constructed by using 96-percent alumina ceramic as the primary hull material. Design curves for 96-percent alumina-ceramic housings are presented that relate the maximum number of operational dive cycles to the maximum allowable stresses in the ceramic housing during each dive cycle. The 96-percent alumina ceramic has been found to be a reliable structural material for the fabrication of cylindrical external pressure housings with a minimum fatigue life of 1,000 dive cycles to nominal design stresses of -160,000 psi in the hoop direction.					
14. SUBJECT TERMS  ceramics external pressure housing ocean engineering				15. NUMBER OF PAGES 100	
				16. PRICE CODE	
17. SECURITY CLASSIFICATION OF REPORT  UNCLASSIFIED	18. SECURITY CLASSIFICATION OF THIS PAGE  UNCLASSIFIED	19. SECURITY CLASSIFICATION OF ABSTRACT  UNCLASSIFIED	20. LIMITATION OF ABSTRACT  SAME AS REPORT		



UNCLASSIFIED

21a. NAME OF RESPONSIBLE INDIVIDUAL R. P. Johnson	21b. TELEPHONE (include Area Code) (619) 553-1935	21c. OFFICE SYMBOL Code 564

## THE AUTHORS



**RICHARD P. JOHNSON** is an Engineer for the Ocean Engineering Division. He has held this position since 1987. Before that, he was a Laboratory Technician for the Ocean Engineering Laboratory, University of California at Santa Barbara from 1985-1986, and Design Engineer in the Energy

Projects Division of SAIC from 1986-1987. His education includes a B.S. in Mechanical Engineering from the University of California at Santa Barbara in 1986, and an M.S. in Structural Engineering from the University of California, San Diego, in 1991. He is a member of the Marine Technology Society and has published "Stress Analysis Considerations for Deep Submergence Ceramic Pressure Housings," *Intervention '92*, and "Structural Design Criteria for Alumina-Ceramic Deep Submergence Pressure Housings," *MTS '93 Proceedings*.



**RAMON R. KURKCHUBASCHE** is a Research Engineer for the Ocean Engineering Division and has worked since November 1990 in the field of deep submergence pressure housings fabricated from ceramic materials. His education includes a B.S. in Structural Engineering from the

University of California at San Diego, 1989; and an M.S. in Aeronautical/Astronautical Engineering from Stanford University in 1990. His experience includes conceptual design, procurement, assembly, testing, and documentation of ceramic housings. Other experience includes buoyancy concepts utilizing ceramic, nondestructive

evaluation of ceramic components. He is a member of the Marine Technology Society, and has published "Elastic Stability Considerations for Deep Submergence Ceramic Pressure Housings," *Intervention '92*, and "Nondestructive Evaluation Techniques for Deep Submergence Housing Components Fabricated from Alumina Ceramic," *MTS '93 Proceedings*.



**DR. JERRY STACHIW** is Staff Scientist for Marine Materials in the Ocean Engineering Division. He received his undergraduate engineering degree from Oklahoma State University in 1955 and graduate degree from Pennsylvania State University in 1961.

Since that time he has devoted his efforts at various U.S. Navy Laboratories to the solution of challenges posed by exploration, exploitation, and surveillance of hydrospace. The primary focus of his work has been the design and fabrication of pressure resistant structural components of diving systems for the whole range of ocean depths. Because of his numerous achievements in the field of ocean engineering, he is considered to be the leading expert in the structural application of plastics and brittle materials to external pressure housings.

Dr. Stachiw is the author of over 100 technical reports, articles, and papers on design and fabrication of pressure resistant viewports of acrylic plastic, glass, germanium, and zinc sulphide, as well as pressure housings made of wood, concrete, glass, acrylic plastic, and ceramics. His book on "Acrylic Plastic Viewports" is the standard reference on that subject.

For the contributions to the Navy's ocean engineering programs, the Navy honored him with the Military Oceanographer Award and the NCCOSC's

## FEATURED RESEARCH

---

RDT&E Division honored him with the Lauritsen-Bennett Award. The American Society of Mechanical Engineers recognized his contributions to the engineering profession by election to the grade of Life-Fellow, as well as the presentation of Centennial Medal, Dedicated Service Award and Pressure Technology Codes Outstanding Performance Certificate.

Dr. Stachiw is past-chairman of ASME Ocean Engineering Division and ASME Committee on

Safety Standards for Pressure Vessels for Human Occupancy. He is a member of the Marine Technology Society, New York Academy of Science, Sigma Xi and Phi Kappa Honorary Society.